Optical studies of X-ray sources in the old open cluster M 67

Figures 1.1 and 8.1, the images in the chapter headings and the images at the end are created from the Digitized Sky Survey

ISBN 90-393-2679-7

Optical studies of X-ray sources in the old open cluster M 67

Optische studies van röntgenbronnen in de oude open sterrenhoop M 67

(met een samenvatting in het Nederlands)

Proefschrift

ter verkrijging van de graad van doctor aan de Universiteit Utrecht
op gezag van de Rector Magnificus prof. dr H.O. Voorma
ingevolge het besluit van het College voor Promoties,
in het openbaar te verdedigen op

woensdag 21 maart 2001 des ochtends te 10.30 uur

door
Maureen Constance van den Berg

geboren op 6 april 1972 te Maastricht

PROMOTOR prof. dr Frank Verbunt

Dit proefschrift werd mede mogelijk gemaakt met financiële steun van de Nederlandse Organisatie voor Wetenschappelijk Onderzoek (NWO).

Contents

Chapter 1

Introduction

1.1 Blue stragglers, yellow stragglers and sub-subgiants

Galactic clusters, also called open clusters, are bound groups of stars, consisting of a few hundred to a few thousand members. Their ages range from millions of years (e.g. the ~ 4 Myr old IC 1590, Guetter & Turner 1997) to billions of years (e.g. the ~ 6 Gyr old NGC 188, Dinescu et al. 1995), where they start to approach the typical age of the older, more dense and populous globular clusters. The field of an open cluster is usually not too crowded so that a probability of cluster membership for individual stars projected in the field can be established by means of proper-motion and radial-velocity measurements with ground-based instruments. Only recently can accurate proper motions also be measured for stars in globular clusters, with the Hubble Space Telescope (e.g. King et al. 1999).

A basic fingerprint of a cluster is its colour-versus-magnitude diagram: comparison of the observed locations in this diagram of the cluster stars with theoretical isochrones provides an estimate of the age, distance and metallicity of the cluster. The advantages of studying stars in clusters are therefore many: we can derive basic stellar parameters like mass, temperature and radius of the individual members from comparison with models. On the other hand, clusters have been used extensively to test stellar evolution models. By studying the properties of clusters of different ages the evolution in time of those properties can be investigated. Also, as the spatial distribution of open clusters is concentrated towards the disc of the Galaxy, they are used to probe the properties and evolution of the Galactic disc.

The open cluster that plays a central role in this thesis is M 67 (NGC 2682, Fig. 1.1). M 67 is one of the best-studied open clusters as a result of several factors: it is a rich cluster, at 850 pc it is relatively nearby, and due to its high Galactic latitude ($b = 32^\circ$) the reddening in the direction of M 67 is low and the field is little contaminated by field stars; also, it is one of the few clusters older than several Gyr. The stars in the colour-magnitude diagram can be fitted with a 4 to 5 Gyr isochrone of solar or slightly subsolar metallicity (e.g. Fan et al. 1996).

Even after the non-members are removed, the colour-magnitude diagram of M 67 still features many stars that straggle from the theoretical isochrone (see Fig. 1.2). This can be

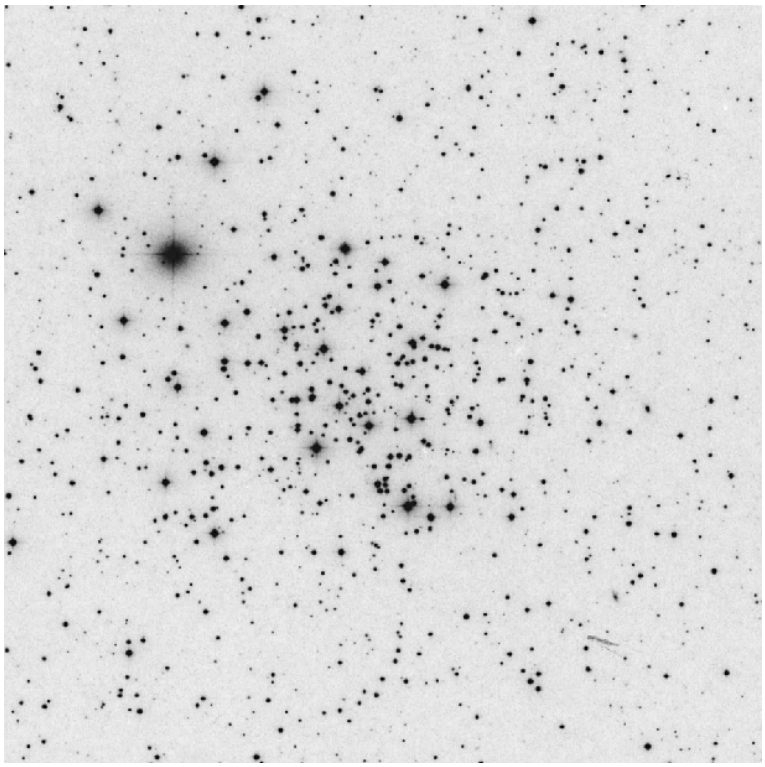

Figure 1.1: Central 25 x 25 arcmin^2 of M 67.

accounted for when we are actually seeing the light of two cluster members in an unresolved binary. For instance, the line of stars that lies above and parallel to the main sequence is likely due to a binary population. However, this cannot be the case for the two sub-subgiants below the base of the giant branch, for the blue stragglers that are brighter and bluer than the main-sequence turnoff and for some of the yellow stragglers that lie between the blue stragglers and the red giants.

What makes these stars so interesting is that we have no explanation for their properties which only involves the evolution of a single isolated star. Therefore, they offer the possibility to study the products of interactions between stars – either between the companions in a binary or between stars in the cluster. Encounters and collisions between single and binary stars in the high-stellar density environment of a cluster have been invoked to explain the formation of strange stars like low-mass X-ray binaries or blue stragglers, especially in globular clusters (see review by Bailyn 1995). The interest in these systems is not only restricted to the desire to understand interacting stars: the exchange of energy that results from interactions between cluster stars can also affect the evolution of the cluster as a whole (Hut et al. 1992).

Two ROSAT observations of M 67 detected many of the peculiar stars in X-rays (Belloni et al. 1993, 1998), possibly providing an important clue to their origin or present state. These X-ray sources were selected for an optical follow-up study, and the results can be read in this thesis. As the X-ray emission of these stars was unexpected (see next Section) our first

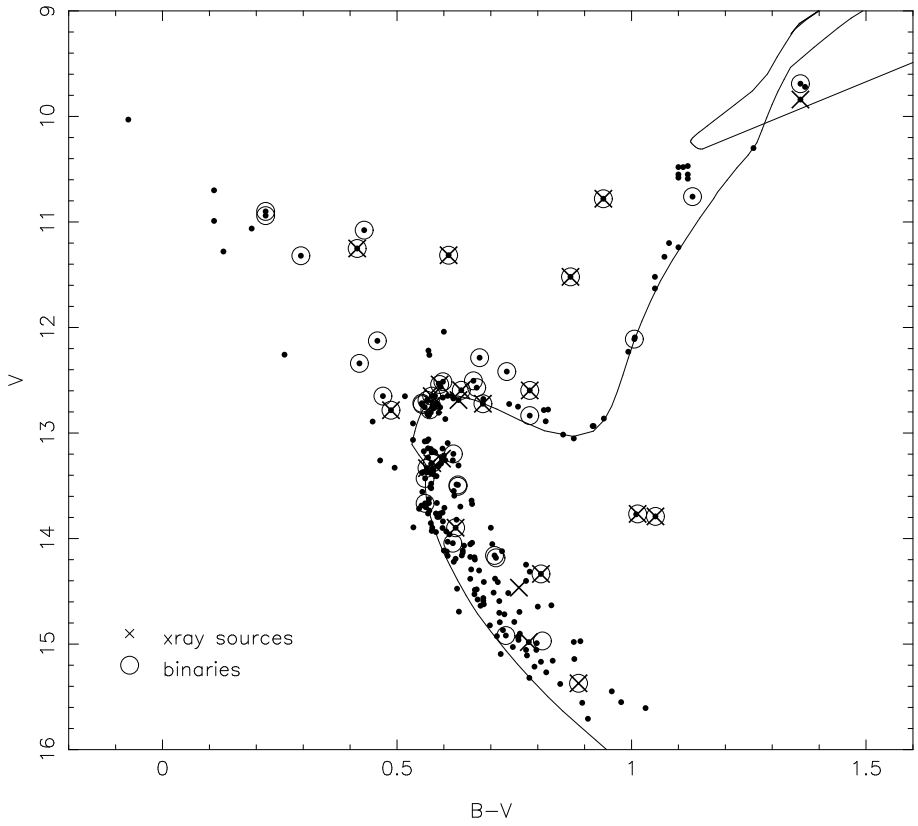

Figure 1.2: Colour-magnitude diagram in which the binaries (Whelan et al. 1979, Mathieu et al. 1990, Gilliland et al. 1991, Latham et al. 1992, Latham et al. private communication) and the X-ray sources (Belloni et al. 1998) are indicated. Only stars with a proper-motion membership probability $>$80% (Girard et al. 1989, for several stars Sanders 1977) are plotted. Photometry is mostly taken from Montgomery et al. (1993), in a few cases from Sanders (1989).

question was whether we can find spectroscopic (Chapter 2) and photometric (Chapter 3) signatures that explain the X-rays. Our photometric-variability study inevitably included many other stars in M 67 – these results are included in Chapter 3 and Chapter 4. Next, three systems were studied in more detail: the blue straggler (Chapter 5) and the two sub-subgiants (Chapter 6). The last chapter adds a study of the peculiar X-ray sources in the old clusters NGC 752 (2 Gyr) and NGC 6940 (1 Gyr).

1.2 X-ray observations of old open clusters

X-ray emission of single stars is generally thought to arise from two mechanisms. For spectral types earlier than A, the X-rays come from shocks in a stellar wind. For types later than A, a hot corona around the star is believed to give rise to X-rays. The presence of the hot coronal

cluster	age	N_X	N_{bin}	N_{act}	N_{pec}
NGC 188	6	2	1	1	1
M 67	4	25	18	12	9
NGC 752	2	7	4	3	1
IC 4651	1.7	2	1	1	1
NGC 6940	0.6	4	3	2	2

Table 1.1: X-ray sources in old open clusters. For each cluster we list the age in Gyr, the number of X-ray sources identified with optical cluster members, the number of binaries among the optical counterparts, the number of sources for which the X-rays are likely the result of coronal activity due to tidal interaction in a binary and the number of peculiar X-ray sources (blue stragglers, yellow stragglers and sub-subgiants; long-period binaries; stars without indication for binarity). Data for NGC 188 and M 67 are taken from Belloni et al. (1998), for NGC 752 from Belloni & Verbunt (1996), for IC 4651 from Belloni & Tagliaferri (1998) and for NGC 6940 from Belloni & Tagliaferri (1997). Cluster ages are taken from Dinescu et al. 1995, except for IC 4651 (Anthony-Twarog & Twarog 2000) and NGC 6940 (Carraro & Chiosi 1994). The number of X-ray sources detected in a cluster depends on many factors not related to the intrinsic properties of the stars in the clusters, like the exposure time of the ROSAT observation, the distance and reddening to the cluster.

medium is related to magnetic activity, generated by the interaction between convection and differential stellar rotation in the outer layers of a star. The two classes are not expected to contribute to the X-rays of an old stellar population: massive stars with strong winds have long since evolved off the main sequence; the rotation of late-type stars decreases as the stars age, and with it the magnetic activity. Consequently, the level of X-ray emission becomes too low to be detected. Randich (1997) has indeed shown that the average level of X-ray emission for G-type stars in the 600 Myr old cluster Hyades is lower than in the 50 Myr old α Per.

None the less, ROSAT observations of old open clusters revealed many X-ray sources, with X-ray luminosities of a few times 10^{30} erg s^{-1}, that were optically identified with cluster members (see Fig. 1.2). While we do not expect to detect X-rays from single main-sequence or giant stars, close binaries are able to emit detectable X-ray at ages of a few Gyr. The reason is that in close binaries the stellar rotation is locked to the orbital motion through tidal interaction, and therefore rapid rotation and magnetic activity can be maintained regardless the age of the component stars. Indeed, many X-ray sources in old open clusters have tidally interacting binaries as optical counterparts (see Table 1.1). These magnetically active binaries – also called RS CVn or BY Dra binaries depending on whether the active star is a giant or main-sequence star, respectively – can be recognised by other properties related to the activity. The orbits are circular due to the tidal interaction. Photometric variability on the orbital period is often observed due to star spots on the corotating stellar surfaces. Optical spectral signatures of activity are strong Ca II H&K emission cores and/or Hα emission. The lifetimes of the (sub)giants in RS CVns in younger clusters are much shorter than in older

clusters, which reduces the chance for detection. The X-ray observations of old clusters were partly aimed at observing homogeneous samples of active binaries (Belloni 1997).

However, a considerable fraction of the X-ray sources in old clusters is not identified with tidally interacting binaries (see last column of Table 1.1). For the hot white dwarf, the cataclysmic variable and the contact binaries the X-rays are understood. But the optical counterparts also include main-sequence stars or giants with no indication for binarity or wide binaries with orbital periods too long for tidal interaction at present[1]; their X-ray emission is not as easily explained and merits further study. Many stars in M 67 that were pointed out in the previous section as stragglers from the theoretical isochrone also belong to this group of sources for which the X-rays are not understood. Apart from their anomalous position in the colour-magnitude diagram this is an extra property that makes them notable. Similar sources have also been identified among the optical counterparts of X-ray sources in other old clusters. To summarise, X-ray observations of old open clusters are valuable as they can efficiently point the way to close and/or interacting binaries and to special cases of stellar and binary evolution.

In the next section I will introduce the peculiar X-ray sources of M 67, NGC 752 and NGC 6940 in more detail and I will summarise the results of our study.

1.3 Summary: peculiar X-ray sources in M 67, NGC 752 and NGC 6940

Many of the X-ray sources that we investigated are binaries. However, we found that the properties of some systems are difficult to understand in the context of binary evolution alone. Therefore, one of the conclusions of this study is that interactions between cluster stars are responsible for making stars that are found away from the 4 Gyr isochrone in M 67 – also outside of the blue straggler region – and that the properties of the stars that are the outcome of such interactions are only poorly understood.

The blue straggler S 1082 is probably a good example of a system that is the product of an encounter or of multiple encounters. Our study solved the apparent contradictions in the observations of this system: the star showed eclipses in a period of 1.07 days (Goranskij et al. 1992) but the radial-velocity variations of the narrow lines in the spectrum are not larger than a few km s^{-1} (Mathieu et al. 1986) and indicate that the star moves in an orbit of $\sim$ 1000 days (Milone 1991). We concluded that the star must be triple, and indeed found the signature of three stars likely bound in a triple (Chapters 2, 5). However, our findings raised new questions: the outer star in the triple is a blue straggler on its own account, the total mass of the inner binary is larger than twice the turnoff mass of M 67 and one of the stars in the inner binary is

[1]The cut-off period for tidal interaction depends on the size of the stars in the binary. For main-sequence stars in M 67 the cut-off period as derived from the longest-period circular orbit observed is 12.4 days (Mathieu et al. 1992). For giant stars for which the radii rapidly vary in time, the evolution of the stellar radii should be taken into account to judge whether a binary could be or have been tidally interacting (Verbunt & Phinney 1995).

subluminous for its mass (see Chapter 5).

Two other blue stragglers in the open clusters NGC 752 and IC 4651 were detected in X-rays. Chapter 7 discusses the optical properties of H 209 in NGC 752. Also for H 209 a long spectroscopic orbital period was detected (Latham et al., private communication) and low-amplitude variability was noted by Hrivnak (1977). Yet our observations have revealed no sign of photometric or spectroscopic variability, and thus its X-rays and evolutionary status remain unexplained.

The two sub-subgiants in M 67, S 1063 and S 1113, both binaries, are located in a position where not many stragglers have been found before. We did spectroscopic (Chapter 2) and photometric (Chapter 3) observations to get more information on their properties. Chapter 6 contains a discussion on the possible origins of these stars. Even though their positions in the colour-magnitude diagram are so similar, we have found that their different orbital properties – S 1063 has an eccentric 18.4 day orbit, S 1113 a circular 2.8 day orbit – make it difficult to find one explanation for their origin. In fact, we have great difficulty to find an explanation for these stars at all, and are left to conclude that these systems were involved in a recent interaction with other cluster stars.

We studied two yellow stragglers in somewhat less detail. S 1072 lies 1.2 mag above the main-sequence turnoff and can therefore be no combination of two turnoff stars. At nearly 1500 days the orbital period is too long for tidal interaction. That the star is a combination of three turnoff stars or of a giant and a blue straggler is excluded, which similarly leaves open the option that the binary contains an anomalous star (Mathieu et al. 1990, Nissen et al. 1987). We observed the star photometrically (Chapter 3) and spectroscopically (Chapter 2) but found nothing that explains the X-rays. S 1040 is composed of a giant and a white dwarf whose first direct observational signature came from ultraviolet observations (Landsman et al. 1997). Its presence was however already predicted from the circular orbit: the giant is too small to have tidal interaction in the orbit of 43 days, which led Verbunt & Phinney (1995) to the conclusion that the progenitor of the now optically invisible white dwarf must have circularised the orbit. Landsman et al. constructed an evolutionary history where the present giant received mass from the white-dwarf progenitor until 75 Myr ago (the cooling time of the white dwarf). As this is one of the ways to make the mass receiver a blue straggler, an explanation is needed why the observed colours of S 1040 are so red. Maybe it just started evolving off the main-sequence into a giant (Landsman et al. 1997); in that case binary evolution can explain the system. The white dwarf is too cool for X-ray emission; we find spectral signatures that point at magnetic activity of the giant, but do not understand the reason for activity (Chapter 2). It has been suggested that when intermediate-mass stars evolve off the main sequence and start developing convective envelopes, they can attain enhanced activity levels (Pizzolato et al. 2000).

We studied several X-rays sources that are not found at strange locations of the colour-magnitude diagram. The position of S 1237 to the blue of the giant branch can actually be accounted for by combining the light of a giant and a turnoff star (Janes & Smith 1984). Its X-rays however are unexplained as the orbital period is nearly 700 days which excludes tidal

interaction. Our observations offer no solution, but we conclude that magnetic activity of the giant is likely not the origin of the X-rays (Chapter 2). Other long-period binaries and stars with no indication for binarity were checked for photometric variability (S 760, S 775, S 1270 – all in M 67) with a negative result (Chapter 3). In NGC 6940, the long-period (3595 day) binary VR 111 and VR 108 with no indication for binarity were observed spectroscopically. Again, we found no sign of strong magnetic activity. We conclude that, provided the optical identification of the X-ray sources is correct, either these stars were also involved in a recent interaction, or they are triples that contain a closer binary with an active component. Alternatively, the X-ray emission of single old stars is just not understood very well.

For X-ray sources that *were* identified with close binaries (Belloni et al. 1998) our findings support the interpretation that their X-rays arise through magnetic activity. In our photometric study (Chapter 3) the orbital period of some of these binaries was also detected in the light curves. Assuming that the brightness modulations are caused by spots on the stellar surface, this confirms that the stars are corotating with the orbit – a signature of tidal interaction. Most of the stars that we found to be periodic variables (within the limits of our sensitivity as described in Chapters 3 and 4) are binaries. This confirms that at the age of M 67 single stars are not rapid rotators.

References

Anthony-Twarog, B. J. & Twarog, B. A. 2000, AJ, 119, 2282
Bailyn, C. D. 1995, ARAA, 33, 133
Belloni, T. 1997, in Cool stars in clusters and associations: magnetic activity and age indicators, ed. G. Micela, R. Pallavicini, & S. Sciortino, Vol. 68, 993
Belloni, T. & Tagliaferri, G. 1997, A&A, 326, 608
—. 1998, A&A, 335, 517
Belloni, T. & Verbunt, F. 1996, A&A, 305, 806
Belloni, T., Verbunt, F., & Mathieu, R. D. 1998, A&A, 339, 431
Belloni, T., Verbunt, F., & Schmitt, J. H. M. M. 1993, A&A, 269, 175
Carraro, G. & Chiosi, C. 1994, A&A, 287, 761
Dinescu, D. I., Demarque, P., Guenther, D. B., & Pinsonneault, M. H. 1995, AJ, 109, 2090
Fan, X., Burstein, D., Chen, J.-S., Zhu, J., Jiang, Z., Wu, H., Yan, H., Zheng, Z., Zhou, X., Fang, L.-Z., Chen, F., Deng, Z., Chu, Y., Hester, J. J., Windhorst, A., Li, Y., Lu, P., Sun, W.-H., Chen, W.-P., Tsay, W.-S., Chiueh, T.-H., Chou, C.-K., Ko, C.-M., Lin, T.-C., Guo, H.-J., & Byun, Y.-I. 1996, AJ, 112, 628
Gilliland, R. L., Brown, T. M., Duncan, D. K., Suntzeff, N. B., Lockwood, G. W., Thompson, D. T., Schild, R. E., Jeffrey, W. A., & Penprase, B. E. 1991, AJ, 101, 541
Girard, T. M., Grundy, W. M., López, C. E., & van Altena, W. F. 1989, AJ, 98, 227
Goranskij, V. P., Kusakin, A. V., Mironov, A. V., Moshkaljov, V. G., & Pastukhova, E. N. 1992, Astron. Astrophys. Trans., 2, 201
Guetter, H. H. & Turner, D. G. 1997, AJ, 113, 2116
Hrivnak, B. J. 1977, IBVS 1293

Hut, P., McMillan, S., Goodman, J., Mateo, M., Phinney, E., Pryor, C., Richer, H., Verbunt, F., & Weinberg, M. 1992, PASP, 104, 981
Janes, K. A. & Smith, G. H. 1984, AJ, 89, 487
King, I. R., Anderson, J., Cool, A. M., & Piotto, G. 1998, ApJ, 492, L37
Landsman, W., Aparicio, J., Bergeron, P., di Stefano, R., & Stecher, T. P. 1997, ApJ, 481, L93
Latham, D. W., Mathieu, R. D., Milone, A. A. E., & Davis, R. J. 1992, in Binaries as tracers of stellar formation, ed. A. Duquennoy & M. Mayor (Cambridge: Cambridge University Press), 132
Mathieu, R. D., Latham, D. W., & Griffin, R. F. 1990, AJ, 100, 1859
Mathieu, R. D., Latham, D. W., Griffin, R. F., & Gunn, J. E. 1986, AJ, 92, 1100
Mathieu, R. D., Latham, D. W., Mazeh, T., Duquennoy, A., Mayor, M., & Mermilliod, J.-C. 1992, in Binaries as tracers of stellar formation, ed. A. Duquennoy & M. Mayor (Cambridge: Cambridge University Press), 278
Milone, A. A. E. 1991, PhD thesis, Univ. of Córdoba
Montgomery, K. A., Marschall, L. A., & Janes, K. A. 1993, AJ, 106, 181
Nissen, P. E., Twarog, B. A., & Crawford, D. L. 1987, AJ, 93, 634
Pizzolato, N., Maggio, A., & Sciortino, S. 2000, A&A, 361, 614
Randich, S. 1997, in Cool stars in clusters and associations: magnetic activity and age indicators, ed. G. Micela, R. Pallavicini, & S. Sciortino, Vol. 68, 971
Sanders, W. L. 1977, A&AS, 27, 89
—. 1989, Rev. Mex. Astron. Astrofis., 17, 31
Verbunt, F. & Phinney, E. S. 1995, A&A, 296, 709
Whelan, J. A. J., Worden, S. P., Ruciński, S. M., & Romanishin, W. 1979, MNRAS, 186, 729

Chapter 2

Optical spectroscopy of X-ray sources in the old open cluster M 67

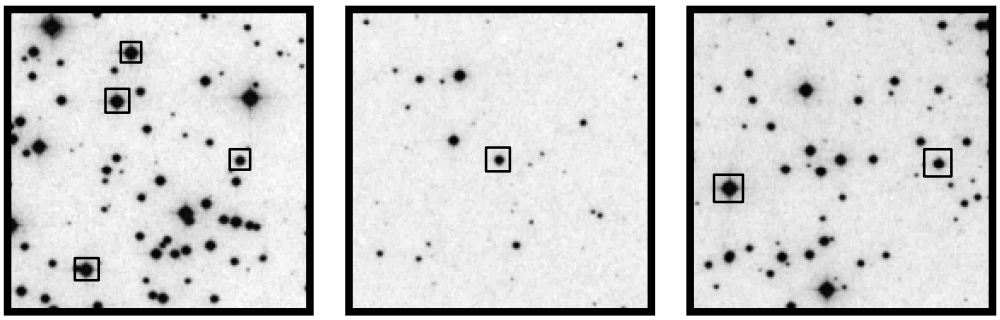

Maureen van den Berg, Frank Verbunt & Robert D. Mathieu
Astronomy & Astrophysics 1999, 347, 866

Abstract – We have obtained optical spectra of seven stars in the old galactic cluster M 67 that are unusual sources of X-rays, and investigate whether the X-ray emission is due to magnetic activity or to mass transfer. The two binaries below the giant branch S 1063 and S 1113, the giant with the white dwarf companion S 1040 and the eccentric binary on the subgiant branch S 1242 show magnetic activity in the form of Ca II H&K emission and Hα emission, suggesting that their X-rays are coronal. The reason for the enhanced activity level in S 1040 is not clear. The two wide, eccentric binaries S 1072 and S 1237 and the blue straggler S 1082 do not show evidence for Ca II H&K emission. A second spectral component is found in the spectrum of S 1082, most clearly in the variable Hα absorption profile. We interpret this as a signature of the proposed hot subluminous companion.

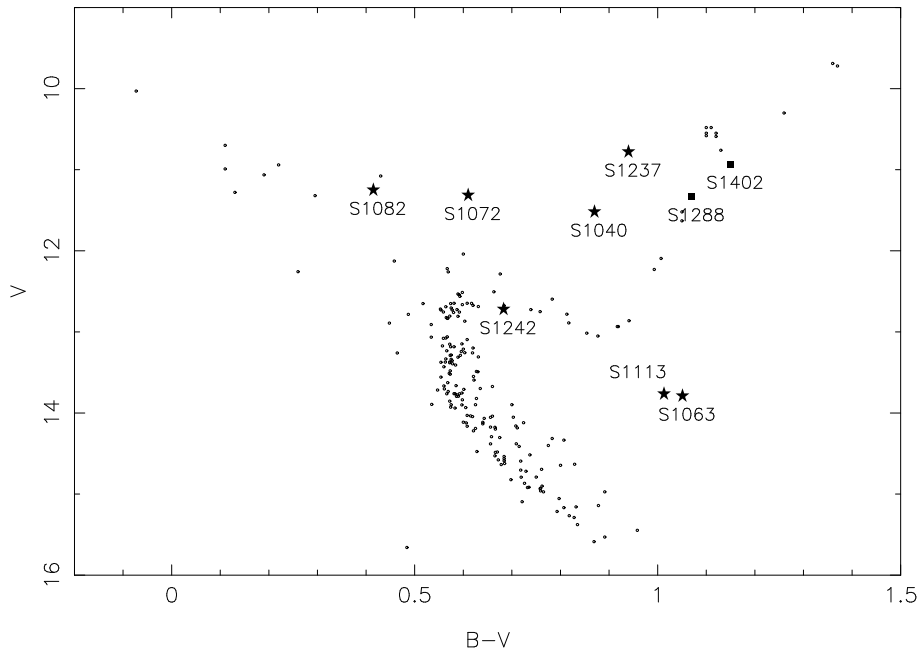

Figure 2.1: Colour-magnitude diagram of M 67. Colours and magnitudes are from Montgomery et al. (1993). Only stars with membership probability >80% (based on their proper motion, Sanders 1977) were selected. Stars indicate the observed X-ray binaries; squares two member giants observed for comparison.

2.1 Introduction

Two observations of M 67 with the ROSAT PSPC resulted in the detection of X-ray emission from 25 members of this old open cluster (Belloni et al. 1993, 1998). The X-ray emission of many of these sources is readily understood. For example, the X-ray emission originates in deep, hot atmospheric layers in a hot white dwarf; is due to mass transfer in a cataclysmic variable; and is caused by magnetic activity in two contact binaries and several RS CVn-type binaries. However, Belloni et al. (1998) point out several X-ray sources in M 67 for which the X-ray emission is unexplained. All but one of these objects are located away from the isochrone formed by the main sequence and the (sub)giant branch of M 67 (Fig. 2.1).

In this paper we investigate the nature of the X-ray emission of these stars through low- and high-resolution optical spectra. In particular, we investigate whether the emission could be coronal as a consequence of magnetic activity, by looking for emission cores in the Ca II H&K lines. Tidal interaction in a close binary orbit is thought to enhance magnetic activity at the stellar surface by spinning up the stars in the binary. Therefore, we also derive projected rotational velocities with the cross correlation method. Finally, we study the Hα profile as a possible indicator of activity or mass transfer.

The observations and the data reduction are described in Sect. 2.2, and the analysis of the spectra in Sect. 2.3. Comparison with chromospherically active binaries is made in Sect. 2.4.

ID	V	$B-V$	sp.type	P_b (d)	e	count rate (s^{-1})
S 1040	11.52	0.87	G4III	42.83	0.027(28)	0.0050(6)
S 1063	13.79	1.05	G8IV	18.39	0.217(14)	0.0047(6)
S 1072	11.32	0.61	G3III–IV	1495.	0.32(7)	0.0013(3)
S 1082	11.25	0.42	F5IV			0.0046(6)
S 1113	13.77	1.01		2.823	0.031(14)	0.0047(6)
S 1237	10.78	0.94	G8III	697.8	0.105(15)	0.0010(3)
S 1242	12.72	0.68		31.78	0.664(18)	0.0007(2)

Table 2.1: Stars of M 67 discussed in this paper. Visual magnitude and colour (from Montgomery et al. 1993), spectral type (from Allen & Strom 1995, and Zhilinskii & Frolov 1994), orbital period and eccentricity (from Mathieu et al. 1990, Latham et al. 1992 and – for S 1113 – Mathieu et al., in preparation [Chapter 6]), and X-ray count rate in PSPC channels 41–240, corresponding to 0.4–2.4 keV (from Belloni et al. 1998).

A discussion of our results is given in Sect. 2.5. In the remainder of the introduction we give brief sketches of the stars studied in this paper; details on many of them are given by Mathieu et al. (1990). The stars are indicated with their number in Sanders (1977), and are listed in Table 2.1.

S 1063 and S 1113 are two binaries located below the subgiant branch in the colour-magnitude diagram of M 67. Their orbital periods, 18.4 and 2.82 days respectively, are too long for them to be contact binaries; also they are too far above the main sequence to be binaries of main-sequence stars. In principle, a (sub)giant can become underluminous when it transfers mass to its companion, as energy is taken from the stellar luminosity to restore hydrostatic equilibrium (e.g. Kippenhahn & Weigert 1967). However, mass transfer through Roche lobe overflow very rapidly leads to circularisation of the binary orbit, whereas S 1063 has an eccentricity $e = 0.217$. The orbit of S 1113 is circular, so mass transfer could be occurring in that system. For the moment, the nature of these binaries is not understood. In both, Pasquini & Belloni (1998) observed emission cores in the Ca II H&K lines. S 1063 is reported to be photometrically variable with ~ 0.10 mag (Rajamohan et al. 1988; Kaluzny & Radczynska 1991), but no period is found. For S 1113, photometric variability with a period of 0.313 days and a total amplitude of 0.6 mag was claimed by Kurochkin (1960), but this has not been confirmed by Kaluzny & Radczynska (1991), who find variability with only 0.05 mag. S 1063 is the only M 67 star in our sample that shows significantly variable X-ray emission (between 0.0081 and 0.0047 cts s^{-1}; Belloni et al. 1998).

S 1072 and S 1237 are binaries with orbital periods of 1495 and 698 days, and with eccentricities $e = 0.32$ and 0.105, respectively. The colour and magnitude of S 1072 cannot be explained with the pairing of a giant and a blue straggler, since this is not compatible with its *ubvy* photometry (Nissen et al. 1987; Mathieu & Latham 1986), nor with superposition of three subgiants, since this is excluded by the radial-velocity correlations (Mathieu et al. 1990).

The absence of the 6708 Å lithium feature in the spectrum of S 1072 indicates that the surface material has undergone mixing (Hobbs & Mathieu 1991; Pritchett & Glaspey 1991). S 1237 could be a binary of a giant and a star at the top of the evolved main sequence (Janes & Smith 1984); high-resolution spectroscopy should be able to detect the main-sequence star in that case (Mathieu et al. 1990). The wide orbits and significant eccentricities appear to exclude both mass transfer and tidal interaction as explanations for the X-ray emission.

S 1242 has the largest eccentricity of the binaries in our sample, at $e = 0.66$ in an orbit of 31.8 days. Its position on the subgiant branch is explained if a subgiant of $1.25\,M_{\odot}$ has a secondary with $V > 15$ (Mathieu et al. 1990). Ca II K line emission is reported by Pasquini & Belloni (1998). Photometric variability with a period of 4.88 days and amplitude of 0.0025 mag has been found by Gilliland et al. (1991). We note that this photometric period corresponds to corotation with the orbit at periastron, which suggests that the X-ray emission may be due to tidal interaction taking place at periastron. The binary would then be an interesting example of a system in transition from an eccentric to a circular orbit. Indeed, according to the diagnostic diagram of Verbunt & Phinney (1995) a giant of $1.25\,M_{\odot}$ with a current radius of $\simeq 2.3\,R_{\odot}$ (as derived from the location of S 1242 in the colour-magnitude diagram) cannot have circularised an orbit of 31.8 days.

S 1040 is a binary consisting of a giant and a white dwarf. The progenitor of the white dwarf circularized the orbit during a phase of mass transfer (Verbunt & Phinney 1995); as a result the mass of the white dwarf is very low (Landsman et al. 1997). The white dwarf is probably too cool, at 16 160 K, to be the X-ray emitter. Indications for magnetic activity are Ca II H&K (Pasquini & Belloni 1998) and Mg II (λλ 2800 Å, Landsman et al. 1997) emission lines. If the X-rays are due to coronal emission of the giant, this must be the consequence of the past evolution of the binary, since the giant is too small for significant tidal interaction to be taking place in the current orbit.

S 1082 is a blue straggler. Photometric variability of 0.08 mag within a few hours was observed by Simoda (1991). Goranskij et al. (1992) found eclipses with a total amplitude of 0.12 mag and a binary period of 1.07 days; however, the radial velocities of the star do not show this period, and vary by about 2 km s^{-1}, far too little for a 1 day eclipsing binary (Mathieu et al. 1986). Landsman et al. (1998) detect a significant excess at 1520 Å with the Ultraviolet Imaging Telescope, and ascribe this to a hot, subluminous secondary. Such a secondary was suggested already by Mathys (1991) on the basis of a broad component in the Na I D and O I absorption lines.

2.2 Observations and data reduction

Optical spectra were obtained on February 28/29, 1996 with the 4.2-m William Herschel Telescope on La Palma, under good weather conditions (seeing $< 1''$ until 4.30h UT, $< 2''$ thereafter). In addition to the X-ray sources in M 67 we observed two ordinary member giants of M 67, S 1288 and S 1402, for comparison. Furthermore one flux standard and three velocity standards were observed. The blue high-resolution spectra of S 1113 were obtained on April

	ISIS		UES blue		UES red	
ID	UT	t_{exp} (s)	UT	t_{exp} (s)	UT	t_{exp} (s)
X-RAY SOURCES						
S 1040	02:43	60	22:03	600	00:46	300
S 1063	02:30	180	20:51	1200	00:11	1200
			21:15	1200	00:33	600
			21:37	1200		
S 1072	02:49	60	22:24	360	01:01	240
S 1082	02:39	60	20:39	300	00:01	360
			23:24	600	01:41	360
					04:11	360
S 1113	03:01	180	22:37*	900	03:36	1200
			22:58*	900	03:58	600
S 1237	02:46	60	22:16	300	00:54	180
S 1242	02:55	120	22:33	1500	01:08	900
COMPARISON GIANTS						
S 1288	02:58	60	23:12	600	01:33	300
S 1402	02:52	60	23:01	450	01:26	240
FLUX STANDARD						
HZ 44	02:21	80	23:42	600	01:57	600
	03:13	80				
	04:43	480				
RADIAL-VELOCITY STANDARDS						
HD 132737			06:04	90	05:13	45
HD 136202			05:55	100	05:42	50
HD 171232					05:34	45

Table 2.2: Log of the observations. For each target we give the UT at start of the exposures and the exposure time for the ISIS and UES blue and red spectra. All observations were obtained on 28/29 February 1996, except the blue UES exposures of S 1113 which were taken on 7/8 April 1998 (indicated with * in the table).

7/8, 1998 with the same telescope through a service observation (seeing 1–2″). A log of the observations is given in Table 2.2.

All spectra have been reduced using the Image Reduction and Analysis Facility (IRAF).

2.2.1 Low-resolution spectra

Low-resolution spectra were taken with the ISIS double-beam spectrograph (Carter et al. 1993). The blue arm of ISIS was used with the 300 lines per mm grating and TEK-CCD, resulting in a wavelength coverage of 3831 to 5404 Å and a dispersion of 1.54 Å per pixel at 4000 Å. The red arm, combined with the 316 lines per mm grating and EEV-CCD, covered a wavelength region of 5619 to 7135 Å with a dispersion of 1.40 Å per pixel at 6500 Å. The format of the frames is 1124×200 pixels^2 which includes the under- and overscan regions. For the object exposures the slit width was set to $4''$. Flatfields were made with a Tungsten lamp while CuAr and CuNe lamp exposures were taken for the purpose of wavelength calibration.

For the ISIS-spectra, basic reduction steps have been done within the IRAF CCDRED-package. These steps include removing the bias signal making use of the under- and overscan regions and zero frames, trimming the frames to remove the under- and overscan, and flatfielding to correct for small pixel-to-pixel gain variations. The remaining reduction has been done with IRAF SPECRED-package tasks. With the optimal extraction algorithm (Horne 1986) the two dimensional images are reduced to one dimensional spectra. Next, the spectra are calibrated in wavelength with the arc frames. A dispersion solution is found by fitting third (blue) and fourth (red) order polynomials to the positions on the CCD of the arclamp lines. The fluxes of the spectra are calibrated with the absolute fluxes of HZ 44, tabulated at 50 Å intervals (Massey et al. 1988), and adopting the standard atmospheric extinction curve for La Palma as given by King (1985). The estimated accuracy of the flux calibration is $\sim 10\%$.

2.2.2 High-resolution spectra

High-resolution echelle spectra were taken with the Utrecht Echelle Spectrograph (UES, Unger et al. 1993). Observations were done with a $\sim 1''$ slit width.

For the 1996 observations, the UES was used in combination with a 1024×1024 pixels^2 TEK-CCD, and the 31.6 lines per mm grating (E31), which resulted in a broad wavelength coverage, but small separation of the echelle orders on the CCD. In this setup, the UES resolving power is 49 000 per resolution element (two pixels), corresponding to a dispersion of 3 km s^{-1} per pixel or 0.06 Å per pixel at 6000 Å. The frames were centred on $\lambda_{\rm cen} = 4250$ Å and $\lambda_{\rm cen} = 5930$ Å in order to get a blue (3820 to 4920 Å) and red (4890 to 7940 Å) echelle spectrum. The number of orders recorded on the CCD is 34 in the blue and 45 in the red, each covering ~ 45 to 80 Å increasing for longer wavelengths. Towards the red, gaps occur between the wavelength coverage of adjacent orders. Exposures of a quartz lamp were taken to make the flatfield corrections. ThAr exposures served as wavelength calibration frames.

For the 1998 observations of S 1113, a 2048×2048 pixels^2 SITe-CCD was used. Two spectra were taken with the 79.0 lines per mm (E79) grating ($\lambda_{\rm cen} = 4343$ Å). The difference between the E79 and the E31 gratings is that E79-spectra have a larger separation of the echelle-orders on the detector, which can improve the determination of the sky-background. The spectral resolution of the gratings is the same (the central dispersion in these observations is ~ 0.04 Å per pixel). The specified wavelength-coverage for this combination of grating and

detector is 3546 to 6163 Å but only the central orders were bright enough to extract spectra (3724 to 5998 Å). Flatfield and ThAr exposures were made for calibration purposes.

The reduction of the UES spectra has been performed using the routines available within the IRAF ECHELLE-package. First, the frames are debiased and the under- and overscan regions removed. After locating the orders on the CCD for both the quartz lamp and the object exposures, we flatfielded the frames. Spectra are extracted with optimal extraction. The small order separation makes sky subtraction difficult; however, our targets are bright, and the resulting error is negligible. In the step of wavelength calibration, the dispersion solution is derived by fitting third and fourth order polynomials leaving rms-residuals of 0.004 Å (red) and 0.002 Å (blue, 0.003 Å for the 1998-spectra). To find absolute fluxes for the Ca II K (λ3933.67 Å) & H (λ3968.47 Å) emission lines (Sect. 2.3), the fluxes of the relevant blue orders of an object have been calibrated with the calibrated ISIS spectrum of the same object. Continuum normalisation of the orders in the red spectra, required for the rotational velocity analysis, is done by fitting third to fifth order polynomials to the wavelength-calibrated spectra.

2.3 Data analysis

We study two indicators of magnetic activity. The direct indicator is emission in the cores of the Ca II H&K lines. Another indicator is the rotational speed: rapid (differential) rotation and convective motions are thought to generate magnetic fields through a dynamo.

2.3.1 Determination of Ca II H&K emission fluxes

To estimate the amount of flux emitted in the Ca II H&K line cores, $F_{\rm Ca}$, we add the fluxes above the H&K absorption profiles as follows. An upper and a lower limit of the level of the absorption pseudo-continuum is estimated by eye and is marked by a straight line. For S 1113 this is illustrated in Fig. 2.7. We obtain a lower and upper limit of the emitted flux by adding the fluxes in each wavelength-bin above these levels. The value given in Table 2.3 is the average of these two results, the uncertainty is half their difference. Use of higher order fits (following Fernández-Figueroa et al. 1994) to the absorption profile gives similar results. If an emission line is not clearly visible, we obtain an upper limit by estimating the minimal detectable emission flux at the H&K line centres within a 1 Å wide region (typical width of the emission lines).

Six of our sources show Ca II H&K line emission (Fig. 2.2). The profiles of S 1113 appear to be double-lined, suggesting that we see activity of both stars (Fig. 2.7). The fluxes given in Table 2.3 are the total fluxes, i.e. no attempt was made to deblend the emission lines. No emission is visible in the spectrum of S 1082.

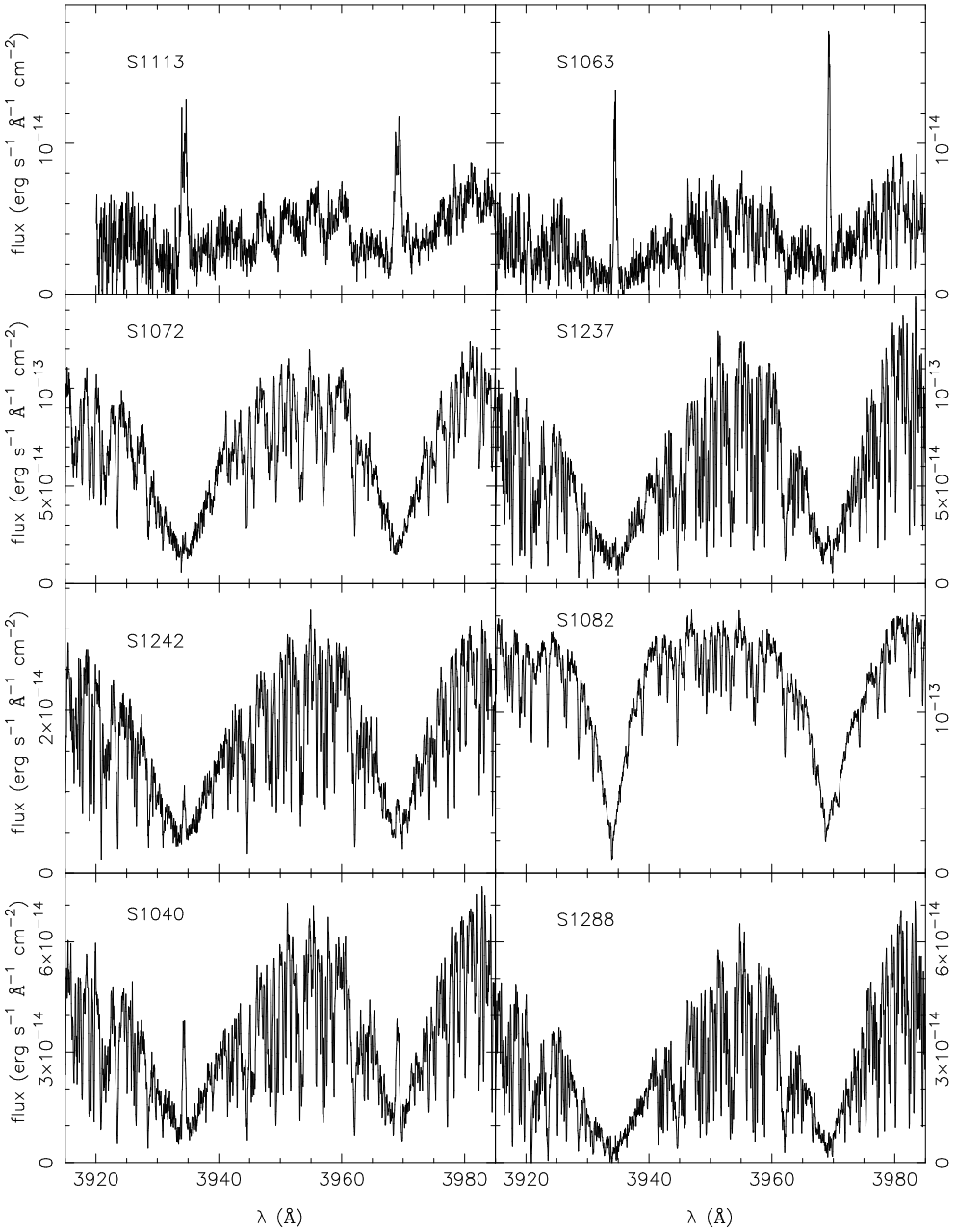

Figure 2.2: The Ca II H&K regions in the high-resolution spectra of our targets. In the lower right corner the spectrum of the non-active comparison giant S 1288 is shown.

ID	$F_{\mathrm{Ca\ K}}$ (erg cm^{-2} s^{-1})	$F_{\mathrm{Ca\ H}}$ (erg cm^{-2} s^{-1})	$v \sin i$ (km s^{-1})
S 1040	$16(4) \times 10^{-15}$	$17(5) \times 10^{-15}$	3.0(1.0)
S 1063	$6(1) \times 10^{-15}$	$7(1) \times 10^{-15}$	3.9(0.8)
S 1072	$3(2) \times 10^{-15}$	$< 13 \times 10^{-15}$	8.1(1.1)
S 1082	$< 11 \times 10^{-15}$	$< 24 \times 10^{-15}$	5.1(0.7)
S 1113	$9(2) \times 10^{-15}$	$10(3) \times 10^{-15}$	45(6)
			12(1)
S 1237	$4(2) \times 10^{-15}$	$8(5) \times 10^{-15}$	< 1.8
S 1242	$2.2(0.5) \times 10^{-15}$	$2(1) \times 10^{-15}$	$< 2.6(1.0)$

Table 2.3: Fluxes of emission cores in Ca II H&K lines and projected rotational velocities derived from our high-resolution spectra. The velocities were determined from cross correlation with the spectrum of HD 136202 (F8III-IV, ESA 1997) for S 1040, S 1072, S 1082 and S 1242; and with the spectrum of HD 171232 (G8III, ESA 1997) for the other stars. Both HD stars have line widths $\tau = 1.8 \pm 0.1$ km s^{-1}. For S 1113 we list both components; the primary contributes $\sim 82\%$ of the light and has broader lines.

2.3.2 Determination of projected rotational velocities

Cross correlation

In order to derive the projected rotational velocity $v \sin i$ of our targets, we apply the cross correlation technique (e.g. Tonry & Davis 1979). This method computes the correlation between the object spectrum and an appropriately chosen template spectrum as function of relative shift. The position of the maximum of the cross correlation function (CCF) provides the value of the radial-velocity difference between object and template. The width of the peak is indicative for the width of the spectral lines and can therefore be used as a measure of the rotational velocity of the stars.

For rotational velocities not too large the line profiles may be approximated with Gaussians, allowing analytical treatment of the cross correlation method. Assuming that the binary spectrum is a shifted, scaled and broadened version of the template spectrum, the broadening can be related to the width of the CCF peak as follows (Gunn et al. 1996). With τ the dispersion in the template's and β the dispersion in the target's spectral lines, μ the dispersion of the CCF peak and σ the dispersion of the Gaussian that describes the broadening of the object's spectrum with respect to the template, one can write:

$$\mu^2 = \tau^2 + \beta^2 = 2\tau^2 + \sigma^2 \tag{2.1}$$

Eq. 2.1 applies to both components in the binary spectrum and their corresponding CCF peaks.

The cross correlations are performed with the IRAF task FXCOR that uses Fourier transforms of the spectra to compute the CCF. Before performing the cross correlation, the continuum is subtracted from the normalised spectra. Filtering in the Fourier domain is applied to

avoid undesirable contributions originating from noise or intrinsically broad lines (see Wyatt 1985).

The templates are chosen from the radial-velocity standards such that their spectral types resemble those of the targets. The value of τ for these stars is determined for each order separately by auto correlation of the template spectrum adopting the same filter used for the cross correlations. In this case σ is zero and therefore τ is found directly from the width of the CCF peak: $\tau^2 = \mu^2/2$.

The template spectra are correlated with our target stars order by order, where we limit ourselves to orders in the red spectra that do not suffer from strong telluric lines. Most CCF peaks can be fitted well with a Gaussian. As the final value for $v \sin i$ we give the broadening σ averaged over the different orders, and for the uncertainty we take the rms of the spread around the average of σ (Table 2.3). Equating $v \sin i$ to σ implicitly assumes that τ is the width of the lines not related to rotation. An upper limit to $v \sin i$ is found from the other extreme in which we assume that the total width of the spectral line β follows from rotation. This creates uncertainties of the order of σ for S 1242. In the case of S 1237 we find that $\beta < \tau$ ($\sigma < 0$), i.e. the lines in S 1237 are narrower than in the template. For these two stars, we give an upper limit of $v \sin i < \beta$ in Table 2.3.

S1113 is the only binary observed whose CCF shows two peaks. The CCF peaks of both stars overlap in the 1998 observation. Therefore we do not use these spectra in the following analysis. For the 1996 spectra, the CCF shows two peaks, one of which is broad indicating the presence of a fast rotating star. Both peaks are clearly separated with a centre-to-centre velocity separation of ~ 110 km s^{-1}. The lines in the spectrum are smeared out and less pronounced, resulting in a noisy CCF. To improve this, we combine four sequential orders before cross correlating (being constrained by the maximum number of points FXCOR can handle). From Eq. 17 in Gunn et al. we derive the relative light contribution of both components to the spectrum from the height and dispersion of the cross correlation peaks, assuming that the binary stars have the same spectrum as the template ($\alpha = 1$ in Eq. 17). According to this the rapidly rotating star contributes $\sim 82\%$ of the light. Note that luminosity ratios derived from cross correlations are uncertain and should be confirmed photometrically.

Fourier-Bessel transformation

The line profile of the fast rotating star in S 1113 is not compatible anymore with a Gaussian, therefore we adopt another method to determine its $v \sin i$, described in Piters et al. (1996). This method uses the property that the Fourier-Bessel transform of a spectral line that is purely rotationally broadened has a maximum at the position of the projected rotational velocity. In practice, this position is a function of the limits over which the Fourier transform is performed. The local maxima of this velocity-versus-cutoff-frequency (vcf) function approach $v \sin i$ within half a percent, the result growing more accurate for maxima at higher frequencies. This error is negligible when compared to errors arising from noise, other line broadening mechanisms, etc. (see Piters et al. 1996). In our determination of $v \sin i$ of the primary of S 1113, we have used the first local maximum in the vcf-plot of the transformation

of four isolated Fe I lines at λλ 6265.14, 6400.15, 6408.03 and 6411.54 Å. The $v \sin i$ in Table 2.3 is an average of the resulting values; the $v \sin i$ of the secondary is found from cross correlation.

The application of the Fourier-Bessel transformation method is limited on the low velocity side by the spectral resolution: the Fourier transform cannot be performed beyond the Nyquist frequency which for slow rotators lies at a frequency that is lower than the cutoff-frequency at which the first maximum occurs in the vcf-plot. For our spectra this means that the method cannot be used for $v \sin i < 5.2$ km s^{-1}. Indeed, for every star for which the cross correlation method gives a $v \sin i$ smaller than this value, the vcf-plot does not reach the first local maximum, except for S 1082 for which we find $v \sin i$ = 9.5(1.6). For S 1072, the Fourier-Bessel transform gives a $v \sin i$ of 12.7(1.0) km s^{-1}. Spectral lines were selected from those used in Groot et al. (1996) and from the additional lines used for S 1113.

2.4 Results

The results of our search for emission cores in the Ca II H&K lines are displayed in Fig. 2.2 and in Table 2.3. The emission lines are strong in S 1063, S 1113 and S 1040; and still detectable in S 1242 which indicates chromospheric activity in these stars. In S 1072 and S 1237 the emission cores are marginal, and on S 1082 we can only determine an upper limit.

The (projected) rotational velocities of all of our stars are relatively small $v \sin i < 10$ km s^{-1}, with the exception of S 1113.

In Sect. 2.4.1 we investigate whether the relations between X-ray emission, strength of the emission cores in the Ca II H&K lines, and the rotational velocities of the unusual X-ray emitters in M 67 are similar to the relations found for well-known magnetically active stars, the RS CVn binaries. In Sect. 2.4.2 we briefly discuss the behaviour of the Hα line and spectral lines other than Ca II H&K that are indicators of chromospheric activity. Individual systems are discussed in Sect. 2.4.3.

2.4.1 Comparison with RS CVn binaries

To investigate whether the X-rays of the M 67 stars studied in this paper are related to magnetic activity, we compare their optical activity indicators and X-ray fluxes with those of a sample of RS CVn binaries. In particular, we select RS CVn binaries for which fluxes of the emission cores in the Ca II H&K lines have been determined from high-resolution spectra by Fernández-Figueroa et al. (1994). To obtain X-ray count rates for these binaries, we searched the ROSAT data archive for PSPC observations of them. We then analysed all these observations, and determined the count rates, in the same bandpass as used in the analysis of M 67, using the standard procedure described in Zimmermann et al. (1994). All pointings that we have analysed actually led to a positive detection of the RS CVn system: even when not the target of the observation, the RS CVn system is usually the brightest object in the field of view. The results of our analysis are listed in Table 2.4.

name	d (pc)	JD	$t_{\rm exp}$ (s)	ctrate (s^{-1})	Δ ($'$)
LUMINOSITY CLASS V (GROUP 1)					
IL Com	107±12	8420.575	16156	0.322(5)	36
		8775.123	8345	0.126(5)	36
TZ CrB	21.7±0.5	8864.531	4267	6.072(15)	0
		9003.872	5776	6.228(11)	0
		8864.595	3651	6.84(2)	24
		9004.871	3151	5.41(2)	24
V772 Her	37.7±1.9	9049.117	14531	1.206(4)	0
BY Dra	16.4±0.2	9247.809	9895	1.009(7)	0
V775 Her[a]	21.4±0.5	9085.714	2140	1.10(2)	0
ER Vul	49.9±2.1	9148.099	1209	1.23(3)	0
KZ And	25.3±4.9	8604.712	5249	0.888(16)	36
LUMINOSITY CLASS IV (GROUP 2)					
V711 Tau	29.0±7	8648.446	3098	6.29(2)	0
UX Com	168±51	8426.486	21428	0.146(3)	33
RS CVn	108±12	8810.279	2526	0.336(17)	44
		8991.040	6214	0.372(11)	44
		8796.874	5076	0.305(12)	51
		8966.506	2904	0.366(18)	51
HR 5110	44.5±1.2	8431.422	71803	2.3152(14)	44
		9158.435	37658	2.403(3)	44
SS Boo[b]	202±57	9030.359	10327	0.059(2)	0
RT Lac[b]	193±39	8789.392	8668	0.198(5)	0
AR Lac[c]	42.0±1.0	8620.767	13460	1.717(4)	0
		9136.873	4892	2.902(13)	0
LUMINOSITY CLASS III/II (GROUP 3)					
12 Cam	192±34	8322.477	3516	0.574(13)	3
σ Gem[d]	37.5±1.1	8346.927	4745	5.269(14)	0
		8904.569	1438	3.43(4)	0
		8735.159	7940	4.753(8)	0
DK Dra	138±10	9272.484	4156	1.32(2)	41
ε UMi	106±7.6	8328.919	14690	0.624(6)	40
DR Dra[e]	103.±8.5	8863.981	10576	1.554(8)	31
HR 7428[e]	323±53	9088.631	24889	0.112(2)	0
IM Peg	96.8±7.1	8589.200	6335	1.692(15)	44
		8769.630	8150	1.422(12)	44
		8973.263	22143	1.909(4)	44
λ And[f,g]	25.8±0.5	8448.155	31165	4.077(2)	0

Table 2.4: ROSAT PSPC count rates for RS CVn binaries, from our analysis of archival data. For each source we list the distance, adopted from the Hipparcos catalogue (ESA 1997), the Julian date (-2440000) of the beginning of the ROSAT exposure, the effective exposure time, the count rate in channels 41–240 (i.e. roughly in the 0.4–2.4 keV band), and the offset of the star to the ROSAT pointing direction. Where applicable we also refer to earlier publication of the ROSAT observation: [a]Singh et al. (1996a), [b]Welty & Ramsey (1995), [c]White et al. (1994), [d]Yi et al. (1997), [e]Singh et al. (1996b), [f]Bauer & Bregman (1996), [g]Ortolani et al. (1997).

To compare systems at different distances, we multiply the ROSAT count rate and the flux of the emission cores for each system with the square of the distance listed in Table 2.4; for M 67 we adopt a distance of 850 pc (Twarog & Anthony-Twarog 1989). No corrections are made for interstellar absorption. The choice of the 0.4–2.4 keV bandpass minimises the effects of interstellar absorption, which are severe at energies < 0.4 keV. As it is unknown which component of the binary emits the X-rays, we plot the total X-ray and Ca II fluxes, adding the contributions of both components where these are given separately by Fernández-Figueroa et al. (1994).

The resulting 'absolute' count rates and fluxes are shown in Fig. 2.3. The M 67 systems with Ca II H&K emission clearly visible in Fig. 2.2, viz. S 1063, S 1113, S 1040 and S 1242 lie on the relation between X-ray and Ca II H&K emission defined by the RS CVn systems, in agreement with the hypothesis that the X-ray flux of these objects is related to the magnetic activity. It is also seen that the upper limits or marginally detected emission cores in S 1082, S 1072 and S 1237 are high enough that we cannot exclude the hypothesis that the X-ray emission in these systems is related to magnetic activity.

The rotational velocity is another indicator of magnetic activity. We investigate the relation between rotational velocity and Ca emission by selecting those stars from the sample of Fernández-Figueroa for which a value of $v \sin i$ is given in the Catalogue of Chromospherically Active Binary Stars (Strassmeier et al. 1993). In Fig. 2.4 the Ca II H&K emission of these stars is compared with their $v \sin i$. In this figure we do discriminate between the separate contributions of both stars to $F_{\rm Ca}$, with the exception of S 1113 for which we combine the total flux $F_{\rm Ca}$ with the $v \sin i$ of the primary. The M 67 stars are found within the range occupied by chromospherically active stars. We note that the correlation between the observed H&K flux and $v \sin i$ is not tight. In particular, high and low Ca II H&K emission flux is found at low values of $v \sin i$. Some of the scatter may be due to the use of $v \sin i$ instead of the stellar rotation period.

Parameters depending on the spectral type (e.g. properties of the convective region) have been used to reduce the scatter in the activity-rotation relation; whereas this is successful for main-sequence stars with $0.5 \lesssim B-V \lesssim 0.8$, it fails for other main-sequence stars and for giants (see discussion in Stępień 1994). For example, the three giants 33 Psc (K0 III), 12 Cam (K0 III) and DR Dra (K0-2 III) have $v \sin i$ values of 10, 10 and 8 km s^{-1}, respectively, but differ in $\log d^2 F_{\rm Ca}$ by three orders of magnitude (see Fig. 2.4).

2.4.2 Activity indicators

The Hα lines (λ 6562.76 Å) of only two stars, S 1063 and S 1113, show clear evidence of emission, as shown in Fig. 2.6. This is described in more detail in their individual subsection in Sect. 2.4.3. For the other M 67 stars, we have used the few (sub)giants in the library of UES-spectra of Montes & Martín (1998) to investigate the behaviour of Hα. We have chosen library spectra of stars that match the spectra of the M 67 stars as closely as possible (see Fig. 2.5). S 1072 and S 1237 show no evidence for filling in of the Hα profile compared to a

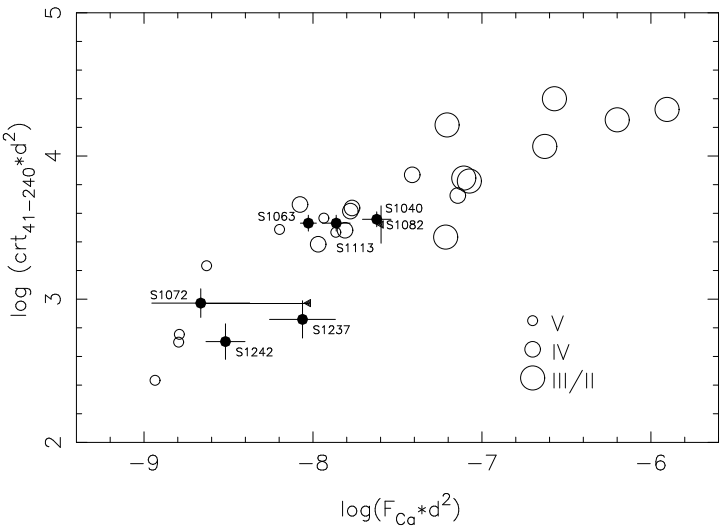

Figure 2.3: PSPC count rates in channels 41–240 versus observed Ca II H&K emission flux $F_{\rm Ca}$ (in erg $s^{-1}cm^{-2}$). Both are multiplied with the square of the distance (in pc). Open circles are chromospherically active binaries from the sample of Fernández-Figueroa (1994). Their size indicates the luminosity class of the active component. When more than one PSPC observation is available, the count rate of the longest exposure is plotted. Filled symbols are the M 67-sources. Triangles indicate upper limits.

G0IV–V and a K0III star, respectively. In S 1040 Hα seems slightly filled in compared to a G8IV and a K0III star. This is also the case for S 1242 compared to a G0IV-V star, but we note that no classification for this star is found in literature. For S 1082, no matching spectrum is available in this wavelength region.

Filling in of the lines in the Mg I b triplet ($\lambda\lambda$ 5167.33, 5172.70 and 5183.62 Å) and in the Na I D doublet ($\lambda\lambda$ 5889.95 and 5895.92 Å) is visible in some active stars. The presence of a He I D_3 (λ 5876.56) absorption or emission feature can also indicate activity (see discussion in Montes & Martín (1998) and references therein). However, in none of the M 67 stars we see filled in Mg I b and Na I D lines. Neither do we see a clear He I D_3 feature. For S 1082 (Mg I b and Na I D) and S 1113 (Mg I b, Na I D and He I D_3) we find no suitable library stars for these features.

2.4.3 Individual systems

S 1063 and S 1113

The two stars below the subgiant branch, S 1063 and S 1113, both show relatively strong Ca II H&K emission, and are the only two stars in our sample showing Hα in emission, shown in Fig. 2.6. We use the orbital solutions for both objects to try and identify the star responsible for these emission lines. The velocities of both components in S 1113, and of one component in S 1063 are indicated in Fig. 2.6.

The Hα line profile of S 1063 is asymmetric, showing emission which is blue-shifted with respect to the absorption. The location of the absorption line is compatible with the velocity of the primary, which dominates the flux; the emission is probably due to the secondary. Remarkably, the Ca II H&K emission peak is at the velocity of the primary. This suggests that the Hα emission is not chromospheric in nature. The Hα emission of S 1063 does not show the double peak that is known to indicate accretion disc emission (Horne & Marsh, 1986).

In S 1113 the Hα emission profile is symmetric and broad, with full width at continuum level of 15 Å. The emission peak is centred on the more massive star, which contributes 82% of the total flux (Table 2.3). This suggests that the Hα emission is due to the primary. The Ca II H&K emission shows marginal evidence for a double peak, suggesting that both stars contribute to the chromospheric emission. In Fig. 2.7 we indicate the expected position of the H&K lines for both stars. For the phase observed, their peaks overlap in the cross correlation function. In the figure we use the velocities resulting from fitting the order that gives the 'cleanest' cross correlation.

S 1072 and S 1237

The Ca II H&K emission in the wide binaries S 1072 and S 1237 is only marginally significant. The level of their X-ray and Ca II emission is more appropriate for active main-sequence stars (Fig.2.3). One might speculate that it is due to the invisible companion of the giant detected in the cross correlation; even if this were the case, we would not understand why this

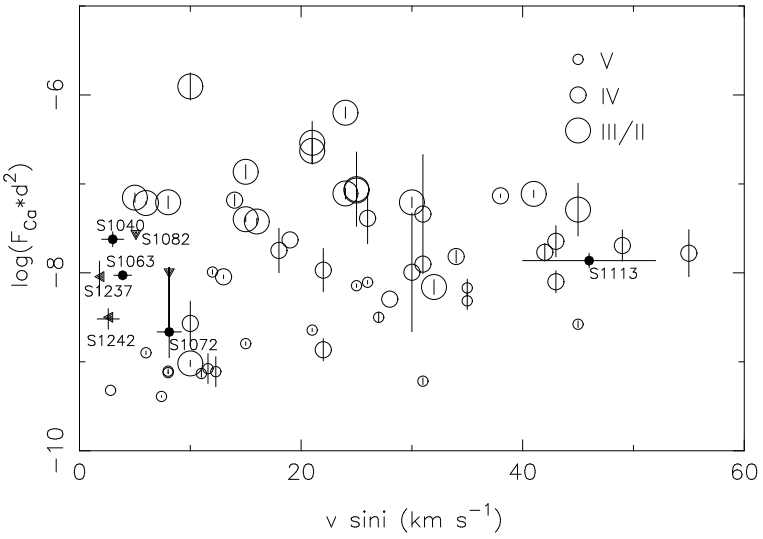

Figure 2.4: Observed Ca II H&K emission flux $F_{\rm Ca}$ versus $v \sin i$. Open circles show the comparison sample of chromospherically active binaries up to 60 km s^{-1} (Strassmeier et al. 1993 and Fernández-Figueroa 1994). Their size indicates the luminosity class of the active star. Vertical bars indicate 1-σ errors due to uncertainty in the distance, for systems with a Hipparcos parallax. M 67 sources are plotted as filled symbols.

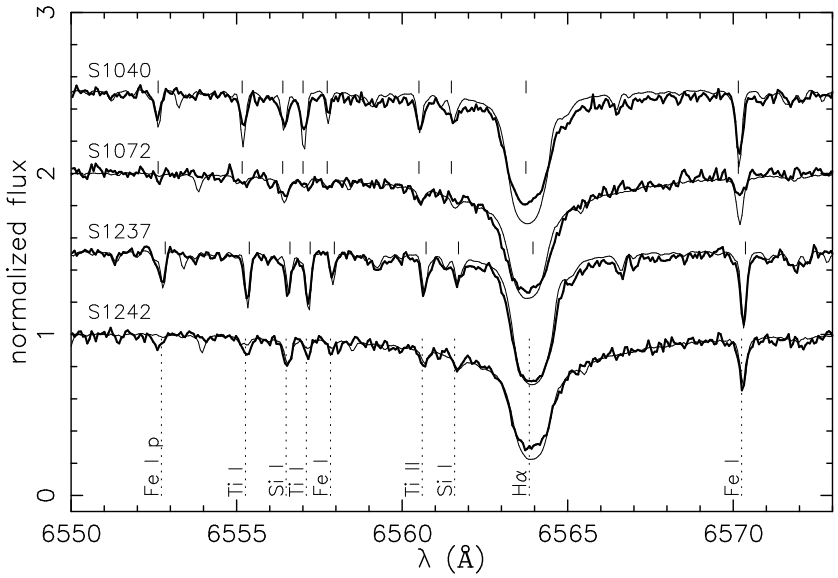

Figure 2.5: Hα profiles of S 1040, S 1072, S 1237 and S 1242. Library UES-spectra (Montes & Martín 1998) are plotted with a thinner line. The comparison star is a K0III giant (HD 48432) for S 1040 and S 1237, and a G0IV–V subgiant (HD 160269) for the other stars. Position of Hα and other lines are indicated with vertical lines.

companion would be chromospherically active. We conclude that we do not understand why these two stars are X-ray sources. We find no indication for a faint secondary in the cross correlation profile of S 1237; at the time of observation, the spectra of two equally massive stars as suggested by Janes & Smith (1984) would be separated by 4 to 7 km s^{-1} (derived from the ephemeris in Mathieu et al. 1990). Since the secondary is 1.6 magnitude fainter in V than the primary, we think that this small separation is compatible with finding a single peak in the cross correlation.

S 1242

S 1242 is chromospherically active, as shown by its Ca II H&K emission. We suggest that this activity, which also explains the X-rays, is due to rapid rotation induced by tidal interaction at periastron, which tries to bring the subgiant into corotation with the orbit at periastron. If we assume that the observed period of photometric variability is the rotation period we derive an inclination of $\sim 9^\circ$ using our maximum value of $v \sin i$ and the estimated radius. This would be in agreement with a companion at the high end of the range 0.14–0.94 $M_\odot$ allowed by the mass function (Mathieu et al. 1990).

S 1040

Our detection of clear chromospheric emission indicates that the X-ray emission of S 1040 is due to the giant. The white dwarf has a low temperature, and is unlikely to contribute to

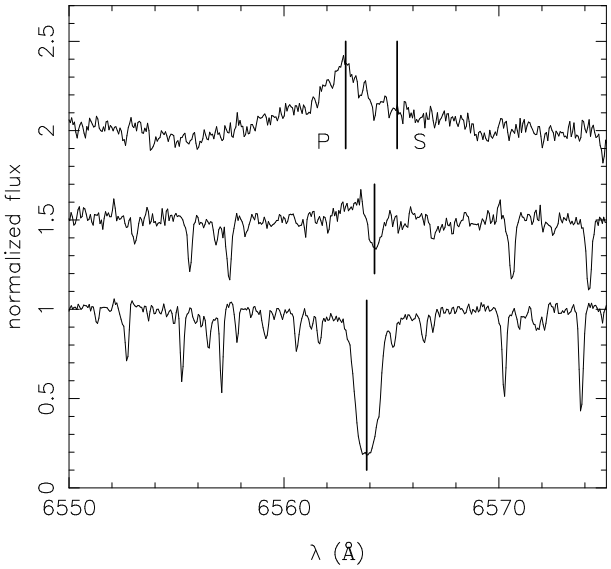

Figure 2.6: Hα in S 1113 (top), S 1063 (middle) and comparison giant S 1288. The intensity is normalised to the continuum level; the upper two spectra are displaced vertically by 0.5 and 1 unit. The line marks the radial-velocity shift of the stars as determined by the cross correlation; for S 1113 the primary (P) and secondary (S) star are separately indicated.

the X-ray flux. We find a rather slow rotational velocity for the giant, 3 km s^{-1}. Gilliland et al. (1991) detected a periodicity of 7.97 days in the visual flux (B and V bandpasses) of S 1040, with an amplitude of 0.012 mag. If this is the rotation period of the giant, the radius of 5.1 $R_\odot$ (Landsman et al. 1997) implies an equatorial rotation velocity of $v = 32$ km s^{-1}. This is compatible with the velocity measured with our cross correlation, $v \sin i$, for an inclination $i \lesssim 5.3°$. This inclination has an a priori probability less than 0.5%; and it implies an unacceptably high mass for the white dwarf, from the measured mass function $f(m) = 0.00268$. We conclude that the 8 days period cannot be the rotation period of the giant. It is doubtful that the white dwarf can be responsible, as its contribution to the B and V flux is small.

S 1082

The Hα absorption profile of the blue straggler S 1082 is variable. If we consider the most symmetric spectrum profile, that of 00:01 UT, as the unperturbed profile of the primary, we find that the changes are due to extra emission. This is illustrated in Fig. 2.8. We suggest that this variation is due to the subluminous companion, possibly to a wind of that star. We have also investigated the presence of a broad shallow depression underlying the Na I D lines (near λ 5895 Å) and the O I triplet (near λ 7775 Å) as found by Mathys (1991). We find that this broad component is variable, as illustrated in Fig. 2.9. Mathys (1991) suggests that the broad component originates in the subluminous companion. This companion outshines the primary by a factor six at λ 1520 Å and thus is presumably hot (Landsman et al. 1998). We note that

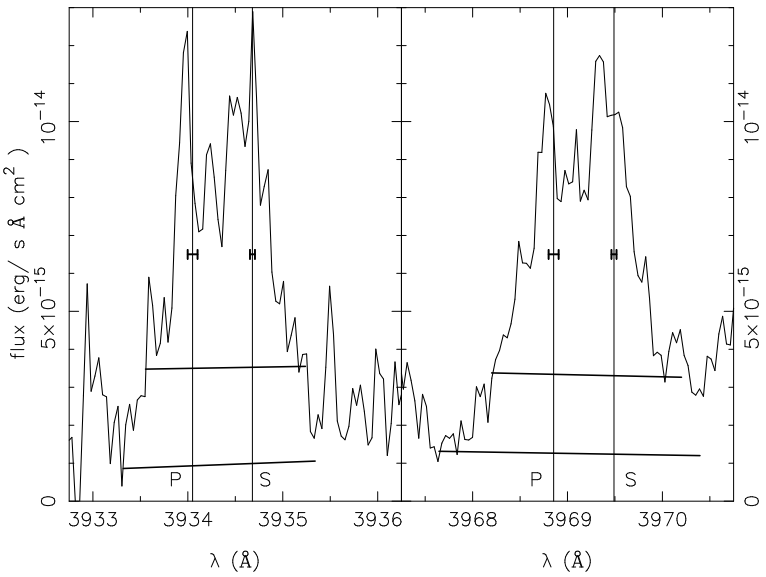

Figure 2.7: Ca II H&K emission cores in S 1113. The vertical lines mark the shifted position of the lines for the primary (P) and secondary (S) as derived from the cross correlation with the radial-velocity standard HD 132737 (K0III, ESA 1997). Errors are also indicated. The long horizontal lines indicate the upper and lower limit chosen to determine the emitted Ca II H&K flux (see Sect. 2.3.1).

the star cannot be too hot or it would not show neutral lines.

2.5 Discussion and conclusions

In this paper we have tried to find an explanation for the X-ray emission of seven sources in M 67.

For S 1242 and S 1040 we have concluded from the Ca II H&K emission cores that magnetic activity is responsible for the X-rays. This is supported by filling in of Hα (see e.g. Montes et al. 1997; Eker et al. 1995). In S 1242, activity is likely to be triggered by interaction at periastron in the eccentric orbit. This is also reflected in the period of photometric variability. For S 1040, the reason for activity is less clear. The explanation could involve mass transfer from the precursor of the white dwarf to the giant and the latter's subsequent expansion during the giant phase. As was already noted by Landsman et al. (1997), a similar system is AY Cet, a binary of a white dwarf of $T_{\rm eff} = 18\,000$ K (Simon et al. 1985) and a G5III giant in an 56.8 days circular orbit. The $v \sin i$ of that giant is also low, 4 km s^{-1}, and the long photometric period of 77.2 days implies asynchronous rotation (Strassmeier et al. 1993). The X-ray luminosity for AY Cet is 1.5×10^{31} erg s^{-1} in the 0.2–4 keV band as measured with Einstein by Walter & Bowyer (1981), somewhat higher than the luminosity of S 1040. (With the coronal model discussed by Belloni et al. (1998), the count rate for S 1040 corresponds to 5.6×10^{30} erg s^{-1} in the 0.2–4 keV band.) Walter & Bowyer attribute the X-rays to coronal

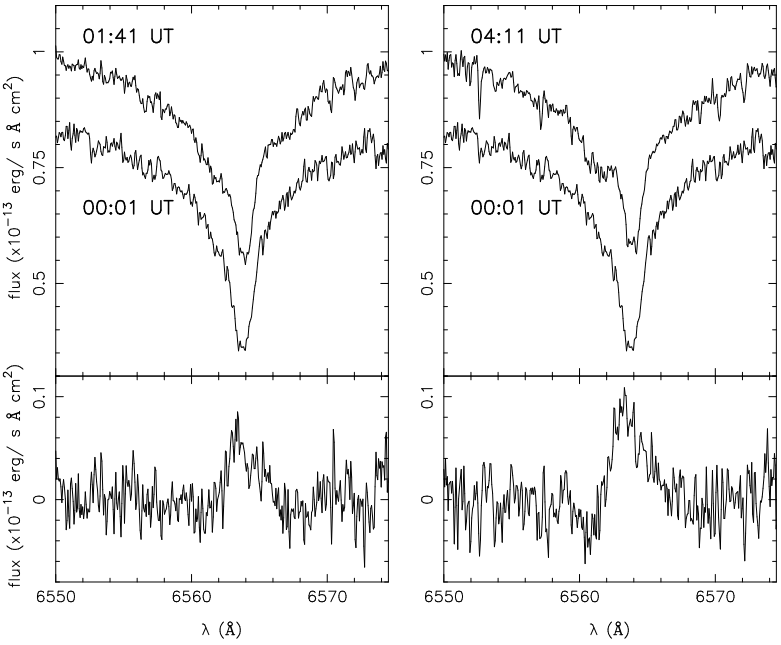

Figure 2.8: Hα profile for the three exposures of S 1082. The spectra are labelled according to the UT at start of the exposure. For clarity, the lower spectrum is offset with -0.2×10^{-13} erg s^{-1} Å^{-1} cm^{-2} in both figures. The lower panels show the difference between the first and second (left) and the first and the third exposure.

activity of the giant.

The Ca II H&K emission cores in S 1063 and S 1113 are very strong. In S 1113 we might even see emission of both stars. Due to the shape of the Hα emission we cannot conclude with certainty that the X-rays arise in an active corona and not in a disc or stream. The wings in the emission peak of S 1113 are very broad. However, Montes et al. (1997) have demonstrated that the excess emission in the Hα lines of the more active binaries is sometimes a composite of a narrow and broad component, the latter having a full width at half maximum of up to 470 km s^{-1}. They ascribe this broad component to microflaring accompanied by large scale motions. We note the similarity between S 1113 and V711 Tau, a well known extremely active binary of a G5IV ($v \sin i = 13$ km s^{-1}) and K1IV ($v \sin i = 38$ km s^{-1}) star in a 2.84 days circular orbit and a mass ratio 0.79 (Strassmeier et al. 1993); the mass ratio of S 1113 is 0.70 (Mathieu et al., in preparation [Chapter 6]). From the count rate of V711 Tau in Table 2.4 we find $L_{\rm x} = 6.8 \times 10^{30}$ erg s^{-1} in the 0.1–2.4 keV band using the same model as in Belloni et al. (1998) with $N_H = 0$, which is comparable to the luminosity of S 1113 in the same band $L_{\rm x} = 7.3 \times 10^{30}$ erg s^{-1} (Belloni et al. 1998). The Hα emission of S 1063 is more difficult to explain. As this system is not double-lined, Hα emission by the (invisible) secondary star would have to be strong to rise above the continuum of the primary.

In the binaries S 1072 and S 1237 we see no Hα emission while the level of Ca II H&K emission is low in comparison with active stars of the same luminosity class. We have no

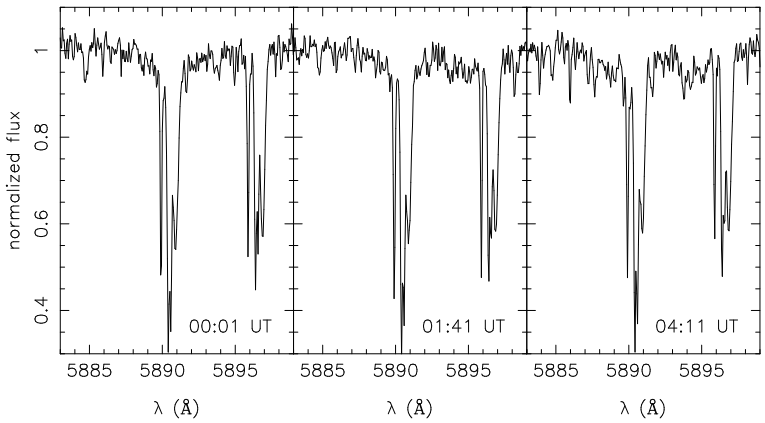

Figure 2.9: Na I D lines in S 1082. Shown from left to right are the three spectra labelled according to the UT at start of the exposure. Variability is most clearly seen left of the Na λ 5895.92 line.

explanation for this. For S 1072, an option is a wrong identification of the X-ray source with an optical counterpart. Belloni et al. (1998) give a probability of 43% that one or two of their twelve identifications of an X-ray source with a binary in M 67 is due to chance.

No Ca II H&K emission is seen in the spectrum of the blue straggler S 1082. Possibly, the X-ray emission has to do with the hot, subluminous secondary that could also cause the photometric variability and whose signature we might have seen in the Hα line.

Acknowledgements – The authors wish to thank G. Geertsema for her help during our observations, P. Groot for providing his program to compute projected rotational velocities with the Fourier-Bessel transformation method and M. van Kerkwijk for comments on the manuscript. The William Herschel Telescope is operated on the island of La Palma by the Isaac Newton Group in the Spanish Observatorio del Roque de los Muchachos of the Instituto de Astrofisica de Canarias. IRAF is distributed by the National Optical Astronomy Observatories, which are operated by the Association of Universities for Research in Astronomy, Inc., under cooperative agreement with the National Science Foundation. MvdB is supported by the Netherlands Organization for Scientific Research (NWO).

References

Allen, L. E. & Strom, K. M. 1995, AJ, 109, 1379

Bauer, F. & Bregman, J. N. 1996, ApJ, 457, 382

Belloni, T., Verbunt, F., & Mathieu, R. D. 1998, A&A, 339, 431

Belloni, T., Verbunt, F., & Schmitt, J. H. M. M. 1993, A&A, 269, 175

Carter, D., Benn, C. R., Rutten, R. G. M., Breare, J. M., Rudd, P. J., King, D. L., Clegg, R. E. S., Dhillon, V. S., Arribas, S., Rasilla, J.-L., Garcia, A., Jenkins, C. R., & Charles, P. A. 1993, ISIS Users' Manual, http://www.ing.iac.es

Eker, Z., Hall, D. S., & Anderson, C. M. 1995, ApJS, 96, 581

ESA SP 1200. 1997, The Hipparcos and Tycho Catalogues
Fernández-Figueroa, M. J., Montes, D., de Castro, E., & Cornide, M. 1994, ApJS, 90, 433
Gilliland, R. L., Brown, T. M., Duncan, D. K., Suntzeff, N. B., Lockwood, G. W., Thompson, D. T., Schild, R. E., Jeffrey, W. A., & Penprase, B. E. 1991, AJ, 101, 541
Goranskij, V. P., Kusakin, A. V., Mironov, A. V., Moshkaljov, V. G., & Pastukhova, E. N. 1992, Astron. Astrophys. Trans., 2, 201
Groot, P. J., Piters, A. J. M., & van Paradijs, J. 1996, A&AS, 118, 545
Gunn, A. G., Hall, J. C., Lockwood, G. W., & Doyle, J. G. 1996, A&A, 305, 146
Hobbs, L. M. & Mathieu, R. D. 1991, PASP, 103, 431
Horne, K. 1986, PASP, 98, 609
Horne, K. & Marsh, T. R. 1986, MNRAS, 218, 761
Janes, K. A. & Smith, G. H. 1984, AJ, 89, 487
Kaluzny, J. & Radczynska, J. 1991, IBVS 3586
King, D. L. 1985, ING Technical Note, 31
Kippenhahn, R. & Weigert, A. 1967, Zeitschrift für Astrophysik, 65, 251
Kurochkin, N. E. 1960, Astron. Circular USSR, 212, 9
Landsman, W., Aparicio, J., Bergeron, P., di Stefano, R., & Stecher, T. P. 1997, ApJ, 481, L93
Landsman, W., Bohlin, R. C., Neff, S. G., O'Connell, R. W., Roberts, M. S., Smith, A. M., & Stecher, T. P. 1998, AJ, 116, 789
Latham, D. W., Mathieu, R. D., Milone, A. A. E., & Davis, R. J. 1992, in Binaries as tracers of stellar formation, ed. A. Duquennoy & M. Mayor (Cambridge: Cambridge University Press), 132
Massey, P., Strobel, K., Barnes, J. V., & Anderson, E. 1988, ApJ, 328, 315
Mathieu, R. D. & Latham, D. W. 1986, AJ, 92, 1364
Mathieu, R. D., Latham, D. W., & Griffin, R. F. 1990, AJ, 100, 1859
Mathieu, R. D., Latham, D. W., Griffin, R. F., & Gunn, J. E. 1986, AJ, 92, 1100
Mathys, G. 1991, A&A, 245, 467
Montes, D., Fernández-Figueroa, M. J., De Castro, E., & Sanz-Forcada, J. 1997, A&AS, 125, 263
Montes, D. & Martín, E. L. 1998, A&AS, 128, 485
Montgomery, K. A., Marschall, L. A., & Janes, K. A. 1993, AJ, 106, 181
Nissen, P. E., Twarog, B. A., & Crawford, D. L. 1987, AJ, 93, 634
Ortolani, A., Maggio, A., Pallavicini, R., Sciortino, S., Drake, J. J., & Drake, S. A. 1997, A&A, 325, 664
Pasquini, L. & Belloni, T. 1998, A&A, 336, 902
Piters, A. J. M., Groot, P. J., & van Paradijs, J. 1996, A&AS, 118, 529
Pritchet, C. J. & Glaspey, J. W. 1991, ApJ, 373, 105
Rajamohan, R., Bhattacharyya, J. C., Subramanian, V., & Kuppuswamy, K. 1988, Bull. Astr. Soc. India, 16, 139
Sanders, W. L. 1977, A&AS, 27, 89
Simoda, M. 1991, IBVS 3675
Simon, T., Fekel, F. C., & Gibson, D. M. 1985, ApJ, 295, 153
Singh, K. P., Drake, S. A., & White, N. E. 1996a, AJ, 111, 2415
Singh, K. P., Drake, S. A., White, N. E., & Simon, T. 1996b, AJ, 112, 221
Stępién, K. 1994, A&A, 292, 191
Strassmeier, K. G., Hall, D. S., Fekel, F. C., & Scheck, M. 1993, A&AS, 100, 173

Tonry, J. & Davis, M. 1979, AJ, 84, 1511
Twarog, B. A. & Anthony-Twarog, B. J. 1989, AJ, 97, 759
Unger, S., Walton, N., Pettini, M., & Tinbergen, J. 1993, UES Users' Manual, http://www.ing.iac.es/
Verbunt, F. & Phinney, E. S. 1995, A&A, 296, 709
Walter, F. M. & Bowyer, S. 1981, ApJ, 245, 671
Welty, A. D. & Ramsey, L. W. 1995, AJ, 109, 2187
White, N. E., Arnaud, K., Day, C. S. R., Ebisawa, K., Gotthelf, E. V., Mukai, K., Soong, Y., Yaqoob, T., & Antunes, A. 1994, PASJ, 46, L97
Wyatt, W. F. 1985, in IAU Coll., Vol. 88, Stellar radial velocities, ed. A. G. Davis Philip & D. W. Latham (Schenectady, N.Y.: L. Davis Press, Inc.), 123
Yi, Z., Elgarøy, Ø., Engvold, O., & Westergaard, N. J. 1997, A&A, 318, 791
Zhilinskii, E. G. & Frolov, V. N. 1994, Astronomy Letters, 20, 80
Zimmermann, H., Becker, W., Belloni, T., Döbereiner, S., Izzo, C., Kahabka, P., & Schwentker, O. 1994, EXSAS User's Guide: Extended scientific analysis system to evaluate data from the astronomical X-ray satellite ROSAT, Technical Report 257, MPE

Chapter 3

Photometric variability in the old open cluster M 67

I. Cluster members detected in X-rays

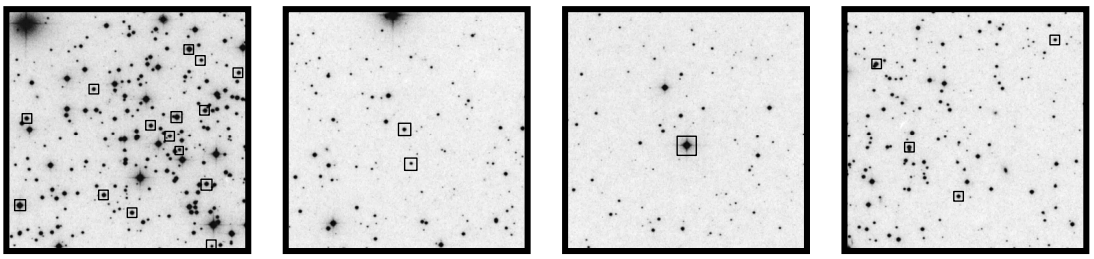

Maureen van den Berg, Keivan G. Stassun, Frank Verbunt & Robert D. Mathieu
submitted to Astronomy & Astrophysics

Abstract – We study photometric variability among the optical counterparts of X-ray sources in the old open cluster M 67. The two puzzling binaries below the giant branch are both variables: for S 1113 the photometric period is compatible with the orbital period, S 1063 either varies on a period longer than the orbital period, or does not vary periodically. For the spectroscopic binaries S 999, S 1070 and S 1077 the photometric and orbital periods are similar. Another new periodic variable is the main-sequence star S 1112, not known to be a binary. An increase of the photometric period in the W UMa system S 1282 (AH Cnc) is in agreement with a previously reported trend. Six of the eight variables we detected are binaries with orbital periods of 10 days or less and equal photometric and orbital periods. This confirms the interpretation that their X-ray emission arises in the corona of tidally locked magnetically active stars. No variability was found for the binaries with orbital periods longer than 40 days; their X-ray emission remains to be explained.

3.1 Introduction

Twenty five members of the old open cluster M 67 have been detected in X-rays (Belloni et al. 1998). At the age of M 67 (4 Gyr, Dinescu et al. 1995) the rotation of single stars is too slow to generate detectable X-rays. Therefore, the X-ray emission of many M 67 sources probably arises in interacting binaries. Indeed, one source is known to be a cataclysmic variable. Nine sources are binaries with orbital periods of 10 days or less, presumably RS CVn type systems, whose X-rays are due to the coronae of magnetically active stars forced to corotate by tidal interaction (see Table 3.2). However, not all X-ray sources are binaries, e.g. one source is a hot white dwarf, and some others are stars which do not show signs of binarity.

There are five peculiar binaries whose evolutionary statuses we currently do not understand. They are found in the colour-magnitude diagram in locations which cannot be reproduced by combining the light from any two members on the main sequence, subgiant and/or giant branches. Two of them have long orbital periods which exclude strong tidal interaction. A sixth binary with a long orbital period lies to the blue of the giant branch which can be explained by the superposition of the light of a giant and a turnoff star.

A spectroscopic study of these peculiar systems was presented in van den Berg et al. (1999) [Chapter 2]. Here we report our photometric study of these sources and of other X-ray sources that happen to be in the same fields of view. The photometry of S 1082 will be published separately (van den Berg et al. 2001) [Chapter 5]. The observations and analyses are described in Sect. 3.2. Results are presented in Sect. 3.3, followed by the interpretation and discussion – including comparison with earlier work – in Sect. 3.4. Sect. 3.5 summarises our conclusions. The variability of stars not detected in X-rays but included in our observations will be the subject of Paper II (Stassun et al., in preparation) [Chapter 4].

3.2 Data and analysis

3.2.1 Observations

U, *B*, *V*, *I* and Gunn *i* photometry was obtained with the 0.90-m telescope at Kitt Peak, the 0.91-m ESO Dutch Telescope at La Silla and the 1-m Jacobus Kapteyn Telescope on La Palma. Combined, the five observation runs span a period of two years (see Table 3.1). Fig. 3.1 shows the location of the observed fields. During run 1 weather conditions were good with a typical seeing of $0\farcs9$ to $1\farcs4$. The observations were made during and around full moon but moon illumination was not a problem. Weather conditions during runs 2 and 3 were good, with a typical seeing of $1\farcs6$. During run 4 the typical seeing was $1\farcs5$ while the quality of some images was affected by the brightness of the nearby moon. The same, at a seeing between $1\farcs5$ and $3''$, is true for the last run, that in addition was troubled by partial cloudiness. This is reflected in the relatively large errors of the last two runs.

Every X-ray source of Belloni et al. (1998) was monitored in at least one run, except for the faint cataclysmic variable EU Cnc and the hot white dwarf. The main purpose of run 1 was

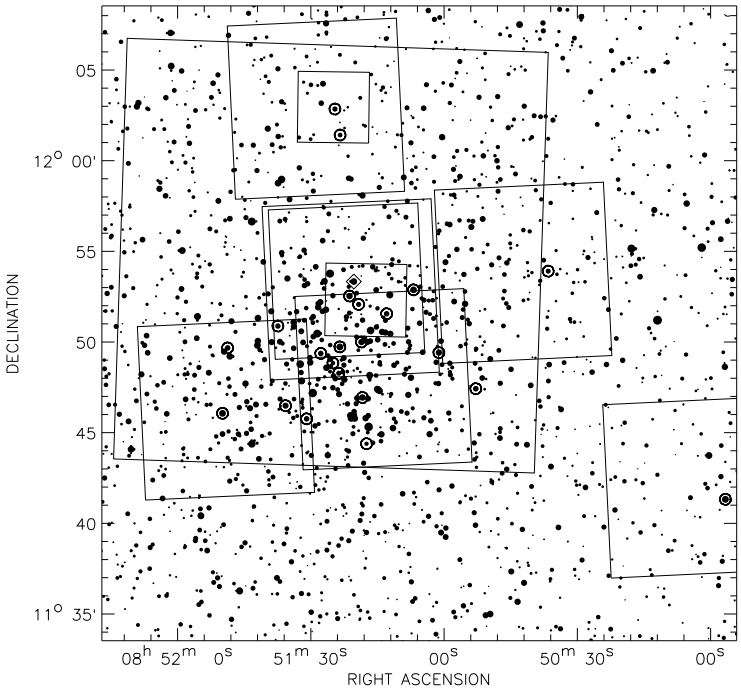

Figure 3.1: A 35 x 35 arcmin^2 region of M 67 centred on the star S 783. The coordinates of the sources in this field are taken from the USNO-A1.0 catalogue. The areas monitored in the five observation runs are indicated by the squares (see also Table 3.1). The open circles mark the optical counterparts to the X-ray sources that are discussed in this paper; the diamond marks S 1082 that we discuss elsewhere (van den Berg et al. 2001) [Chapter 5].

to monitor variability of S 1113 and S 1063, of run 2 to monitor S 1113 and of runs 3 to 5 to monitor S 1082. This means that exposure times were chosen to optimise the measurements of these stars. During run 5, five additional fields containing X-ray sources were observed in *B* and *V* once or twice per night to search for obvious signs of variability. As S 364 and S 1237 are very bright stars (see Table 3.2) the quality of the images of fainter stars in these fields are poor. This affects the quality of the light curves of the X-ray sources in the field of view of S 1237 (i.e. S 1242, S 1270 and S 1282).

3.2.2 Data reduction and light curve solution

Standard IRAF routines were used to remove the bias signal and flatfield the images. Aperture photometry for all the stars was done with the DAOPHOT.PHOT task. For each individual run, source counts were extracted within a fixed radius with a value depending on the seeing conditions. The stars in M 67 are separated well enough to avoid problems of crowding.

The light curve solution was computed with the algorithm of ensemble photometry as described by Honeycutt (1992). In this method, the magnitudes of all the stars on every frame

Run	Dates	Telescope	Centre	FOV	Filters	t_{exp} (s)	P_{min}	P_{max}
1	Jan 4-16 1998	0.90-m KPNO	S 1084	$23' \times 23'$	*BV I*	90 60 60	2.4 hr	10 d
2	Feb 12,14-17,21,24-28 1998, Mar 1-3,6,8 1998	0.91-m ESO Dutch	S 1113	$3\farcm8 \times 3\farcm8$	*U BV* Gunn *i*	300 120 120 120	5 hr	25 d
3	Feb 2-19 1999	0.91-m ESO Dutch	S 1068*	$3\farcm8 \times 3\farcm8$	*U BV* Gunn *i*	360 100 50 30	30 mn	18 d
4	Dec 25, 26 1999	1-m ING JKT	S 1082	$10' \times 10'$	*BV*	75 30	12 mn	1 d
5	Feb 13-16, 20 2000	1-m ING JKT	S 1082	$10' \times 10'$	*U BV I*	350 30 15 8	30 mn	8 d
			S 364	$10' \times 10'$	*BV*	15 4	4 hr	8 d
			S 628	$10' \times 10'$	*BV*	150 80	4 hr	8 d
			S 1013	$10' \times 10'$	*BV*	20 8	4 hr	8 d
			S 1113	$10' \times 10'$	*BV*	200 100	4 hr	8 d
			S 1237	$10' \times 10'$	*BV*	20 10	4 hr	8 d

* S 1063 starting from February 8

Table 3.1: Log of the observations. From left to right: number and dates of the observation run; telescope; Sanders number of the star near the centre of the field; field of view; filters; typical exposure time in seconds for each filter; the minimum and maximum period P_{min} and P_{max} used to compute periodograms for the specified run.

S	X	V	$B-V$	$P_{\rm orb}$ (d)	e	run	var	$P_{\rm phot}$ (d)		$d\phi_{\rm max}$	log FAP	remarks
364	19	9.84	1.36			5	n					
628	35	14.47	0.76			5	n					
760	49	13.29	0.57	954(12)	0.43(9)	1	n					3
775	44	12.69	0.63			1,5	n					
972	17	15.37	0.89	1.166412(2)	0.009(6)	1,5	n					3
999	13	12.60	0.78	10.05525(19)	0.	1,5	y	9.2(2.0)[a]	[1;B]	0.3	−2.62	2
1019	11	14.34	0.81	1.360217(18)	0.023(13)	1,5	n					3
1027	46	13.24	0.60			1,4,5	n					
1036	45	12.78	0.49			1,4,5	y	0.44144(1)[a]	[all;B]	0.05	−18.6	EV Cnc
								0.44144(1)[a]	[all;V]	0.05	−17.0	
								0.44144(1)[a]	[1+5;I]	0.05	−6.4	
1040	10	11.52	0.87	42.8271(22)	0.	1,4,5	n					
1045	41	12.54	0.59	7.64521(11)	0.	1,4,5	n					
1063	8	13.79	1.05	18.396(5)	0.206(14)	1,3,4,5	y	17-18[b]	[1;U], [1+3;B,V,I]			1
1070	38	13.90	0.63	2.66059(8)	0.	1,3,4,5	y	2.6(1)	[3;B]	0.3	−17.6	3
								2.6(1)	[3;V]	0.3	−31.5	
1072	37	11.32	0.61	1495(16)	0.32(7)	1,3,4,5	n					2
[c]1077	7	12.60	0.64	1.358766(8)	0.095(33)	1,3,5	y	1.42(9)	[3;B]	0.3	−3.3	3
								1.44(9)[a]	[3;V]	0.3	−7.2	
								1.38(9)	[3;I]	0.3	−5.5	
1112	28	14.98	0.78			1,2,5	y	2.7(2)	[1;B]	0.3	−3.0	
								2.65(3)	[1+2;V]	0.3	−7.8	
1113	26	13.77	1.01	2.823105(14)	0.022(10)	1,2,5	y	2.84(8)	[2;U]	0.1	−3.9	1, AG Cnc
								2.834(1)	[all;B]	0.1	−14.5	
								2.833(1)	[all;V]	0.1	−14.9	
								2.84(3)	[1+2;I]	0.1	−11.2	
[c]1234	53	12.65	0.57	4.35563(25)	0.	1	n					2
1237	52	10.78	0.94	697.8(7)	0.105(15)	5	n					2
1242	50	12.72	0.68	31.7797(27)	0.664(18)	1,5	n					2
1270	43	12.73	0.58			1,5	n					
1282	40	13.33	0.56			1,4,5	y	0.360452(8)[a]	[all;B]	0.05	−19.2	AH Cnc
								0.360452(8)[a]	[all;V]	0.05	−21.9	

[a] period does not correspond to the highest peak in the periodogram [b] folded light curves do not look convincing [c] this system is a triple system; the period listed is for the inner binary

Table 3.2: Properties of the X-ray sources of Belloni et al. (1998) discussed in this paper. From left to right: Sanders number (Sanders 1977); X-ray source number from Belloni et al. (1998); V magnitude and $B-V$ colour (Montgomery et al. 1993); for spectroscopic binaries: orbital period $P_{\rm orb}$ in days and eccentricity e; observation runs during which the star was observed; a variability indicator n (y) if the probability that the source is constant is larger (smaller) than 0.3%; photometric period $P_{\rm phot}$ in days with the run number(s) and the filter for which the period was detected in square brackets; maximum phase shift used to estimate the error in the period; logarithm of the false-alarm probability of the period detection; remarks and references for information on the spectroscopic binaries (1=Mathieu et al., in preparation [Chapter 6], 2=Mathieu et al. 1990, 3=preliminary solution by Latham et al., private communication).

are used to create an ensemble average with respect to which the brightness variations are defined. Frames that have a large offset from this average (e.g. due to bad seeing) show up as deviant observations and can be excluded. For a given star, errors were assigned to the data points by estimating the typical spread in the light curves of stars of similar magnitude. In most cases the formal errors from the PHOT task are negligible; if not, we used this error instead. The different datasets were analysed individually.

As exposure times were chosen to optimise the measurements of the X-ray sources in each field, the photometric precision as a function of stellar brightness varies from one run to the next. Generally speaking, the photometric precision of the brightest (unsaturated) stars in our exposures is flat-field limited to 5–10 mmag. This precision level typically holds for stars up to 2–2.5 mag fainter than the brightest sources, and then becomes photon-noise limited and degrades for still fainter stars. The best overall precision was achieved on our Kitt Peak frames (run 1; Table 3.1), for which the brightest stars ($B \approx 12$, $V \approx 12$, $I \approx 11.5$) have $\sigma_{\rm mag} = 0.007$, 0.005, 0.005 in B, V, and I, respectively. The precision begins to degrade at around 14th mag. For the faintest sources, at about 18.5 mag, the precision is 0.05–0.1 mag. We refer the reader to Paper II [Chapter 4] for a full discussion of the photometric precision in our observations.

A simple zero-point shift is applied to the measurements in each filter to roughly place the instrumental magnitudes on an absolute scale as described in Paper II [Chapter 4]. The light and colour curves that are presented in Fig.3.3-3.5 show the variations with respect to the mean magnitude and colour (see Table 2 of Paper II) [Table 4.2].

3.2.3 Search for variability

Our search for variability is a two-step process. First we perform a χ^2-test on the individual light curves for each filter for each run, to calculate the probability that the light curves of the X-ray sources are compatible with being constant. As the intrinsic properties of the variability need not be the same in light curves of different runs (in particular for brightness variations due to spots), we consider each light curve separately. To remove accidental outliers, the minimum and maximum data points are excluded. A star is labeled as a probable variable if the probability for being constant is smaller than 0.3% in any of the light curves. Eight stars are marked as probable variables (see column *var* in Table 3.2). For six of these stars the variability is not detected in every light curve. In most cases we can ascribe this to differences in sensitivity between runs or between different filters of a certain run, or to different durations of runs. For S 1063, S 1070 and S 1077 it seems that the variability itself has changed as discussed below.

We next perform a Lomb-Scargle time-series analysis (Scargle 1982) to search for periodicity in the light curves. In cases when multiple light curves in a given filter are marked as variable, those light curves are combined for the period search; no distinction was made between I and Gunn i. If the resulting period does not produce a smooth folded light curve, data from different runs are analysed separately; this will be indicated for each source in Sect. 3.3. A periodogram is computed with 1000 frequencies between a minimum and maximum period

$P_{\rm min}$ and $P_{\rm max}$ corresponding to twice the typical sampling period and the full length of the longest observation run, respectively (see Table 3.1). We choose the period of the highest peak in the periodogram as our first estimate for periodicity in the data. However, as will be discussed below, external information often leads us to immediately neighbouring peaks of comparable significance.

Photometric periods have been determined previously for the two contact binaries S 1036 (Gilliland et al. 1991) and S 1282 (e.g. Kurochkin 1979). Therefore, we look for periods in a narrow window instead of the range limited by $P_{\rm min}$ and $P_{\rm max}$. In both cases, we find that the power at half the photometric period is far higher than at the photometric period, due to the symmetry in the light curve. For S 1036 we search for periods between 0.215 and 0.225 days, for S 1282 between 0.175 and 0.185 days. The periodogram is computed for 5000 points to increase the resolution.

An estimate for the chance detection of a period, i.e. the probability that the light curve does not have the periodicity indicated by the highest peak, is expressed by the false-alarm probability. In the case of the Lomb-Scargle periodogram the false-alarm probability follows the expression: $1-[1-\exp(-z)]^m$, where z is the height of the peak and m is the number of independent frequencies. Horne & Baliunas (1986) demonstrated that this number can be smaller than the number of data points especially in sets of unevenly sampled data. The value of m is obtained by fitting this expression to a probability distribution generated by measuring the maximum peak heights in periodograms of 5000 simulated random datasets with the same time-sampling and the same spread in the measurements as the actual light curve.

Photometric periods with a false-alarm probability smaller than 1% are summarised in Table 3.2. These correspond to the position of the highest peak in the periodogram unless indicated otherwise. To estimate the error in the best period we proceed as follows. For the correct period the light curves defined by the first and last observations coincide. A small change dP in the period causes a small phaseshift: $d\phi = T/(P+dP) - T/P$, where T is the time span of the dataset. For each light curve we estimate, by visual inspection, a maximum $d\phi_{\rm max}$ for which the light curves do not split perceptibly. This corresponds to a maximum acceptable period change of

$$\frac{dP}{P} = \frac{-d\phi_{\rm max}P}{T + d\phi_{\rm max}P} \tag{3.1}$$

The value for $d\phi_{\rm max}$ that we choose is listed in Table 3.2.

3.3 Results

We have divided the sources into periodically (Sect. 3.3.1) or non-periodically (Sect. 3.3.2) varying stars. The periodically varying stars are two W UMa systems, four spectroscopic binaries and one star not known to be a binary, i.e. S 1112.

3.3.1 Periodic variables

W UMa systems

The W UMa light curves are plotted versus *photometric* phase where phase 0 corresponds to the moment of photometric primary minimum (see Fig. 3.3).

S 1282 is the W UMa variable AH Cnc discovered by Kurochkin (1960). The periodograms of the total B and V datasets show peaks with a spacing of $\sim 4\ 10^{-5}$ and $\sim 6\ 10^{-4}$ days due to the two-year and the two-month gaps in our observations, respectively (see Fig.3.2). The highest peaks in the B and V periodograms are found at 0.180226 and 0.180270 days, respectively, which corresponds to two neighbouring peaks in the periodogram. We folded the data on twice those periods but find that the peak at 0.180226 days represents best the true period: when we use the longer period, the deeper primary minima of the first run fall on top of the secondary minima of the fourth run. Thus we conclude that the photometric period is 0.360452 days. I data were only obtained during run 1 and cannot provide an equally precise period.

In addition to short-term variations on a time scale of roughly 9 to 10 years, Kurochkin (1979) finds a secular increase of the period of AH Cnc. His ephemeris for the primary minimum is:

$$\begin{aligned} \text{Min I} &= 2\,441\,740.7166(27) + 0\overset{\text{d}}{.}36044098(53)E \\ &\quad + 1\overset{\text{d}}{.}56(38)10^{-10}E^2 \end{aligned} \tag{3.2}$$

This ephemeris predicts a period during the time of our observations between 0.3604447 days and 0.3604479 days, in agreement with our result. We note that period changes of similar magnitude have been found for other contact binaries.

We observe no significant colour changes in $V-I$ and $B-V$.

S 1036, or EV Cnc, was discovered to be a contact binary by Gilliland et al. (1991) who report a period of 0.44125 days. The B and V periodograms show fine structure from the two-year and two-month gaps in the data. In both sets, that include data from run 1, 4 and 5, we find the same best period of 0.22078 days. When folded on this period, the light curves show the same effect of interchanging primary and secondary minima as described for S 1282. Proper phasing is obtained with the period of 0.22072 days derived from the peak next to the highest. The period that corresponds to the highest peak in the periodogram of the I data is 0.22091 days, but again interchanges minima. The period of 0.22072 days coincides with a nearby peak of similar height. U data were only obtained during run 5 and cannot provide an equally precise period. In Fig. 3.3 the light curves are folded on the double period of 0.44144 days.

A light curve folded on the period given by Gilliland et al. shows that this period cannot be correct for the epoch of our observations. Since Gilliland et al. do not specify the error in the period, we cannot tell whether the period has changed significantly.

We see no significant changes in any of the colours $U-V$, $B-V$ or $V-I$.

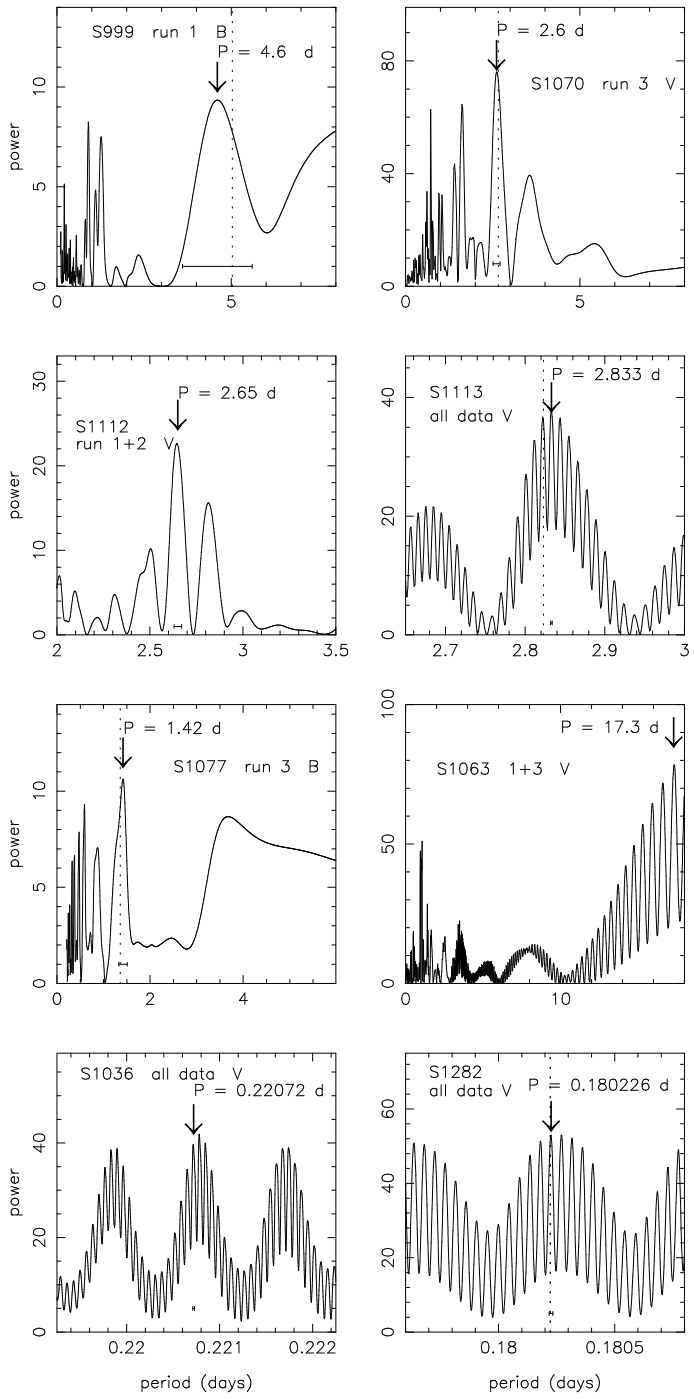

Figure 3.2: Periodograms for the variable stars. The arrow indicates the photometric period or half the photometric period listed in Table 3.2. The dotted line marks the position of the orbital period for S 1070, S 1077 and S 1113, half the orbital period for S 999 and the position of the period as predicted by Kurochkin (1979) for S 1282. The horizontal error bars give our estimate for the uncertainty in the period.

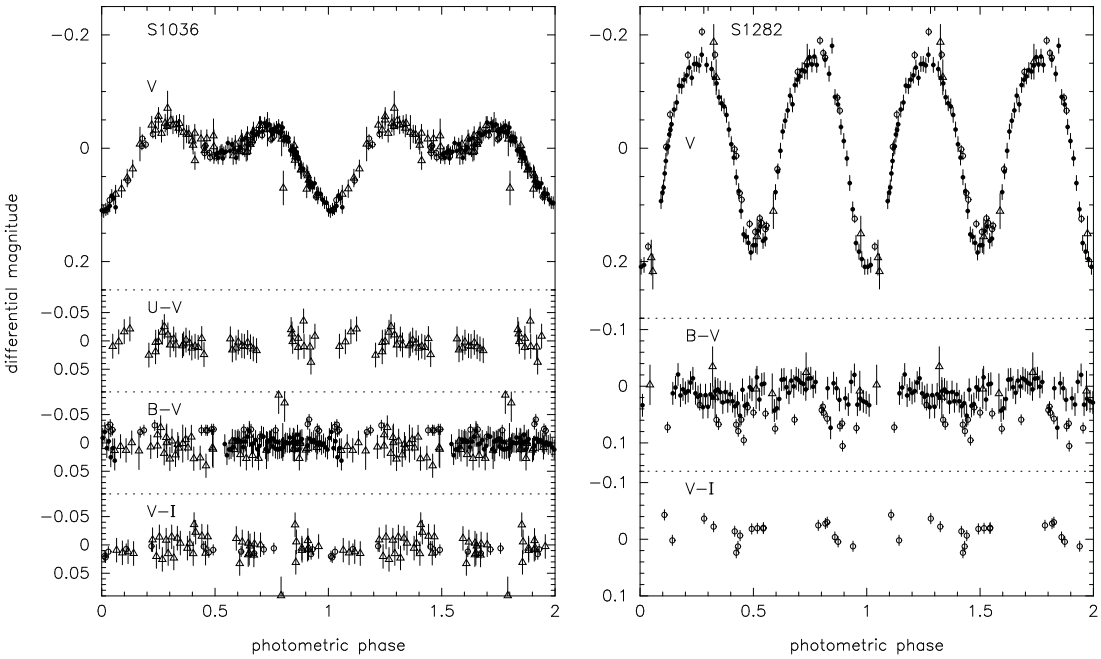

Figure 3.3: Light curves of the two contact binaries S 1036 (EV Cnc) and S 1282 (AH Cnc) folded on the newly derived periods (see Table 3.2). Data from different observing runs are marked with different symbols: open circles for run 1, filled circles for run 4 and open triangles for run 5.

Spectroscopic binaries

We note that the light curves of the spectroscopic binaries are gives as function of *orbital* phase where phase 0 corresponds to the moment of maximum positive radial velocity of the primary star (primary receding).

S 999 The *B* and *V* data of the first run show variability with a semi-amplitude of ~ 0.03 mag. Only the period found in the *B* data has a false-alarm probability smaller than 1%. The highest peak in the periodogram is found at 4.6 ± 1.0 days (Fig. 3.2), but this period does not produce a smooth light curve. We suggest that the peak at 4.6 days is a harmonic of photometric variation on or near the orbital period of 10.06 days. Note that the duration of the first run was 10 nights, so our period search does not extend up to the orbital period. Gilliland et al. (1991) report a period of 9.79 days (no error is given) with an amplitude of only 0.013 mag.

In Fig. 3.4 we fold the *B* and *V* data on the orbital period. According to the orbital solution of Mathieu et al. (1990), the minimum brightness occurs around orbital phase 0. The $B-V$ colour does not vary significantly.

S 1070 A period of 2.6 ± 0.1 days is detected in the *B* and *V* light curves of run 3 with a semi-amplitude of the variation of ~ 0.03 mag.

The photometric properties of S 1070 have changed with respect to run 1. If the variations

seen in the third run ($\sigma \approx 0.014$ mag in V) were present in the first run, they would have been detected.

In Fig. 3.4 all data of run 3 are folded on the orbital period which is compatible with the photometric period. The photometric minimum occurs around orbital phase 0.1-0.2 (ephemeris from Latham et al., private communication). The $V-$Gunn i colour curve shows periodic variations with a semi-amplitude of ~ 0.03 mag such that the star becomes bluer as it gets brighter.

S 1077 All light curves of this star are marked as variable except for the U and B data of run 5, probably due to the reduced sensitivity of run 5, and the V and I data of run 1. The latter can point at a real absence of variation as could be the case in S 1070; the variations of run 3 ($\sigma \approx 0.018$ mag in V) were not seen in run 1. In the periodograms of the combined data peaks with a false-alarm probability smaller than 1% are found near 0.6 and 1.3 days. However, when folded on these periods, the light curves do not look smooth. Therefore we also analysed data of the different runs separately. Only the light curves of run 3, with the highest precision, look smooth when folded on the periods of about 1.4 days (see Table 3.2) which have a false-alarm probability smaller than 1% only in B, V and Gunn i. This period does not correspond to the highest peak in the V periodogram, which is found at 0.60 days. The semi-amplitude of the variation is small, ~ 0.03 mag in V.

The photometric period is compatible with the orbital period; we consider the latter to be the true period for the photometric variability. The data of run 3 are folded on the orbital period in Fig. 3.4. The photometric minimum occurs around phase 0.9-0. The colours do not vary significantly.

S 1113 As already noted by Kaluzny & Radczynska (1991) this star is a photometric variable. In our observations, the B and V data cover the longest timespan and can therefore provide the most accurate photometric period. The periodogram is computed for 25000 periods to make the period bins smaller than the accuracy of our period determination (0.001). The periodogram (see Fig. 3.2) again shows fine structure with a spacing as expected from the two-year gap between runs 1 and 5. The maximum peak indicates a period of 2.833 ± 0.001 days, which is not compatible with the orbital period. The orbital period corresponds to a neighbouring peak in the periodogram at 2.822 ± 0.001 days (in V; 2.823 ± 0.001 days in B). Given the lack of significant difference in peak heights, the photometric and orbital periods may be the same. Therefore, the light curves in Fig. 3.4 are folded on the orbital period. For the B light curve we find a similar result. The periods found in the U and I band are compatible, but less accurate (see Table 3.2).

Data taken during different runs at the same orbital phase give rise to scatter in the light curve, as seen in the top panel of Fig. 3.4. This could be explained if the amplitude, phase and/or the period of the variability has changed between the runs. When analysed separately, the light curves of run 1 and 2 give a period of 2.8 ± 0.1 and 2.83 ± 0.03 days, respectively; the uncertainty is too large to detect a period change. Assuming that the photometric period is the orbital period we conclude that the amplitude or the phase of the variations has changed,

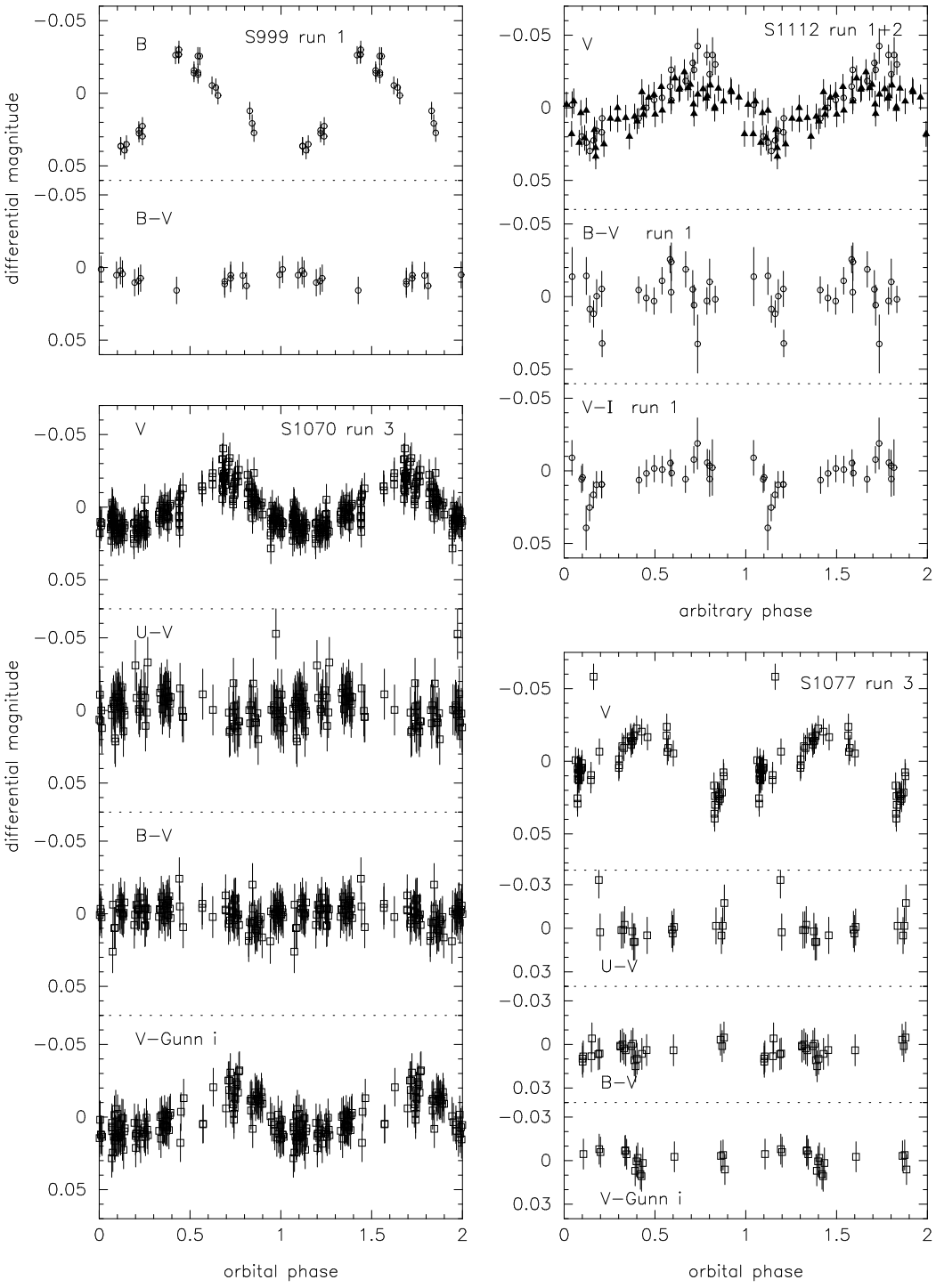

Figure 3.4: Light curves of S 1112 (folded on the photometric period) and of S 999, S 1070, S 1077. Data from different observing runs are marked with different symbols: open circles for run 1, filled triangles for run 2, and open squares for run 3.

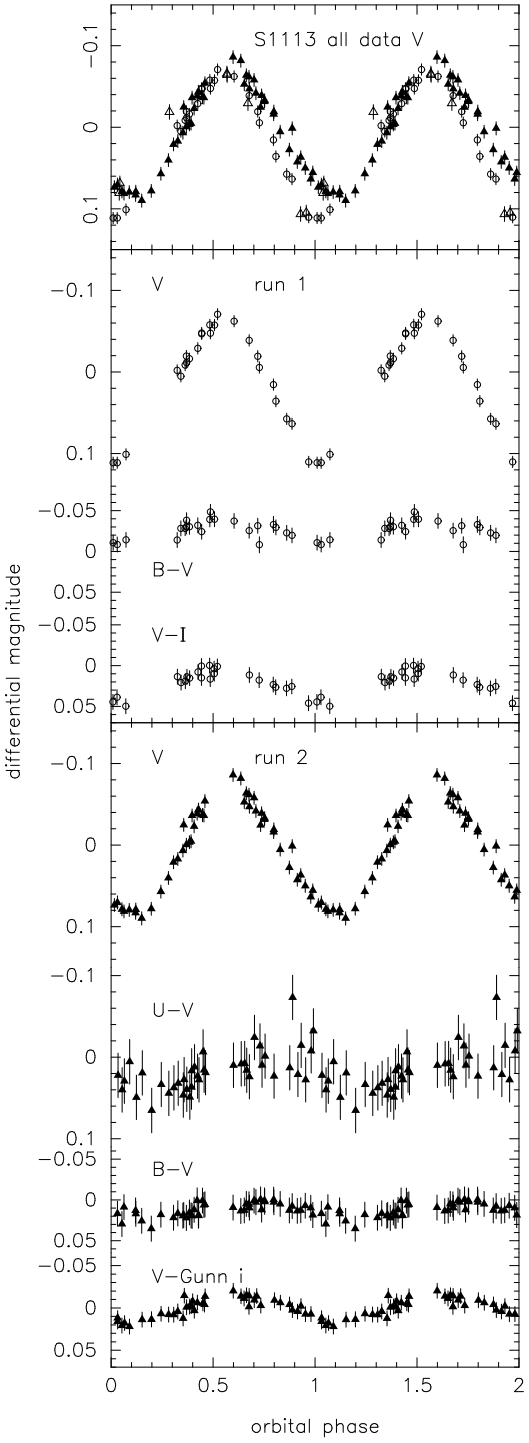

Figure 3.4 – continued: Light curves of S 1113 (folded on the orbital period). Data from different observing runs are marked with different symbols: open circles for run 1, filled triangles for run 2, and open triangles for run 5.

either of which is possible if the variation is caused by a star spot.

We show separately the light and colour curves from runs 1 and 3 in the lower panels of Fig. 3.4. The colour variation is significant only in $V-I$ in run 1 and $B-V$ and $V-$ Gunn i in run 3, such that the star becomes bluer as it brightens.

S 1112

The data of the first (B, V, I) and second (V) runs show variability but only in the B and V light curves do we find significant periods of 2.7 ± 0.2 and 2.65 ± 0.03 days, respectively. In Fig. 3.4 the data are folded on the latter period. The amplitude of the variation is again small, only ~ 0.04 mag. Weak colour variations are only seen in $V-$Gunn i and appear to be in phase with the light curve; the star becomes bluer as it brightens. No information on binarity from radial-velocity measurements exists for this star.

3.3.2 Non-periodic variable: S 1063

Photometric variability of this star up to 0.18 mag was inferred by Racine (1971) from the differences between published values of the magnitude. Rajamohan et al. (1988) and Kaluzny & Radczynska (1991) also noted its variability, but only the latter provide light curves (for December 9 to 15 1986, see Fig. 3.5). This binary was included in all our runs except the second. The light curves of run 1 and 3 clearly show variability (see Fig. 3.5) on a long time scale. The variability during run 1 is similar to that observed by Kaluzny & Radczynska. The longest interval of continuous observation was eighteen consecutive nights during run 3, which is almost the length of the orbital period (18.39 days). Therefore during any one run we could not have established periodicity on the orbital period.

Data from run 1 and 3 were combined to look for periods up to 18 days. The highest peaks in the periodogram are found between 17 and 18 days, all with a false-alarm probability smaller than 1%. However, the folded light curves show no convincing periodicity. Therefore, no actual period is specified in Table 3.2.

The amplitude of the variation increases towards the blue.

3.4 Discussion

We have studied the optical photometric properties of X-ray sources in M 67. Eight photometric variables, including three new variables, were found among the twenty two sources that are discussed in this paper. In all cases the amplitudes of the variations are small, ranging from 0.03 to 0.4 mag in V.

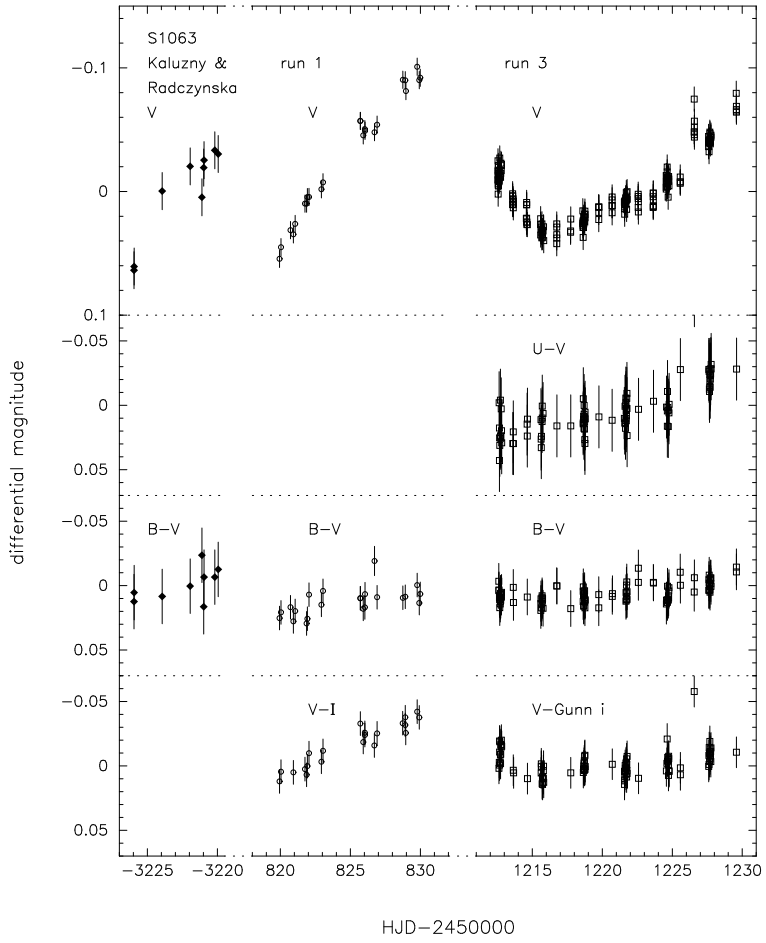

Figure 3.5: Light curves and colour curves of S 1063. Data from different observing runs are marked as in Fig. 3.3. The data from Kaluzny & Radczynka (1991) of December 9-15 1986 are included on the left; the brightness variations are defined with respect to the mean magnitude of the light curve.

The light curves of the two contact binaries S 1036 and S 1282 arise through partial eclipses and ellipsoidal variations of the tidally deformed stars. Their X-rays are believed to be emitted by the hot coronae of the magnetically active components.

The primary and secondary eclipses of contact binaries usually are of similar depth. This has been interpreted as evidence that both stars have almost the same temperature, which in turn is evidence for energy exchange between the two stars in contact. Unequal depths of the primary and secondary eclipses then implies different temperatures for both stars, i.e. poor thermal contact. The thermal contact can be suppressed when the system becomes (semi-) detached. It has been suggested that such phases of poor thermal contact occur periodically in contact binaries (Lucy & Wilson 1979). In view of this interpretation it may appear surprising that we see unequal eclipses but no evidence of colour i.e. temperature variations in S 1036.

S 1036 is interesting as either an immediate progenitor of a contact binary, or because it

is in the semi-detached phase of the thermal cycle of a contact binary. The upper limit on the colour variations in S 1036 is about 0.05 in $B-V$ (Fig. 3.3). Radial-velocity measurements are required to determine the evolutionary status of this system and to convert the upper limit to the colour variations into an upper limit on temperature difference.

The small amplitude of the S 1036 light curve indicates either a small inclination or an extreme mass ratio (e.g. Rucinski 1997). In a volume-limited sample of contact binaries, Rucinski (1997) found that only two among the 98 systems have light curves with unequal minima. One of those two also has a relatively small amplitude of variation of about 0.25 mag.

Another feature of W UMa light curves associated with unequal eclipses is that at first quadrature (phase 0.25) the star is brighter than at second quadrature (phase 0.75). This has been explained with a hot spot on the secondary, possibly as a result of mass transfer in a semi-detached system (e.g. Rucinski 1997). This effect is also visible in S 1036.

Within the two years of our observations we see evidence for variability of the light curve of S 1282: the secondary minimum of run 1 appears to be less deep and flatter than observed in run 4. A similar variation was seen by Gilliland et al. (1991) who noted that in their observations of 1988 the secondary eclipse had a flat shape, while the observations by Whelan et al. (1979) done from 1973 to 1976 showed a rounded secondary minimum. The timescale of these variations is indicative of the presence of spots.

The light curves of the periodic variables S 999, S 1070, S 1077 and S 1113 display only one maximum per cycle. S 1113 and S 1070 also show colour variations in phase with the brightness. For all four systems there is indication for variability in the light curves. The amplitude of the variation in S 999 is different in our observations and those of Gilliland et al. (1991); in S 1070 and S 1077 there has likely been a change between run 1 and run 3 and in S 1113 between run 1 and 2. The short timescale of this variation is an indication of brightness modulations by spots. Remarkably, in all cases the minimum occurs around orbital phase 0. We have no explanation for this.

All four systems are spectroscopic binaries with photometric periods compatible with the orbital period. The circular orbital periods, their X-ray luminosity, and the Ca II K emission in the case of S 999, S 1077 and S 1113 (Pasquini & Belloni 1998, van den Berg et al. 1999 [Chapter 2]) make these stars likely candidates for magnetically active systems due to one or both stars being tidally locked. This was already suggested by Belloni et al. (1998) and our light curves support their interpretation.

The light curve of S 1112 shows low-amplitude periodic light and colour variations similar to those seen in these four binaries. This star has not been monitored for radial-velocity variations but the X-ray luminosity and the light curve are typical for magnetically active systems which suggests that S 1112 is a binary with an orbital period of about 2.65 days.

We do not understand the variability that we observe for S 1063. The source shows spectroscopic signatures of magnetic activity (van den Berg et al. 1999) [Chapter 2]. However, if one of the stars in this binary would be corotating near periastron, we expect a rotation period of 14.6 days (Eq. 42 of Hut 1981) which is excluded by the observations of run 3.

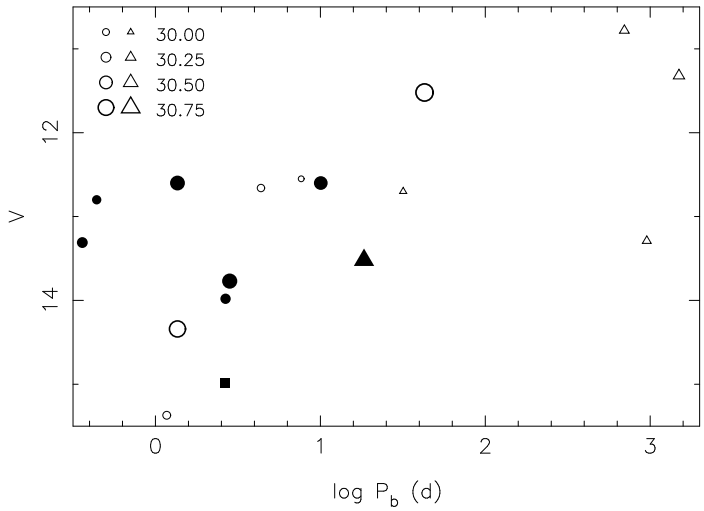

Figure 3.6: Visual magnitude versus orbital period of the M 67 binaries detected in X-rays. The size of the symbol is a measure for the logarithm of the X-ray luminosity (0.1-2.4 keV, in erg s^{-1}) as indicated in the figure. Eccentric binaries are indicated with triangles, binaries with eccentricities compatible with zero (within the 3σ-error) with circles. Filled symbols are systems for which we detected photometric variability. S 1112 is indicated with a filled square.

We conclude that either the star does not vary periodically or that the period of variability is longer than 18 days. More observations covering a longer timespan are required to understand the nature of the variability. Our findings are in contrast with the suggestion by Kaluzny & Radczynska (1991) that S 1063, as well as S 1113, are highly evolved W UMa-type binaries.

3.5 Conclusion

Of the twenty two X-ray sources in M 67 that we discuss, sixteen are spectroscopic binaries with known orbital periods. Our survey for optical photometric variables among these X-ray sources has established eight variables. Seven of these are among the sixteen binaries, the binary status of the eighth, S 1112, is not yet known. In addition, Gilliland et al. (1991) observed periodic optical variation in three more of the X-ray binaries with amplitudes too low to be detected by us: S 1019 (semi-amplitude 0.015 mag), S 1242 (semi-amplitude 0.0025 mag) and S 1040 (semi-amplitude 0.012) mag. Thus ten of the sixteen X-ray binaries in M 67 are optical variables at the $\gtrsim 0.01$ mag level.

Belloni et al. (1998) have suggested that rapid stellar rotation resulting from tidal locking results in enhanced magnetic activity and X-ray emission. Fig. 3.6 shows the visual magnitude versus orbital period of the spectroscopic binaries. With the exception of S 1040 and S 1112, all variables have orbital periods less than 20 days and $V > 15$. In all cases but S 1019 and

S 1063, the photometric period is equal to the orbital period or, in the case of S 1242, the orbital period near periastron. Evidently tidal locking has been established, leading to rotation of at least the primary star that is more rapid than typical for solar-mass stars at 4 Gyr. Thus our results establish a key premise of the Belloni et al. (1998) picture for the X-ray emission. Furthermore, if the cause of the observed optical variability is indeed spot modulation of the observed flux, then the presence of the required large spots is consistent with enhanced magnetic activity in these stars. The X-ray emission and optical variability properties of S 1019 and S 1063 require further investigation.

Three binaries were not detected as variables despite their short orbital periods. S 972 is the faintest of the binary sample at $V = 15.37$, and so its variability may have gone undetected. The X-ray luminosities of S 1045 ($P_{\rm orb} = 7.6$ days) and S 1234 ($P_{\rm orb} = 4.3$ days) are among the lowest of the binary X-ray sources and indicate low activity levels; this can explain the absence of optical variability due to spots. Rajamohan et al. (1998) have noted S 1234 as a possible optical variable (semi-amplitude ~ 0.16 mag) which suggests that time-variability of the spot phenomenon can also explain the absence of optical variation.

The interpretation of S 1040 and of the remaining three X-ray binaries S 760, S 1072 and S 1237 may be the most challenging. All have long orbital periods. Given their wider separations tidal locking is not expected and so the consequent stellar rotations may be characteristic of single stars. As such, their lack of large spots and consequent photometric variability is not a surprise. Nonetheless, these binaries are X-ray sources. Their X-ray emission remains to be explained.

No large radial-velocity variations were found for S 775 and S 1270 (σ is 0.9 km s^{-1} in 12 observations spanning 5200 days and 0.7 km s^{-1} in 7 observations spanning 800 days, respectively, see Mathieu et al. 1986); if these stars are binaries their periods must be relatively long. Thus their X-ray luminosities, as those of S 364, S 628 and S 1027 for which no radial-velocity information is available, remain unexplained.

Acknowledgements – The authors wish to thank Magiel Janson, Rien Dijkstra, Gertie Geertsema, Remon Cornelisse and Gijs Nelemans for obtaining part of the data used in the paper. We also want to thank David Latham for computing preliminary orbital solutions for four spectroscropic binaries to support this research; the radial-velocity measurements are part of a larger study of M 67 binaries carried out by D. Latham, A. Milone and R.D. Mathieu. The Kitt Peak National Observatory is part of the National Optical Astronomy Observatories, which is operated by the Association of Universities for Research in Astronomy, Inc. (AURA) under cooperative agreement with the National Science Foundation. The Jacobus Kapteyn Telescope is operated on the island of La Palma by the Isaac Newton Group in the Spanish Observatorio del Roque de los Muchachos of the Instituto de Astrofisica de Canarias. The Dutch 0.91-m Telescope is operated at La Silla by the European Southern Observatory. IRAF is distributed by the National Optical Astronomy Observatories, which are operated by the Association of Universities for Research in Astronomy, Inc., under cooperative agreement with the National Science Foundation. MvdB is supported by the Netherlands Organization for Scientific Research (NWO).

References

Belloni, T., Verbunt, F., & Mathieu, R. D. 1998, A&A, 339, 431
Dinescu, D. I., Demarque, P., Guenther, D. B., & Pinsonneault, M. H. 1995, AJ, 109, 2090
Gilliland, R. L., Brown, T. M., Duncan, D. K., Suntzeff, N. B., Lockwood, G. W., Thompson, D. T., Schild, R. E., Jeffrey, W. A., & Penprase, B. E. 1991, AJ, 101, 541
Honeycutt, R. K. 1992, PASP, 104, 435
Horne, J. H. & Baliunas, S. L. 1986, ApJ, 302, 757
Hut, P. 1981, A&A, 99, 126
Kaluzny, J. & Radczynska, J. 1991, IBVS 3586
Kurochkin, N. E. 1960, Astron. Circular USSR, 212, 9
—. 1979, Astron. Circular USSR, 1076, 2
Lucy, L. B. & Wilson, R. E. 1979, ApJ, 231, 502
Mathieu, R. D., Latham, D. W., & Griffin, R. F. 1990, AJ, 100, 1859
Mathieu, R. D., Latham, D. W., Griffin, R. F., & Gunn, J. E. 1986, AJ, 92, 1100
Montgomery, K. A., Marschall, L. A., & Janes, K. A. 1993, AJ, 106, 181
Pasquini, L. & Belloni, T. 1998, A&A, 336, 902
Rajamohan, R., Bhattacharyya, J. C., Subramanian, V., & Kuppuswamy, K. 1988, Bull. Astr. Soc. India, 16, 139
Sanders, W. L. 1977, A&AS, 27, 89
Scargle, J. D. 1982, ApJ, 263, 835
van den Berg, M., Orosz, J., Verbunt, F., & Stassun, K. 2001, A&A, 375, 375
van den Berg, M., Verbunt, F., & Mathieu, R. D. 1999, A&A, 347, 866
Whelan, J. A. J., Worden, S. P., Ruciński, S. M., & Romanishin, W. 1979, MNRAS, 186, 729

Chapter 4

Photometric variability in the old open cluster M 67

II. Other stars

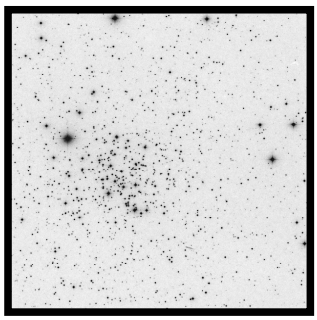

Keivan G. Stassun, Maureen van den Berg, Robert D. Mathieu & Frank Verbunt

to be submitted to Astronomy & Astrophysics
(WIYN Open Cluster Study. VII.)

Abstract – We use differential CCD photometry to search for variability in *BVI* among 991 stars projected in and around the old open cluster M 67. Our previous paper [Chapter 3] reported results for 22 cluster members that are optical counterparts to X-ray sources; this study focuses on the other stars in our observations. A variety of sampling rates were employed, allowing variability on time scales ranging from ~ 0.3 hours to ~ 20 days to be studied. Among the brightest sources studied, sensitivity to variations as small as 10–15 mmag (3σ r.m.s.) is achieved. The study is reasonably complete for stars with $12.5 < B < 18.5$, $12.5 < V < 18.5$, and $12 < I < 18$ within a radius of about 10 arcmin from the cluster centre. In addition, stars with $10 < BVI < 12.5$ were monitored in a few

small regions in the cluster. We present astrometry and photometry for all 991 sources studied, and report the variability characteristics of those stars found to be variable at a statistically significant level. Among the variables, we highlight several sources that merit future study, including stars located on the cluster binary sequence, blue stragglers, a faint blue star that exhibits periodic variability, and a newly discovered W UMa system.

4.1 Introduction

With the intent of studying the photometric variability of optical counterparts to known X-ray sources scattered throughout the old open cluster M 67, we have obtained sensitive photometry of stars projected in a region approximately one-third degree in size around the cluster centre. The results of these observations for the X-ray sources are described in Paper I of this series (van den Berg et al. 2001b) [Chapter 3].

While the X-ray sources were the principal aim of the observations, light curves for nearly 1000 other stars were produced in the course of our analyses. In this paper we present the results of an extensive time-series analysis of the 967 stars included in our observations that are not the optical counterparts of X-ray sources known to be members of the cluster.

Our basic goal is to identify those stars that exhibit statistically significant photometric variability of any kind. At the old age of M 67 (4 Gyr, Dinescu et al. 1995), most single stars rotate too slowly to exhibit strong dynamo-generated activity, and the sensitivity of our photometry is insufficient to detect the extremely low-level ($\sim$ few μmag) variations that may arise from solar-analog *p*-mode oscillations (Woodward & Hudson 1983). Thus, photometric variability in our observations may be an indicator of, e.g., spot-modulated stellar rotation, binary interaction (eclipses or ellipsoidal variations), or stellar activity at levels not detectable in existing X-ray surveys. Periodic variability is especially interesting in these contexts, as a periodicity in the light curve may be fundamentally related to a stellar rotation period, a binary orbital period, etc. But even if a periodicity is not apparent in our data, the detection of photometric variability may point the way to objects that merit special consideration and further study.

Many objects of interest may be identified simply from their location in the colour-magnitude diagram, photometric variability notwithstanding. Thus, a basic product of this work is a colour-magnitude diagram of all of the sources studied.

Basic photometry and time-series analysis have been performed in M 67 by numerous other authors. Most notably, Gilliland et al. (1991) conducted a very sensitive ($\sim 100\mu$mag), highly temporally sampled ($\sim$ 1 min) study of stars in the core of the cluster, resulting in several tentative detections of stellar oscillations as well as the serendipitous discovery of a few δ Scuti variables and W UMa systems. However, this study was confined for the most part to the central few arcmin of the cluster. Montgomery et al. (1993) have presented a deep ($V \sim 20$) colour-magnitude diagram of the central one-half degree of the cluster.

The present study complements and extends these previous studies by combining a relatively precise (5–10 mmag) variability study with a reasonably deep ($V \sim 18.5$) colour-

magnitude diagram for stars covering a large area around the cluster centre. Furthermore, the ongoing spectroscopic surveys of the WOCS (WIYN Open Cluster Study) project and others (e.g. Latham et al. 1992) have identified numerous spectroscopic binaries in the cluster among stars brighter than about $V \sim 14$; in this study we incorporate the available knowledge of binarity into our analyses where appropriate.

In Sect. 4.2, we summarise the photometric data and their analyses. We provide astrometry and photometry for all of the sources included in our observations, as well as cross-identifications of our sources with those of several previous authors. In Sect. 4.3, we present the basic results of this study, including an identification of stars exhibiting statistically significant photometric variability, and a colour-magnitude diagram of all sources studied. We discuss the results of select individual sources in greater detail in Sect. 4.4, and summarise our findings in Sect. 4.5.

4.2 Data and analysis

In this section we provide a summary of our observations and of the procedures used in their analysis. Complete details of the data and of the analysis procedures used are given in Paper I; the reader is referred to that paper for a more thorough discussion.

4.2.1 Observations

Differential *BVI* photometry of M 67 was performed during five separate epochs with a total time span of two years. The observations were obtained with 1-meter telescopes at three different observing sites, each with a different field of view (ranging from $3\farcm8$ to $23'$) and under a range of observing conditions. The five observing runs differ considerably in time span and sampling frequency; the shortest run is the most highly sampled, spanning 2 days with individual measurements taken at roughly 5-minute intervals, while the longest run spans nearly 25 days with measurements taken at intervals of several hours. As each observing run had as its primary target a different set of X-ray sources, the five runs differ in depth and range of stellar magnitudes covered. The reader is encouraged to consult the map (Fig. 1) and table (Table 1) in Paper I [Fig. 3.1 and Table 3.1] that more fully describe these observation details.

The result is a database of differential photometric measurements for 991 stars in a region roughly $23'$ on a side, centred approximately $5'$ north of the cluster centre. The database is relatively complete in this large area for stars with $12.5 < B < 18.5$, $12.5 < V < 18.5$, and $12 < I < 18$. In addition, the database includes stars with $10 < BVI < 12.5$ in a few small regions within this larger area. Some U-band photometry was obtained as well, but as only a small number of stars in a few select regions were observed we do not include the analysis of the U-band data here.

Due to the differences in depth and areal coverage of the five observing runs, there is relatively little overlap of stars among the five epochs of data, so that the light curve of a given star spans anywhere from 2 to 25 days with the specific time-sampling depending on

the particular epoch contributing data to that star. Furthermore, stars near the bright or faint extremes of the database may not be present in all three filters depending on the stellar colours.

4.2.2 Data reduction and light curve solution

The roughly 1200 data frames produced in the course of the five observing runs were reduced using standard IRAF procedures. All stellar sources on our data frames with S/N > 10 were identified with the DAOPHOT task and aperture photometry was performed using the APPHOT.PHOT task. Astrometry was extracted for all stellar sources identified using the STSDAS.GASP package, producing astrometric solutions with formal internal uncertainties of approximately $0\farcs1$ in each direction. Astrometric positions are calibrated to the coordinate system adopted by Montgomery et al. (1993), resulting in an external uncertainty of approximately $0\farcs4$ in each direction.

In Table 4.1[1] we present the master list of all 991 stellar sources included in our observations, sorted in order of increasing right ascension. Stellar positions derived from our data frames are provided for all sources. Cross-identifications with the studies of various other authors are also given, and various cluster membership estimates from those studies are also provided when available.

Given the highly inhomogeneous nature of our photometric data (all stars do not appear on all data frames), differential photometric light curves are derived with the algorithm for differential photometry of an inhomogeneous ensemble described by Honeycutt (1992), as described in Paper I.

The limiting precision of our differential photometry is a function of stellar brightness and can be established from an examination of the scatter present in the light curves of non-variable stars at each magnitude. The limiting photometric precision as a function of stellar magnitude varies among the five observing runs, but generally speaking the precision of the brightest (unsaturated) stars in our exposures is flat-field limited to 5–10 mmag. This precision level typically holds for stars up to 2–2.5 mag fainter than the brightest sources, and then becomes photon-noise limited and degrades for still fainter stars. The best overall precision was achieved on our Kitt Peak frames (run 1; see Table 1 in Paper I [Table 3.1]). In Fig. 4.1 we show the r.m.s. variations in the *BVI* light curves of stars from this observing run as a function of mean stellar magnitude. The non-variable stars are defined by the lower envelope of points in this figure. The brightest non-variable stars show r.m.s. variations of 0.007, 0.005, and 0.005 mag in *B*, *V*, and *I*, respectively. The precision begins to degrade noticeably at around 14th mag. For the faintest sources, at about 18.5 mag, the precision is 0.05–0.1 mag.

We have applied a simple zero-point shift to the instrumental magnitudes in each filter to roughly place our instrumental magnitudes on an absolute scale. The zero-point shift for each filter was determined by taking the average difference between our instrumental magnitudes and the published values of Montgomery et al. (1993) for at least 10 stars common to our two

[1]Tables 4.1 and 4.2 are only available in electronic form via URL
`http://www.astro.wisc.edu/~keivan/maureen`

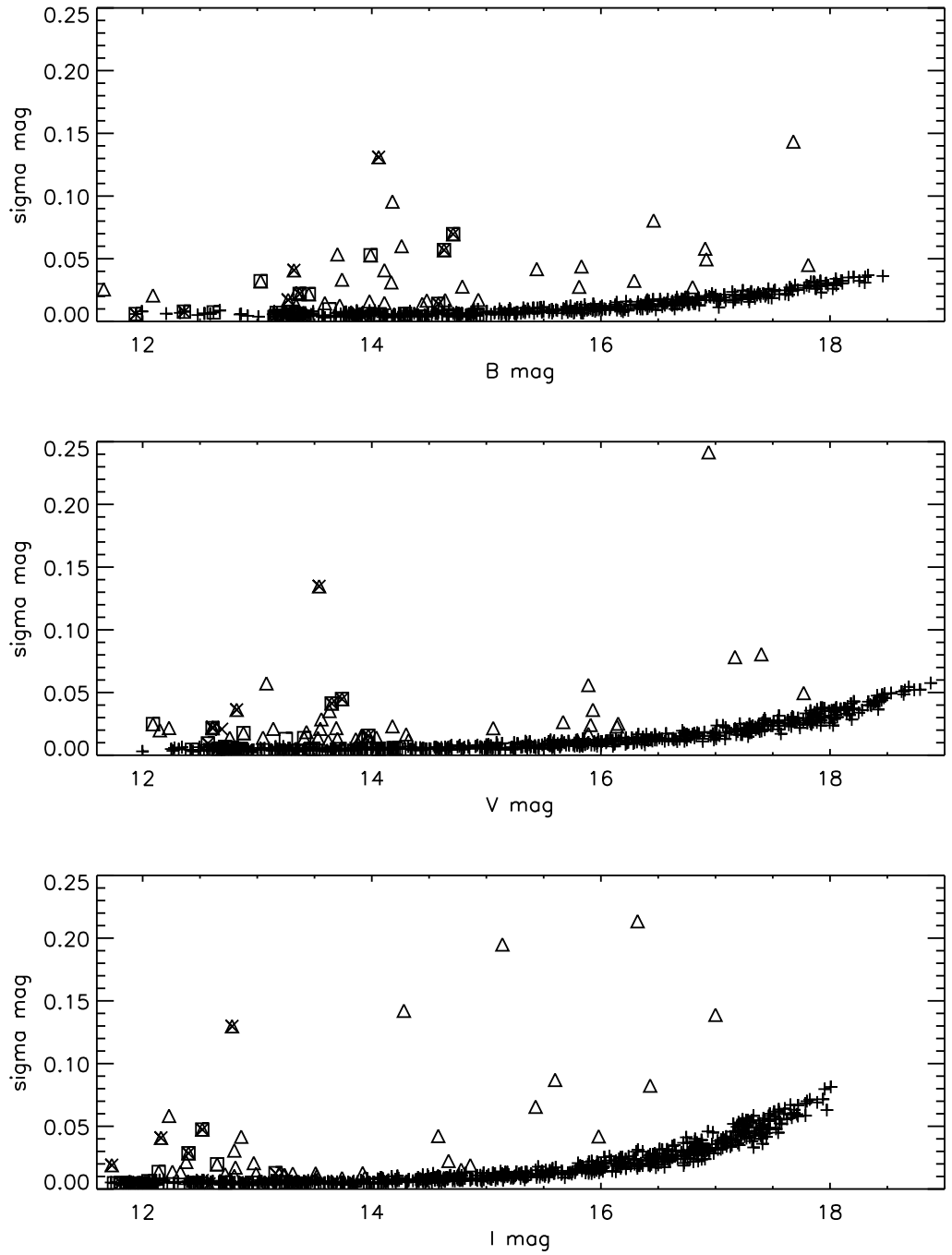

Figure 4.1: Mean stellar magnitude versus r.m.s. variations in the *B* (top), *V* (middle) and *I* light curves of run 1. Variables are indicated with triangles, spectroscopic binaries with squares, X-ray sources with crosses. Non-variable stars are defined by the lower envelope of points.

samples.

In Table 4.2[1] we present mean *BVI* photometry for the 991 stellar sources in our database. As discussed above, uncertainties in the values listed are a function of stellar brightness: formal uncertainties in the brightest sources are 0.01 mag or less, while the faintest sources have formal uncertainties of $\sim 10\%$. We note, however, that our photometry has not been strictly calibrated, so that the uncertainty in the values listed in Table 4.2 is more likely limited to a few percent. In Sect. 4.3 we use these stellar magnitudes to construct colour-magnitude diagrams for identifying objects of interest. The light and colour curves in Figs. 4.3-4.6 show the variations with respect to the mean magnitude and colour as listed in Table 4.2

4.2.3 Search for variability

To identify photometric variability among the stars in our database, we apply a χ^2-test, as described in Paper I, to compute the probability that each star's light curve is consistent with being constant. As our photometric precision is a function of stellar brightness, our ability to detect low-level photometric variations is necessarily a function of stellar brightness as well. Among the brightest sources, the variability search is sensitive to variations larger than $\sim 10-15$ mmag. Depending upon the specific observing runs contributing data to each star's light curve, the variability search is sensitive to variations on time scales ranging from ~ 0.3 hours to ~ 20 days.

Stars with data in multiple runs were analysed on a run-by-run basis, and the results of the variability analysis for the different runs were checked for agreement. All instances in which the variability analysis gives a different result in different runs can be ascribed to differences in sensitivity between runs.

Among those stars found to be variables, we perform a Lomb-Scargle time-series analysis (Scargle 1982) to search for the presence of a periodic signal. For each star, a periodogram is computed at 1000 frequencies between a minimum and maximum frequency corresponding to the full time span of the light curve and one-half the typical sampling rate, respectively. We choose the highest peak in the periodogram as the best estimate for a possible periodicity in the data and estimate the statistical significance of this best period by computing a false-alarm probability (the probability that the detected period could result from random variations). The false-alarm probability is computed via a Monte Carlo simulation in which periodograms are computed for 100 purely random light curves with the same temporal sampling as the actual light curve, and the height of the highest peak in these 100 test light curves is taken to correspond to the level of 99% significance. We report a period only if its peak in the periodogram exceeds that of the 99% significance level so derived. Uncertainties in the periods are estimated as is described in Paper I.

4.3 Results

Our database of differential photometry allows us to identify photometric variables among nearly 1000 stars in M 67 on a variety of time scales. In this section we report the basic photometric results of this study as well as our time-series analysis.

4.3.1 Colour-magnitude diagrams

Though not strictly calibrated, the stellar magnitudes reported in Table 4.2 allow us to place most of the stars in our database on a colour-magnitude diagram. In Fig. 4.2 we present V versus $(B-V)$ and V versus $(V-I)$ colour-magnitude diagrams. The colours plotted have not been de-reddened (reddening towards M 67 is relatively small, $E(B-V) = 0.032$, Nissen et al. 1987).

The cluster main sequence is clearly apparent amid a field of apparent non-members, extending from the cluster turnoff at $V \sim 12.5$ down to the faint limit of our database at $V \sim 18.5$[2] (the range within which our database is roughly complete). The cluster binary sequence is also clearly apparent along this full range. The wall of stars lying below the cluster main sequence has been noted in studies of M 67 before and is likely due to field stars in the halo (e.g. Richer et al. 1998). From the observing runs intended to study brighter sources (covering a few small areas in the cluster; see Table 1 [Table 3.1] and Fig. 1 [Table 3.1] in Paper I), some blue stragglers and a portion of the giant branch (as well as the red giant clump) are also present for approximately $10 < V < 12.5$.

4.3.2 Photometric variability

In Table 4.3 we present the 69 stars in our photometric database that meet the criteria for photometric variability discussed in Sect 4.2.3. For each star we give our own identification number (from Table 4.1), the identification number and proper-motion membership probability from Sanders (1977) if available, V magnitudes and colours from our photometry, and the r.m.s. of the star's light curves in each of the B, V, and I passbands. Stars listed in this table did not necessarily show statistically significant variability in all three passbands (due to differences in the sensitivity of our photometry in the different passbands and in different observing runs); r.m.s. values listed in *italics* are not statistically significant in that passband. Table 4.3 also provides comments for most of the stars listed. These comments give additional information such as possible periodicities, evolutionary status, binarity, etc. Stars without comments are stars situated on or near the cluster main sequence whose light curves show only apparently non-periodic variability in our observations.

We note that the criterion that we adopted to call a star variable is that the probability that its light curve is consistent with being constant is smaller than 0.3%. Therefore, one expects

[2]Note that the $B-V$ colour-magnitude diagram cuts off at $V \sim 17.5$ due to the limiting B magnitude ($B \sim 18.5$) and the stellar colours at that magnitude ($B-V \sim 1$); see Fig. 4.2.

#	S ID	Memb.	V	$B-V$	$V-I$	σ_B	σ_V	σ_I	Comments
35			14.70	1.43	2.44	*0.025*	*0.014*	0.014	long period ($\sim$ 10 d)? nearby M dwarf?
40	647	0.99	13.91	0.57	0.72	0.017	0.015	0.012	
56			13.43	0.55	0.71	0.016	0.019	0.012	long period ($\sim$ 10 d)?
59			15.68	0.61	0.82	0.032	*0.026*	0.019	
70	828	0.00	14.53	0.59	0.79	*0.010*	*0.011*	0.009	
74			17.77	0.31	0.43	*0.052*	0.050	*0.067*	periodic white dwarf? $P = 0.14/0.28$ d
86	745	0.96	13.16	0.56	0.73	0.013	*0.007*	*0.008*	
107			13.70	0.55	0.71	*0.012*	0.013	0.012	
142			14.72	0.66	0.80	*0.013*	*0.012*	0.013	
146			16.99	0.82	1.02	0.045	*0.028*	*0.022*	flares? below M-S, K0 colors
154								0.139	
167			15.93	0.99	1.28	0.050	0.036	*0.020*	$P = 3.6$ d, on binary sequence
188	848	0.97	14.04	0.60	0.73	0.017	0.014	0.012	
208	845	0.00	13.92	0.50	0.68	*0.012*	0.015	0.011	below M-S, late F colors
265	846	0.90	13.62	0.56	0.74	*0.011*	0.011	*0.008*	
267	757	0.95	13.56	0.61	0.76	0.031	0.029	0.031	new W UMa, $P = 0.36$ d
287	1077	0.80	12.61	0.66	0.88	0.017	0.022	0.019	x-ray source
308								0.142	$P \sim 11$ d?
321	2227	0.00	13.69	0.57	0.72	0.060	0.022	0.021	
322	1109	0.34	13.55	0.56	0.74	0.041	0.021	0.017	long period ($\sim$ 20 d)?
365	1063	0.93	13.65	0.98	1.25	0.057	0.041	0.029	x-ray source
381	974	0.00	15.67	0.79	1.00	0.080	0.026	0.022	
418			17.17		1.74		0.078	0.066	on binary sequence
420								0.082	
439	1093	0.96	14.18	0.61	0.77	0.028	0.023	*0.062*	
440	999	0.95	12.61	0.76		0.022	0.022		x-ray source
454	1070	0.89	13.97	0.61	0.81	0.014	0.015	*0.013*	x-ray source
463			16.94		1.34		0.242	0.087	long period ($\sim$ 40 d)?
465			15.91	0.64	0.85	*0.014*	0.024	*0.018*	below M-S, G2 colors
471	1082	0.94	11.25	0.41	0.57	0.026	0.023	0.025	x-ray source, blue straggler
523	1112	0.95	15.06	0.75	0.99	0.028	0.022	*0.016*	x-ray source
525			15.89	0.87	1.13	*0.019*	0.017	*0.012*	
526	1209a[1]	0.00	13.14	0.60	0.76	0.033	0.021	0.022	
529			15.91		0.77		0.386	0.195	below M-S
533	2216	0.74	15.09	0.74	0.94	0.044	*0.010*	*0.013*	
542			13.74	0.97	1.22	0.070	0.045	0.047	x-ray source
561			15.89	1.02	1.31	0.058	0.056	0.042	W UMa, $P = 0.27$ d
579								0.213	
580	1036	0.91	12.82	0.50	0.66	0.041	0.036	0.041	x-ray source
591	1279	0.92	10.56	1.08	1.07	*0.006*	*0.006*	0.014	giant
612	1264[1]	0.75	12.09	0.94	1.08	0.032	0.025	*0.014*	spectroscopic binary, giant
614			14.79	0.69	0.85	*0.011*	*0.011*	0.009	
615	1264b[1]	0.00	13.08	0.62	0.85	0.054	0.057	0.058	
655	1263	0.89	11.15	0.21	0.32	0.016	0.027	0.015	blue straggler
679	1284	0.95	10.98	0.29	0.28	*0.009*	*0.007*	0.013	blue straggler, spectroscopic binary
690	1305	0.95	12.31	0.96	0.98	*0.016*	*0.012*	0.021	giant
716	1282	0.95	13.54	0.52	0.76	0.131	0.135	0.130	x-ray source
719			17.40		1.33		0.080	*0.050*	below M-S
720	1344	0.96	13.86	0.58	0.77	0.014	0.013	*0.008*	
732	1293	0.93	12.15	0.99		*0.006*	0.020		giant
734			15.86	0.87	1.08	*0.019*	*0.022*	0.015	
829	1224b[1]	0.00	13.63	0.55	0.77	0.096	0.035	0.042	
831	1224[1]	0.77	13.41	0.58	0.76	0.053	0.014	0.020	
843	1507	0.95	13.53	0.58	0.73	0.015	0.014	0.010	long period ($\sim$ 20 d)?
851	1506	0.93	12.76	0.58	0.75	0.013	0.014	*0.011*	
856	1504	0.91	13.99	0.59	0.76	*0.012*	0.011	0.011	
872			16.15	0.94	1.23	*0.032*	0.025	*0.016*	
877	1497	0.00	14.32	0.61	0.80	*0.010*	0.012	*0.007*	long period ($\sim$ 10 d)?
893								0.042	
911			12.88	0.57	0.74	0.022	0.018	0.014	spectroscopic binary
921			14.56	0.85	1.04	*0.011*	*0.007*	0.010	on binary sequence
922			14.30	0.63	0.79	0.017	0.017	0.013	
929	1509	0.00				0.021			
936			13.05	0.54	0.72	0.015	0.014	0.013	
940			16.73	0.95	1.28	0.143	*0.024*	*0.018*	long period ($\sim$ 20 d)?
957			16.17	0.63	0.81	0.027	*0.019*	*0.020*	below M-S, G2 colors
963			16.14	0.58	0.75	*0.022*	0.023	*0.018*	below M-S, G0 colors
969			14.76	0.68	0.84	0.042	*0.007*	*0.009*	
973			12.23	1.11		0.023	0.022		repeating dips? giant?

[1] Photometry possibly contaminated by close neighbour.

Table 4.3: List of variable stars. From left to right: identification number from Table 4.1; identification number and proper-motion membership probability from Sanders (1977) if available; average V magnitude and $B-V$ and $V-I$ colours from our photometry as listed in Table 4.2; r.m.s. of the light curves in B, V and I, values in *italics* are not significant at the 3σ-level; comments.

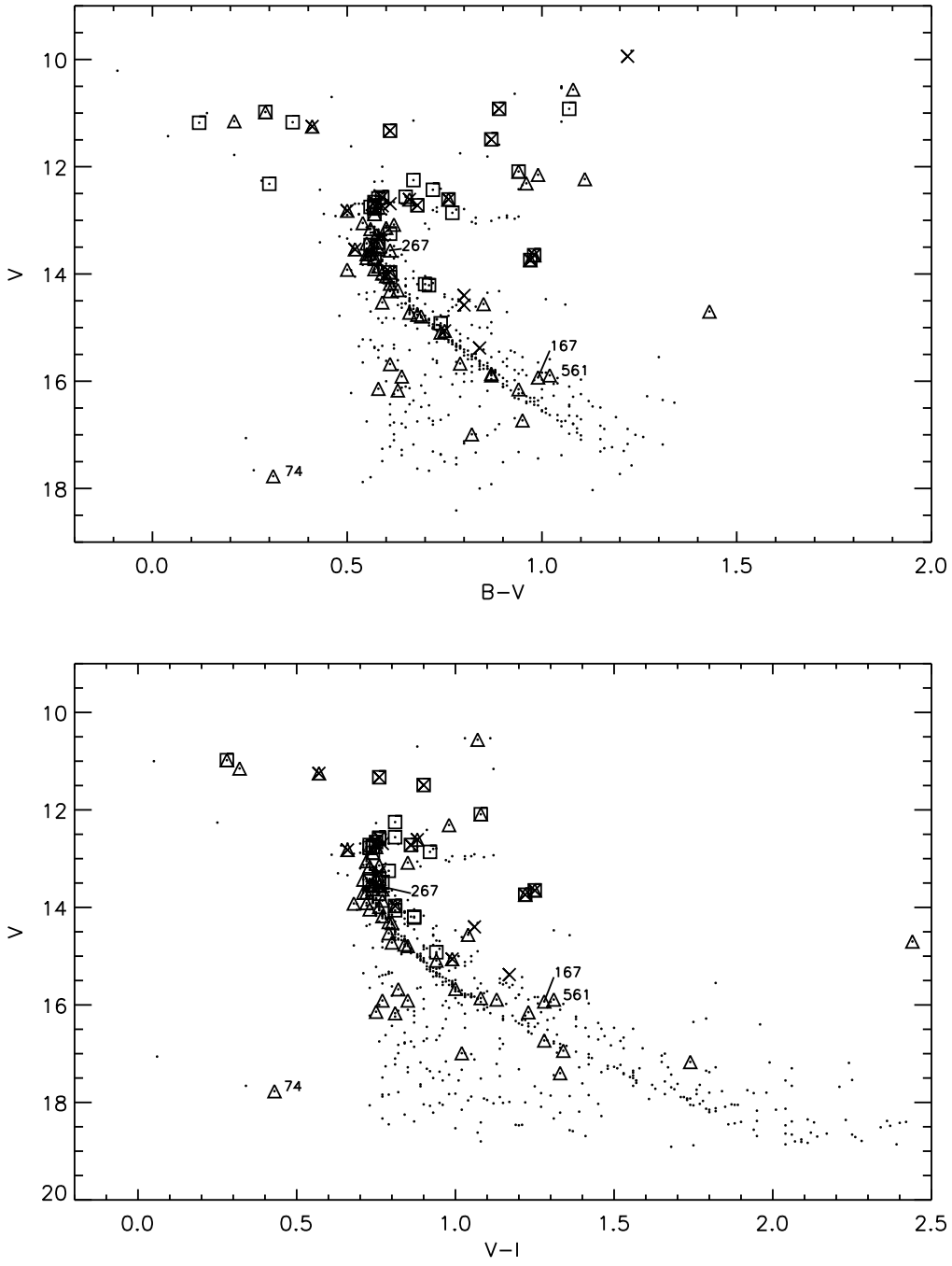

Figure 4.2: Colour-magnitude diagrams that show V versus $(B-V)$ and V versus $(V-I)$ for all the stars in our observations. The variables listed in Table 4.3 are indicated with triangles, spectroscopic binaries with squares and X-ray sources with crosses. Periodic variables discussed in Sect. 4.3.2 are indicated.

that a small number of stars (~ 3) has been classified as a variable by chance.

Variable stars

To give some clue as to the nature of the stars listed in Table 4.3 and, ultimately, to the physical origin of the observed photometric variability, we plot these stars in the colour-magnitude diagrams shown in Fig. 4.2. In addition to these variables (shown as triangles), we also indicate the known X-ray sources (shown as X's) and the known spectroscopic binaries (shown as squares). The paucity of spectroscopic binaries below $V \sim 14$ is a bias effect due to the sensitivity limit of present spectroscopic surveys in the cluster (e.g. Latham et al. 1992). We find photometric variables in all regions of the cluster colour-magnitude diagram; we discuss stars in each of the various regions in more detail in the following section.

Periodic variables

Aside from the X-ray sources which are the subject of Paper I, we detected definitive periods in the light curves of only four stars.

For **star 74** it is unclear whether the correct photometric period is 0.1444(2) days (the best period as determined by the period search) or twice that: the data points at minimum light have sufficiently large errors that it is unclear whether or not the light curve consists of two dips with unequal depths. In Fig. 4.3 the data are folded on the 0.1444 days. The $(B-V)$ and $(V-I)$ colour variations are not significant. We discuss this star in greater detail in Sect. 4.6.

Star 167 is located on the cluster binary sequence and exhibits a periodic light curve with $P = 3.7(3)$ days in V, $P = 3.4(2)$ days in B, both retrieved from data of run 1. The I data show no significant periodic variation. The V-band light curve of this star is shown in Fig. 4.3. The $(B-V)$ and $(V-I)$ colour variations are not significant.

For **star 267** (S 757) the period was determined by the combined data of run 1 and 5 (B and V), that together cover a time span of 2 years. As with star 74, it is not entirely certain whether the correct photometric period is 0.3600(1) days (assuming its light curve is intrinsically double-peaked) or half that value, 0.18000(5) days, which is in fact the best period as determined by the period search. In Fig. 4.3 the data are folded on the longer period. This star was first noted to be a photometric variable by Rajamohan (1988), although no periodicity was reported. The star shows no significant $(B-V)$ and $(V-I)$ colour variations. We discuss this star and our reasons for labelling it a (previously unknown) W UMa system in Sect. 4.4.3.

Star 561 (ET Cnc, or III-79 in the nomenclature of Eggen & Sandage 1964) was identified as a W UMa system with a period of 6.49 hours by Gilliland et al. (1991) but no error in the period was specified. We searched for a period in a narrow window between 0.1 and 0.15 days (the power at half the period is much larger than at the full period) and find a best period from

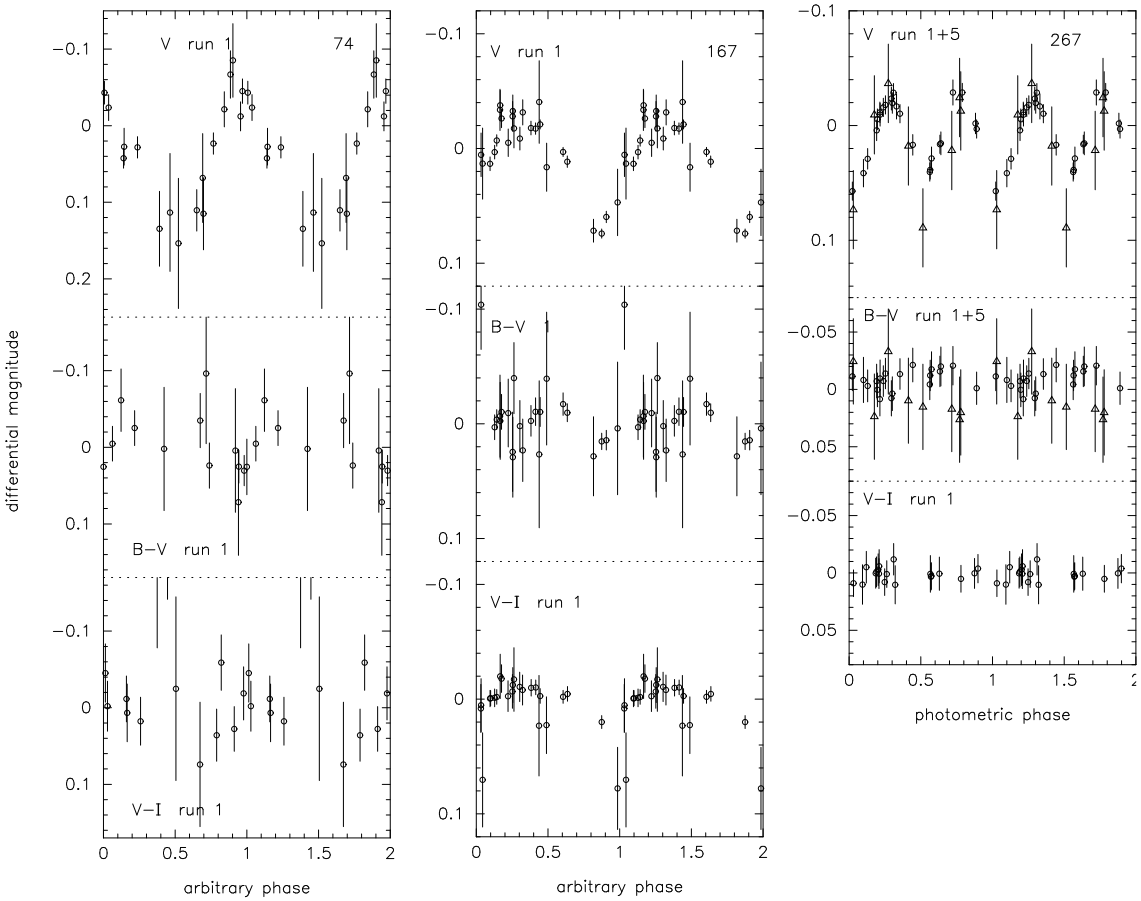

Figure 4.3: Light and colour curves for stars 74, 167 and 267 (S 757) folded on the photometric period of 0.1444, 3.7 and 0.3600 days, respectively. Data from different observing runs are marked with different symbols: open circles for run 1, open triangles for run 5.

our photometry of run 1 of 0.1356(4) days (in B and V, 0.1351(4) days in I) which gives a full period of 6.51(2) hours, compatible with Gilliland's measurement. The data are folded on this period in Fig. 4.4. The system is slightly redder during primary eclipse than during secondary eclipse. This star is discussed further along with star 267 in Sect. 4.4.3.

Tentative periods

In addition to the four variables showing statistically significant periods, we indicate in Table 4.3 possible periods for another eight stars, whose light curves show some evidence for coherent variations on time scales longer than our observing windows. While our period searches did not reveal statistically significant periods for these stars, we include them here as candidate objects for follow-up study. We caution that the periods listed are based solely on our

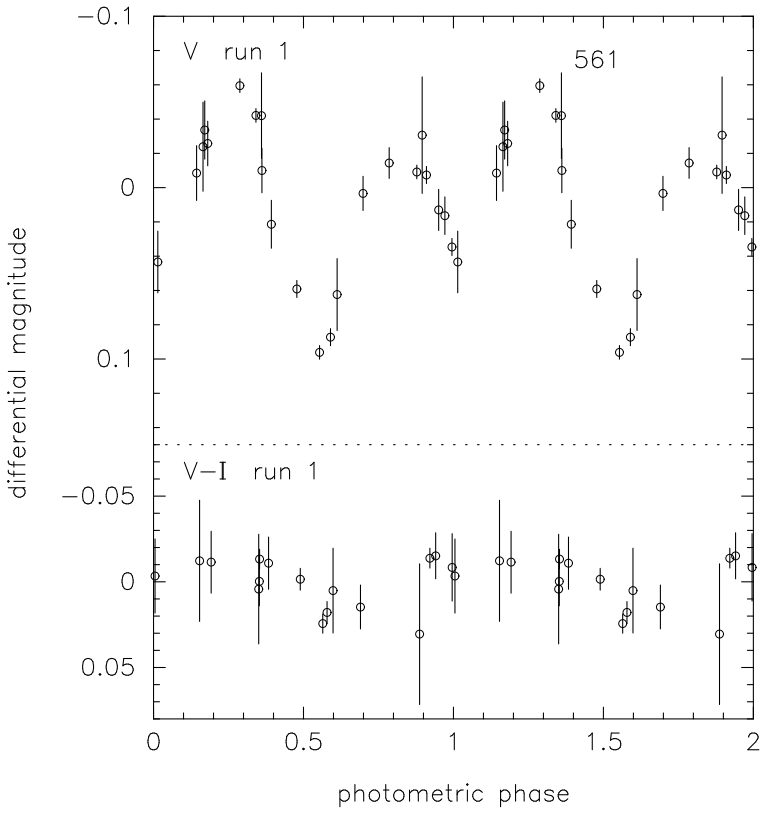

Figure 4.4: Light and colour curves for the contact binary 561 (ET Cnc or III-79) folded on the photometric period of 0.2712 days.

visual impression of the light curves, and should be taken only as a qualitative suggestion of periodicity on the time scale indicated. Of course, these stars do still exhibit statistically significant variability, whether or not that variability is indeed periodic. Of these, star 35 is peculiar in that it is located far to the red of the cluster main sequence in the colour-magnitude diagram. Its colours are those of an M dwarf, so its position in the colour-magnitude diagram suggests that it is a nearby star of the M spectral type. Except for star 308 which does not have the requisite colours to be placed on the colour-magnitude diagram, the rest of these stars are situated on the cluster main sequence.

4.4 Discussion

We turn now to a discussion of the nature of those stars identified as photometric variables, using the locations of these stars in the colour-magnitude diagram as a way of organising the discussion.

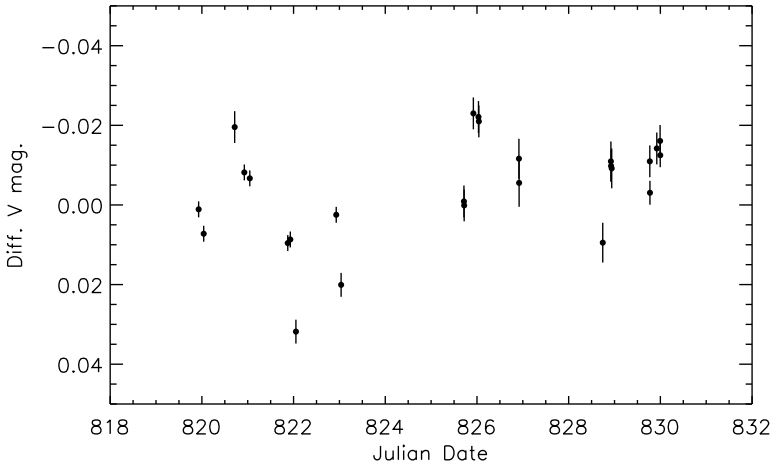

Figure 4.5: Light curve for the star 208.

4.4.1 Stars below the cluster main sequence

Cluster non-members

To begin, we immediately dispense with those stars located below the cluster main sequence. In all 7 cases, our light curves show only apparently low-level random photometric variations (although in one case, star 529, the variations are > 0.2 mag), and the available proper-motion membership probabilities confirm non-membership in the cluster. While our data provide very limited information about the nature of the observed variability, we speculate that it is due to flares. Fig. 4.5 shows the V-band light curve for star 208 as an example of the variable stars located below the cluster main sequence.

Possible new white dwarf?

One of the stars showing periodic photometric variability in our database is star number 74. The light curve shows a best period of 0.1444 days. While no membership information is available for this star, its position in the colour-magnitude diagram together with its photometric behaviour make this object worthy of further study.

Without additional information, it is difficult to make definitive statements about the nature of this star, especially with respect to its evolutionary status. One obvious possibility given its position in the colour-magnitude diagram is that it is a cooling white dwarf. Another possibility based on its light curve is that it is a field W UMa system (in which case the photometric period would be twice the observed one, 0.2888 days).

With $V = 17.8$, $(B-V) = 0.31$, and $(V-I) = 0.43$ (see Table 4.3), the star's colours are somewhat redder than the theoretical white dwarf cooling curve for the cluster. The cooling curve for M 67 presented by Richer et al. (1998) has $(V-I) \sim -0.1$ for the same V magnitude. Nonetheless, the far-ultraviolet photometric study of Landsman et al. (1998) identified several

white dwarf candidates in M 67, and two of them (BATC 4672 and BATC 3009) are similarly situated in the colour-magnitude diagram, with $V \sim 17.5$ and $(B-V) \sim 0.3$ (star 74 is *not* one of these objects). If star 74 is indeed a single white dwarf, the nature of its short-period photometric variability remains unknown. The period of 0.14 days is much longer than the periods of pulsation commonly ascribed to ZZ Ceti white dwarf variables ($\sim$ few minutes). Perhaps a faint, red dwarf companion is responsible for this star's position in the colour-magnitude diagram. In that case, the variability most likely originates from eclipses or interaction in the binary while the period of 0.1444 days reflects (half) the orbital period.

With the colours of a main-sequence early-F star, an alternative explanation for star 74 may be that it is a distant δ Scuti variable; such stars are typically of type A or F, with periods of pulsation of less than 0.3 days and light curve amplitudes of ~ 0.2 mag (Feast 1996). On the other hand, if star 74 is a W UMa system, its photometric period is much too short to place it on the standard W UMa period-colour relation (e.g. Rucinski 1993). A period of 0.28 days is appropriate to W UMa variables with $(B-V) \approx 0.9$; however, star 74 is considerably bluer. Thus, the nature of this star remains unclear.

4.4.2 Stars on the cluster main sequence

In Sect. 4.3.2 we mentioned several stars situated on the cluster main sequence that show some evidence for periodic variability. If these tentative periods are upheld, they may be related to the stellar rotation periods (due to, e.g., starspot modulation). In addition, we have found 30 stars whose light curves show non-periodic variations at a statistically significant level. The amplitudes of variability exhibited by a few of these stars is remarkably large (few tenths of a mag; see Fig. 4.1). Our data do not shed much light on the nature and physical origins of this variability. Perhaps the variations we observe have their origin in stochastic activity on the surfaces of these G and K stars.

Two of the variable stars on the cluster main sequence have been monitored spectroscopically. Star 851 (S 1506) was monitored by Mathieu et al. (1986) for radial-velocity variations, but no indication of binarity was found ($\sigma = 1$ km s^{-1} in 8 observations spanning 2 years). On the other hand, star 911 (S 1508), situated at the cluster turnoff, was found by Mathieu et al. (1990) to be a spectroscopic binary with an orbital period of 25.9 days and an eccentricity of 0.44. The *BVI* light curves of this star do not show evidence for periodic variability on the spectroscopic orbital period or the pseudo-synchronous period (Hut 1981) of 11.2 days.

4.4.3 Stars on the cluster binary sequence

Photometric variables on the cluster binary sequence are interesting because such variability can point the way to the discovery of interacting binary systems. If periodic, the observed variability may be intimately related to the dynamics of the binary system. Three of the variables for which we found a photometric period are located on the binary sequence.

ET Cnc has a semi-amplitude of only 0.08 mag, which is relatively small for a contact system. The unequal eclipses in the observed light curve potentially indicate that the system

is in poor thermal contact or is semi-detached (see also discussion in Paper I on the X-ray source W UMa S 1036).

We have discovered that star 267 (S 757) is a strong candidate for being a W UMa system in M 67. Sanders (1977) gives this star a proper-motion membership probability of 95%, making it a very likely member of the cluster. The most likely period from our time-series analysis is 0.1800 days, which we interpret as the half-period of 0.3600 days, assuming that the light curve consists of two eclipses of very similar depth. Spectroscopic radial-velocity measurements will be needed to confirm this period. Nonetheless, a period of 0.36 days places this star on the W UMa period-colour relation very well, given its $(B-V)$ colour of 0.61.

In addition to these two contact binary systems, we have also discovered periodic variability in another star on the cluster binary sequence, star 167 with a period of 3.6 days. While our data permit us to say little about this star, its location in the colour-magnitude diagram and its periodic light curve make this a prime candidate for follow-up spectroscopic monitoring. Perhaps the observed photometric period corresponds to the binary orbital period. No membership information is presently available for this star.

Finally, we note that we have found two more stars situated on the cluster binary sequence that did not evince periodic variability in our data, but nonetheless showed statistically significant variability. These stars deserve spectroscopic follow-up to determine if they are interacting binary systems. These stars do not presently possess membership probability measurements.

4.4.4 Giant stars

Four of the variables reside on the red giant branch of the cluster colour-magnitude diagram (we discount star 612 as its photometry is suspect due to the presence of a close neighbour). These variables show relatively low levels of variability, with r.m.s. ~ 0.02 mag. For the other giant stars included in our observations, we can place 3σ upper limits on variability of ~ 0.015 mag, based on the limiting photometric precision of our photometry for the brightest sources.

The variable star 591 (S 1279) is a K1 III star that was monitored for radial-velocity variations by Mathieu et al. (1986), but no indication of binarity was found. Similarly, Mathieu et al. monitored the giants 732 (S 1293) and 690 (S 1305), but found no evidence for radial-velocity variations ($\sigma \leq 0.5$ km s^{-1} in about 15 observations spanning more than 10 years, for all three stars). Thus we consider it unlikely that the variability is related to binarity. Henry et al. (2000) found a large fraction of low-amplitude (~ 0.01 mag) photometric variables among a sample of 187 G ($\sim 25\%$) and K ($\sim 50\%$) giants. For the group of giants of type earlier than K2 – that also includes our four variable giants – they exclude both radial pulsation and rotational spot-modulation as the origin of the brightness variations. Henry et al. suggest that non-radial, *g*-mode pulsations most likely give rise to the variability.

Interestingly, star 973 shows a peculiar light curve, with rapid, short-duration dips (Fig. 4.6).

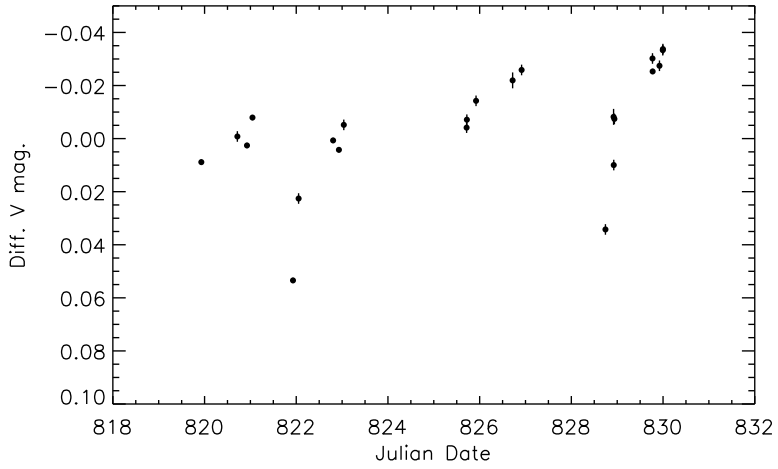

Figure 4.6: Light curve for the giant star 973.

4.4.5 Blue stragglers

Two of the blue stragglers in M 67 not detected in X-rays show statistically significant photometric variability in our data. Photometric variability among blue stragglers is particularly interesting in light of the uncertain evolutionary status of these objects. Photometric variability may be a clue to the presence of a binary companion (e.g. in the case of the eclipsing blue straggler S 1082, see Goranskij et al. 1992, van den Berg et al. 2001a [Chapter 5]) or may provide information on the stellar structure of the stars (in the case of oscillations, see discussion in Gilliland & Brown 1992).

Star 679 (EX Cnc or S 1284) is a spectroscopic binary that shows low-amplitude photometric variations with a period of ~ 1.3 hours first discovered by Gilliland et al. (1991, 1992) and Simoda (1991). The *B* and *V* light curves we obtained during the highly sampled run 4 show a similar behaviour. These short-timescale variations are probably related to the star's position within the δ Scuti instability strip and not to the orbital period of 4.2 days (Milone & Latham 1992)

Star 655 (S 1263) was monitored spectroscopically by Milone et al. (1992), but no orbit was determined. Gilliland et al. included this star in their search for solar-analog oscillations, but no evidence for variability was found. Simoda (1991) similarly found no evidence for photometric variability, but Kim et al. (1996) do report a high dispersion in the light curve of this star. The light curves that results from our observations also display a large scatter up to 0.04 mag around the average magnitude in all four bands.

4.5 Conclusions

Our survey of photometric variability among 991 stars in the old open cluster M 67 detected 69 variable stars. Membership information is available for 405 stars (36 variables) included in

our observations and marks 316 (27 variables) as members with a probability larger than 35% (Girard et al. 1989). Out of this group of 27 variable members, 9 show periodic variations.

In all cases the amplitude of variability is low, ranging from a few hundredths to a few tenths of a magnitude. Our study is sensitive to brightness variations on time scales of 0.3 hours to $\sim$ 20 days. Apparently, at the age of M 67 periodic variability on these time scales at these amplitudes is rare for single stars, as in 7 (probably 8 if we include the new candidate contact system S 757) cases, all X-ray sources, the variability finds its origin in the binary nature of the stars (eclipses, ellipsoidal variations, rotational spot-modulation in tidally locked binaries). This confirms the picture that rapid rotation in an old population can only be maintained in close binaries.

In the contact binary 561 (ET Cnc), for which no membership information exists, the variability is the result of binarity as well. We encourage spectroscopic observations of the three remaining stars that exhibit periodic variations (the faint and blue star 74 and star 167 on the binary sequence, both without membership information) and the member 523 (S 1112, discussed in paper I) to establish their binary status and/or obtain an indication for membership from their radial velocity. Also, more observations should be obtained of the stars for which we provide tentative periods, in the first place to further examine if their photometric variability is indeed periodic and secondly to establish if they are single or binary.

The origin of the photometric variability for the remaining stars discussed in this paper is in most cases unknown. As possible causes for the variations we suggest low-level surface activity, stellar pulsations or, especially for the stars on the binary sequence, binary interaction.

Caption to Table 4.1. Master list of all 991 stellar sources included in our observations, sorted in order of increasing right ascension. From left to right: identification number; right ascension and declination in 1950-coordinates; Sanders' identification number and proper-motion cluster-membership probability (Sanders 1977); Girard et al.'s identification number, proper-motion cluster-membership probability P_μ, proper-motion membership probability taking into account the star's position relative to the cluster centre $P_{\mu,\mathrm{r}}$ and radial-velocity membership probability P_{rv}(Girard et al. 1989); Zhao et al. identification number and proper-motion membership probability (Zhao et al. 1993); Eggen & Sandage (1964) identification number; Fagerholm (1906) identification number; Montgomery et al. (1993) identificaton number.

Caption to Table 4.2. Mean *BVI* photometry for the 991 stellar sources in our database.

Acknowledgements – The authors wish to thank Magiel Janson, Rien Dijkstra, Gertie Geertsema, Remon Cornelisse and Gijs Nelemans for obtaining part of the data used in the paper. The Kitt Peak National Observatory is part of the National Optical Astronomy Observatories, which is operated by the Association of Universities for Research in Astronomy, Inc. (AURA) under cooperative agreement with the National Science Foundation. The Jacobus Kapteyn Telescope is operated on the island of

La Palma by the Isaac Newton Group in the Spanish Observatorio del Roque de los Muchachos of the Instituto de Astrofisica de Canarias. The Dutch 0.91-m Telescope is operated at La Silla by the European Southern Observatory. IRAF is distributed by the National Optical Astronomy Observatories, which are operated by the Association of Universities for Research in Astronomy, Inc., under cooperative agreement with the National Science Foundation. This research made extensive use of the WEBDA Open Cluster Database developed and maintained by J.-C. Mermilliod. MvdB is supported by the Netherlands Organization for Scientific Research (NWO).

References

Dinescu, D. I., Demarque, P., Guenther, D. B., & Pinsonneault, M. H. 1995, AJ, 109, 2090

Eggen, O. J. & Sandage, A. R. 1964, ApJ, 140, 130

Fagerholm, E. 1906, PhD thesis, Uppsala Univ.

Feast, M. W. 1996, in Light curves of variable stars - A pictorial atlas, ed. C. Sterken & C. Jaschek (Cambridge University Press), 81

Gilliland, R. L. & Brown, T. M. 1992, AJ, 103, 1945

Gilliland, R. L., Brown, T. M., Duncan, D. K., Suntzeff, N. B., Lockwood, G. W., Thompson, D. T., Schild, R. E., Jeffrey, W. A., & Penprase, B. E. 1991, AJ, 101, 541

Girard, T. M., Grundy, W. M., López, C. E., & van Altena, W. F. 1989, AJ, 98, 227

Goranskij, V. P., Kusakin, A. V., Mironov, A. V., Moshkaljov, V. G., & Pastukhova, E. N. 1992, Astron. Astrophys. Trans., 2, 201

Henry, G. W., Fekel, F. C., Henry, S. M., & Hall, D. S. 2000, ApJS, 130, 201

Honeycutt, R. K. 1992, PASP, 104, 435

Hut, P. 1981, A&A, 99, 126

Kim, S.-L., Chun, M.-Y., Park, B.-G., & Lee, S.-W. 1996, Journal of the Korean Astronomical Society, 29, 43

Landsman, W., Bohlin, R. C., Neff, S. G., O'Connell, R. W., Roberts, M. S., Smith, A. M., & Stecher, T. P. 1998, AJ, 116, 789

Latham, D. W., Mathieu, R. D., Milone, A. A. E., & Davis, R. J. 1992, in Binaries as tracers of stellar formation, ed. A. Duquennoy & M. Mayor (Cambridge: Cambridge University Press), 132

Mathieu, R. D., Latham, D. W., & Griffin, R. F. 1990, AJ, 100, 1859

Mathieu, R. D., Latham, D. W., Griffin, R. F., & Gunn, J. E. 1986, AJ, 92, 1100

Milone, A. A. E. & Latham, D. W. 1992, in Evolutionary processes in interacting binary stars, ed. Y. Kondo, R. F. Sistero, & R. S. Polidan, 475

Milone, A. A. E., Latham, D. W., Mathieu, R. D., Morse, J. A., & Davis, R. J. 1992, in Evolutionary Processes in interacting binary stars, ed. Y. Kondo, R. F. Sistero, & R. S. Polidan, 473

Montgomery, K. A., Marschall, L. A., & Janes, K. A. 1993, AJ, 106, 181

Nissen, P. E., Twarog, B. A., & Crawford, D. L. 1987, AJ, 93, 634

Rajamohan, R., Bhattacharyya, J. C., Subramanian, V., & Kuppuswamy, K. 1988, Bull. Astr. Soc. India, 16, 139

Richer, H. B., Fahlman, G. G., Rosvick, J., & Ibata, R. 1998, ApJ, 116, L91

Rucinski, S. M. 1993, in The realm of interacting binary stars, ed. J. Sahade, G. McCluskey, & Y. Kondo (Astrophysics and Space Science Library, Dordrecht: Kluwer), 111

Sanders, W. L. 1977, A&AS, 27, 89
Scargle, J. D. 1982, ApJ, 263, 835
Simoda, M. 1991, IBVS 3675
van den Berg, M., Orosz, J., Verbunt, F., & Stassun, K. 2001a, A&A, 375, 375
van den Berg, M., Stassun, K., Verbunt, F., & Mathieu, R. D. 2001b, A&A, submitted (Paper I)
Woodward, M. & Hudson, H. S. 1983, Nat, 305, 589
Zhao, J. L., Tian, K. P., Pan, R. S., He, Y. P., & Shi, H. M. 1993, A&AS, 100, 243

Chapter 5

The blue straggler S 1082: a triple system in the old open cluster M 67

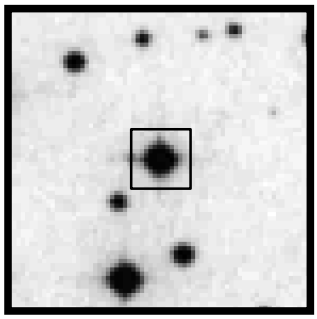

Maureen van den Berg, Jerome Orosz, Frank Verbunt & Keivan G. Stassun
Astronomy & Astrophysics 2001, 375, 375

Abstract – We present a photometric and spectroscopic study of the blue straggler S 1082 in the open cluster M 67. Our observations confirm the previously reported 1.07 day eclipse light curve and the absence of large radial-velocity variations of the narrow-lined star. However, we find two more spectral components which *do* vary on the 1.07 day period. We conclude that the system is triple. We fit the light and radial-velocity curves and find that the total mass of the inner binary is more than twice the turnoff mass and that the outer companion to the binary is a blue straggler on its own account. We briefly discuss formation scenarios for this multiple system.

5.1 Introduction

Blue stragglers are stars that are bluer and more luminous than the main-sequence turnoff of the population to which they belong. Hence they appear to be either younger than the

other stars or have main-sequence lifetimes that exceed those of stars of similar mass. Blue stragglers are easiest to distinguish in globular and open clusters but are also found among field halo stars. Formation scenarios that require anomalous evolution of a single star are considered less likely than explanations that involve the interaction of stars in a binary or in a multiple-star encounter. For example, a blue straggler may be formed when one star in a binary accretes a substantial amount of mass from its companion or when two stars merge either in a binary or in a collision. In the last case, blue stragglers carry information about the high-stellar density environments in which they are found. Reviews on blue stragglers are given by e.g. Stryker (1993) and Bailyn (1995).

The blue stragglers in M 67 have received frequent attention. Ten of them were monitored for radial-velocity variations for nearly twenty years; this revealed one short-period (4.2 day) eccentric binary and five circular and eccentric binaries with periods between 850 and 5000 days (Milone & Latham 1992, Latham & Milone 1996). Leonard (1996) and Hurley et al. (2001) concluded that not one of the proposed blue-straggler formation mechanisms alone can explain the properties of these binaries.

S 1082 is one of the remaining four blue stragglers without an orbital solution. Its spectrum shows the lines of an early F-type subgiant. These lines show only small radial-velocity variations ($v_{\rm rad} < 7$ km s^{-1} peak-to-peak, Mathieu et al. 1986) and little rotational broadening ($v_{\rm rot} \sin i = 4$–11 km s^{-1}, van den Berg et al. 1999 [Chapter 2]). This appears to be in contradiction to the eclipse light curve with a period of 1.07 days found by Goranskij et al. (1992). The relative velocity v of two stars in a 1.07 day binary is v=208 $(M/M_\odot)^{1/3}$ km s^{-1} where M is the total mass of the binary; the stellar rotation in such a short-period binary is expected to be synchronised with the orbit, giving $v_{\rm rot} = (R/a)v$, with a the distance between the binary stars and R the stellar radius. The eclipse light curve excludes the low inclination as well as the extreme mass ratio required to bring the observed velocity limits in agreement with the predicted values *for an F star in the binary*. We therefore tentatively conclude that S 1082 is a (visual or physical) triple.

Evidence for a short orbital period is also furnished by the variation detected in a broad, shallow component (Mathys 1991) in e.g. the Hα line on time scales of hours (van den Berg et al. 1999) [Chapter 2]. Evidence for a wide orbital period of about 1000 days was found from the radial-velocity variations of the narrow lines of the F star (Milone 1991).

We have collected multiband photometry of S 1082 together with high-resolution spectra that sample the light curves at different phases. Our goal was to investigate the eclipses found by Goranskij et al., to monitor the variability of the second spectral component as function of photometric phase and to model the light curve together with the radial-velocity curves. Sect. 5.2 describes the observations and data reduction. The results of the spectroscopic and light curve analysis are presented in Sect. 5.3 and Sect. 5.4. In Sect. 5.5 we summarise our interpretation of the nature of this blue straggler.

Run	Dates	Telescope	Filters	$t_{\rm exp}$ (s)
1	1999 Feb 8-19	0.91-m ESO	U, B, V, Gunn i	300, 120, 120, 120
2	1999 Dec 25, 26	1-m ING JKT	B, V	75, 30
3	2000 Feb 13-16, 20	1-m ING JKT	U, B, V, I	350, 30, 15, 8

Table 5.1: Log of the photometric observations. For each run we give the date of the observations, the telescope and filters used and the typical exposure time for each filter.

5.2 Observations and data reduction

5.2.1 Photometry

S 1082 was monitored in the U, B, V, I and Gunn i bands on three occasions (see Table 5.1). In run 1 we observed the star during twelve nights with the 0.91-m ESO Dutch telescope at La Silla. The observing schedule was divided in four blocks of three nights; every first night the star was observed for an average of 5 consecutive hours in a UBV Gunn i-exposure sequence while every second and third night typically one to three exposures were taken in each filter. During both nights of run 2, S 1082 was observed for several hours with the 1-m Jacobus Kapteyn Telescope on La Palma. In run 3, also on the Jacobus Kapteyn Telescope, we aimed to complete the phase coverage of the light curve between phases 0–0.3.

Standard reduction steps of bias subtraction and flatfielding were performed with IRAF routines. Aperture photometry for all the stars in the field was done with the DAOPHOT.PHOT task. Differential light curves for each individual dataset were computed with ensemble photometry (Honeycutt 1992). The variability properties of the other stars in the fields are discussed in van den Berg et al. (2001) [Chapter 3] and Stassun et al. (in preparation) [Chapter 4]. We refer the readers to these papers for a full description of the observations and the photometry reduction.

5.2.2 Spectroscopy

High-resolution spectra

High-resolution (R $\approx$ 49 000) echelle spectra were taken with the Utrecht Echelle Spectrograph on the 4.2-m William Herschel Telescope on La Palma. S 1082 was observed on four nights in 1996 and 2000 (see Table 5.2 for a log of all spectroscopic observations).

The 1996-spectra were centred on a blue (4250 Å) and red (5930 Å) wavelength. The 31 lines mm^{-1} grating was used in combination with the 1024x1024 pixels^2 TEK-CCD. For a full description of the spectra of run 1 we refer to van den Berg et al. (1999) [Chapter 2].

The spectra of 2000 were all taken with the same instrumental setup: the 79 lines mm^{-1} grating was used with the 2148x2148 pixels^2 SITe1-CCD while the spectra were centred on 5584 Å. In run 2 the seeing was about 2″, while light clouds were present during the start

Run	Dates	$\Delta\lambda$	#	$t_{\rm exp}$ (s)	Inst	RV
1	1996 Feb 28	3920–4920	2	600, 300	UES	HD 136202[a]
		4890–7940	3	360	UES	HD 136202
2	2000 Feb 16	4380–8650	17	1200	UES	HD 89449[b]
3	2000 Feb 20	3535–5035	1	900	IDS	–
4	2000 Feb 22	3535–5035	1	900	IDS	–
5	2000 Mar 13	4380–8650	4	1800	UES	HD 89449
6	2000 Mar 20	4380–8650	5	1200	UES	HD 89449

[a]F8III-IV, [b]F6IV (Simbad)

Table 5.2: Log of the spectroscopic observations. For each run we give the date of the observations, the wavelength coverage in Å, the number of observations, the exposure time in seconds, the spectrograph used and (if applicable) the radial-velocity standard.

of the run. The slit width was set to $1''$. To secure stability, no changes were made to the instrumental setup during the night. In the first two observations of run 5 the seeing was about $2''$; this deteriorated to $3''$ with cloudiness during the last two observations. As the slit width was kept fixed at $1''$, these spectra are of bad quality. In run 6 the seeing was $2''$ during the first two observations but later improved to $1\farcs6$. The slit width was accordingly changed from 2 to $1\farcs2$. Due to the wider slit these spectra have a lower resolution than the spectra of run 1 and 5. All frames were exposed for 1200 s, except for those of run 5 that were exposed for 1800 s to account for the bad seeing conditions. During each run we observed radial-velocity standards. Flatfield images were made with exposures of a Tungsten lamp. Thorium-Argon lamp emission-line spectra were taken for wavelength calibration.

Data-reduction was done in IRAF with CCDRED and ECHELLE routines. After correcting the frames for the electronic bias and after flat fielding, spectra for each echelle-order were extracted with optimal extraction. Towards the red, gaps occur in the wavelength coverage. For the wavelength calibration, fifth-order polynomials were fitted in both directions to the positions of the arclines on the CCD; the maximum residuals to the fit were ~ 0.0125 Å corresponding to 0.75 km s^{-1}. Low-order polynomials were fitted to the spectra for continuum normalisation.

Intermediate-resolution spectra

Two intermediate-resolution (R $\approx$ 3600) spectra were obtained with the Intermediate Dispersion Spectrograph (IDS) mounted on the 2.5-m Isaac Newton Telescope on La Palma, on February 20.90214, 2000 (UT) and February 22.85523 (UT). The R1200B grating and the EEV10 CCD combination gave a spectral resolution of 1.19 Å (FWHM) and a useful wavelength range of 3533-4825Å. The exposure times were 900 s each, and the signal-to-noise level in the extracted spectra ranged from about 65 per pixel near the Balmer jump to about 150 near 4750 Å.

5.3 Results

5.3.1 Eclipse light curve

The new light curves of S 1082 confirm the findings of Goranskij et al. (1992) and fill in the gap in their data between photometric phase 0.53 and 0.74 (with phase 0 corresponding to primary minimum). In Fig. 5.1 our data are folded on their ephemeris for the primary minimum:

$$\mathrm{Min\ I} = 2\,444\,643.253(5) + 1\overset{\mathrm{d}}{.}0677978(50)\,E \qquad (5.1)$$

Two unequal eclipses with an amplitude of about 0.09 and 0.05 mag in V are clearly visible with the deeper, primary eclipses occurring around phase 0 as expected from Eq. 5.1. Goranskij et al. note that the light curve near second quadrature (phase 0.75) is systematically higher than near first quadrature (phase 0.25) by 0.01 to 0.02 mag in V. This might also be the case in our data, but the scatter between phases 0.1 and 0.3 makes this difficult to see. The scatter is probably related to the bad observing conditions (nearby moon) of the last run.

5.3.2 Spectral line profiles

The spectra of S 1082 are dominated by a narrow-lined component resembling a star of type early-F. In addition, the presence of a broad and shallow component in the high-resolution spectra is prominent in the Hα line (see also van den Berg et al. 1999 [Chapter 2]). When the spectra are arranged in order of light curve phase using Eq. 5.1, it is clear that the position and strength of the asymmetric absorption in the wings vary regularly (Fig. 5.2); the spectra that were included in Fig. 8 of van den Berg et al. (1999) [Fig 2.8] correspond to photometric phases 0.092, 0.16 and 0.25. Around first quadrature (phase 0.25) the depth of Hα is smallest while the asymmetric absorption in the wings is maximally blue-shifted; for phases between 0.5 and 1 the phase-coverage is sparser, but in the spectra of phases 0.88 and 0.90 it can be seen that the asymmetric absorption has moved to the red wing. The timing of the velocity shift with respect to the eclipses associates the broad-lined feature with the brighter star in the eclipsing binary (the brighter star must approach us after the primary eclipse). Similar variable line profiles are visible in the Hβ, Na I D, Mg I b and Ca II infrared lines (Fig. 5.3).

The temperature of the narrow-lined star in S 1082 can be measured with the low-resolution spectra. We assume that its light is least contaminated by its companion star(s) in the blue and therefore concentrate on the region around the Balmer jump. In Fig. 5.4 synthetic spectra for various effective temperatures T_{eff} are compared with the IDS spectrum between 3535 Å and 4050 Å. The spectra were computed with model atmospheres for solar metallicity (Kurucz 1979). The observed spectrum was corrected for the reddening towards M 67 ($E(B-V) = 0.032 \pm 0.006$, Nissen et al. 1987) and for a radial-velocity difference with respect to the model spectra. From the relative strength of the Ca II H&K lines, a sensitive temperature indicator in this region (e.g. Gray & Garrison 1989), and the contrast in the Balmer jump it is clear that the observed spectrum is hotter than that of a 6500 K star.

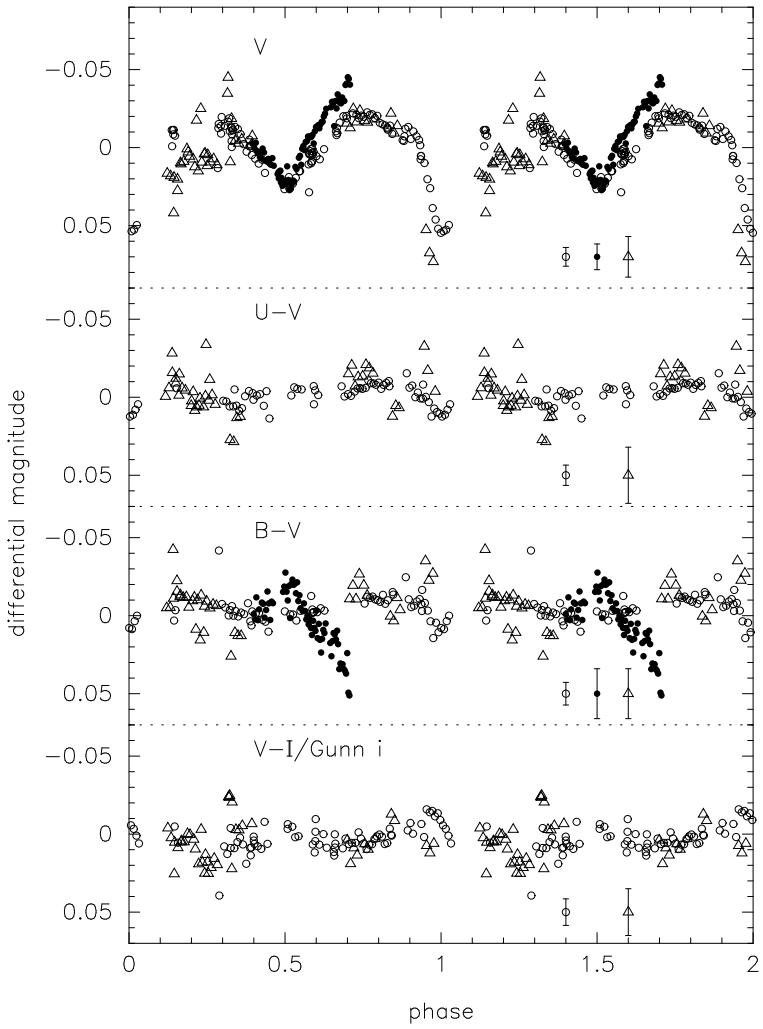

Figure 5.1: Light and colour curves for S 1082 folded on the ephemeris of Goranskij et al. (1992). Data from the three runs are indicated with different symbols: open circles for run 1, filled circles for run 2 and triangles for run 3. A typical error bar is shown for each run. Magnitude and colours are plotted relative to the average V (11.25), U–V (0.45), B–V (0.41) and V–I (0.57) values in our measurements.

This part of the spectrum was fitted to model spectra with surface gravity $\log g$ ranging from 0.5 to 5.0 in steps of 0.5, $T_{\rm eff}$ from 6000 to 8000 K in steps of 250 K and a fixed projected rotational velocity $v_{\rm rot} \sin i$ of 10 km s^{-1}. A free parameter is a wavelength-independent scale factor ranging from 0.025 to 1 in increments of 0.025 that is a measure of the relative contribution of the narrow-lined star. Observed and model spectra were normalised to the flux at 4050 Å. A straight line was fitted to the difference between the observed and each scaled model spectrum. The model that produces the smallest residuals to the fit has $T_{\rm eff} = 7500$ K, $\log g = 4.5$ and scale factor 0.85. If the temperature of the hot star is indeed 7500 K, it is

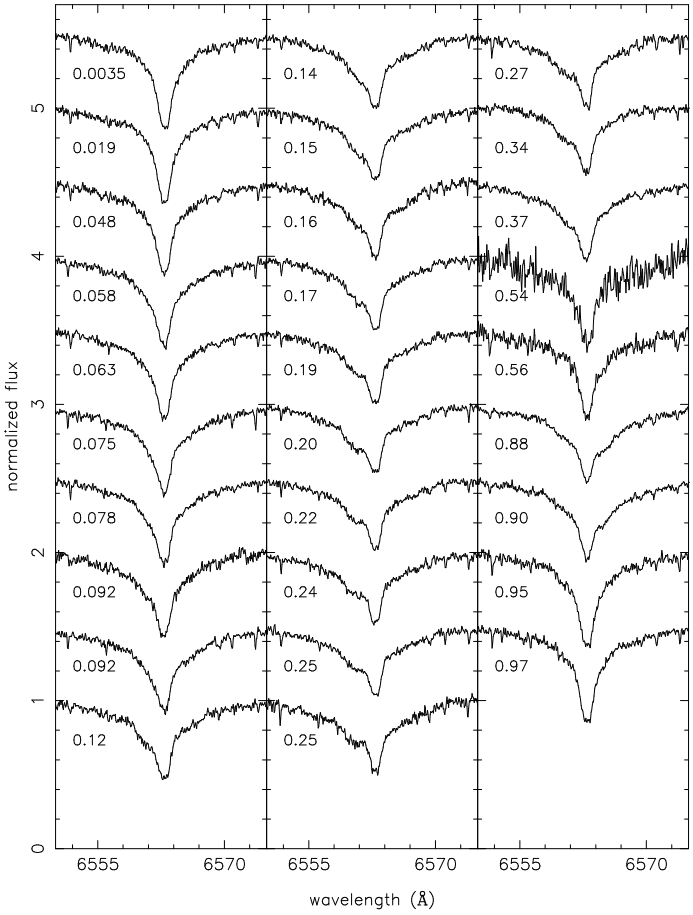

Figure 5.2: Series of Hα profiles in S 1082. The phase of the light curve is indicated for each spectrum. Note the central depth of the line and the asymmetric wings. The observations during phase 0.54 and 0.58 are noisy due to the bad weather conditions of run 5. The continuum separation between the spectra is 0.5 unit.

a late A rather than an F star; the value of $\log g$ is close to that of a main-sequence star for which $\log g \approx 4.25$ (Gray 1992). This shows that the narrow-lined component dominates the spectrum in the blue and it implies that one of the individual components of S 1082 remains a blue straggler. A more accurate decomposition of S 1082 is given in Sect. 5.4.

5.3.3 Radial-velocity curves

Radial velocities were measured via cross correlation of the high-resolution spectra with appropriate template spectra (Table 5.3). To determine the radial velocities of the narrow-lined star in S 1082 we adopted as templates spectra of F-type radial-velocity standards observed during the same run (Table 5.2). Velocities were derived for each order separately. Only orders without strong telluric lines were selected, and included 4890-6820 Å for the 1996-

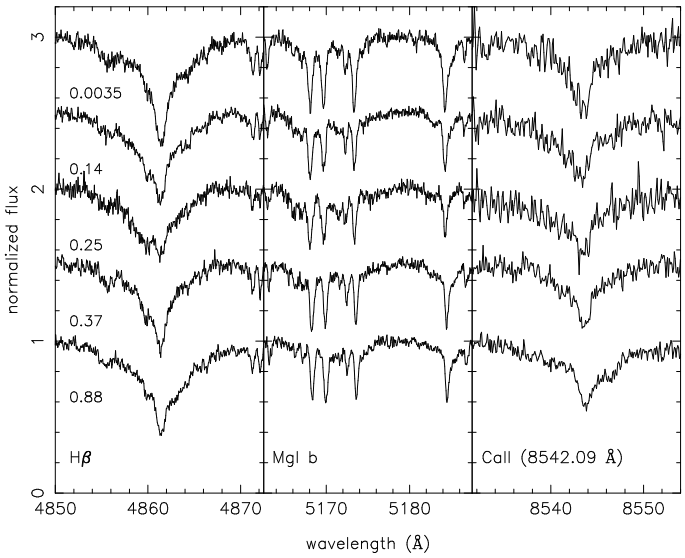

Figure 5.3: Hβ, Mg I b and Ca II infrared lines in S 1082 for a selected set of observations. Light curve phases are indicated. The continuum separation between the spectra is 0.5 unit.

spectra and 4435-6820 Å for the 2000-spectra. The radial velocities listed in the third column of Table 5.3 are the averages of the values from the individual orders; the errors represent the spread around the average. Note that systematic errors can still be included, e.g. due to the wavelength calibration. We expect the latter not to exceed 0.75 km s^{-1} (see Sect. 5.2.2). Our measurements confirm that the narrow-lined component in S 1082 shows radial-velocity variations of only a few km s^{-1}.

The radial-velocity curves of the stars in the eclipsing binary were measured after the contribution of the hot, narrow-lined star to the total spectrum was removed. To that end, all spectra were first brought to the rest frame of the hot star. Then, a hot-star template spectrum was constructed by taking the median of the spectra obtained at phases 0.95, 0.97, 0.0035, 0.019 and 0.048; these particular phases were chosen in order to let the spectral line profiles of the template be as symmetric as possible. For the 1996-spectra, taken with a different instrumental setup, the spectrum obtained at phase 0.092 was chosen as a template. The relative contribution of the hot-star template to the remaining spectra was derived with the same fitting procedure as described in Sect. 5.3.2: the template multiplied with scaling factors ranging from 0.025 to 1 was subtracted from each individual spectrum, and the scaling that produces the smallest residuals around a fit to a straight line was chosen as the appropriate scaling for that particular spectrum. The scaled template was then subtracted from the total spectrum to obtain the spectrum of the binary at various phases.

Next, these residual spectra were correlated against a synthetic spectrum of $T_{\rm eff} = 5250$ K and $\log g = 3.5$. For this model spectrum we chose $v_{\rm rot} \sin i = 50$ km s^{-1} to roughly match the apparently broader lines in the spectrum of the binary. This procedure was repeated for every order between 4380 and 6435 Å, excluding the order that contains the broad Hβ line and

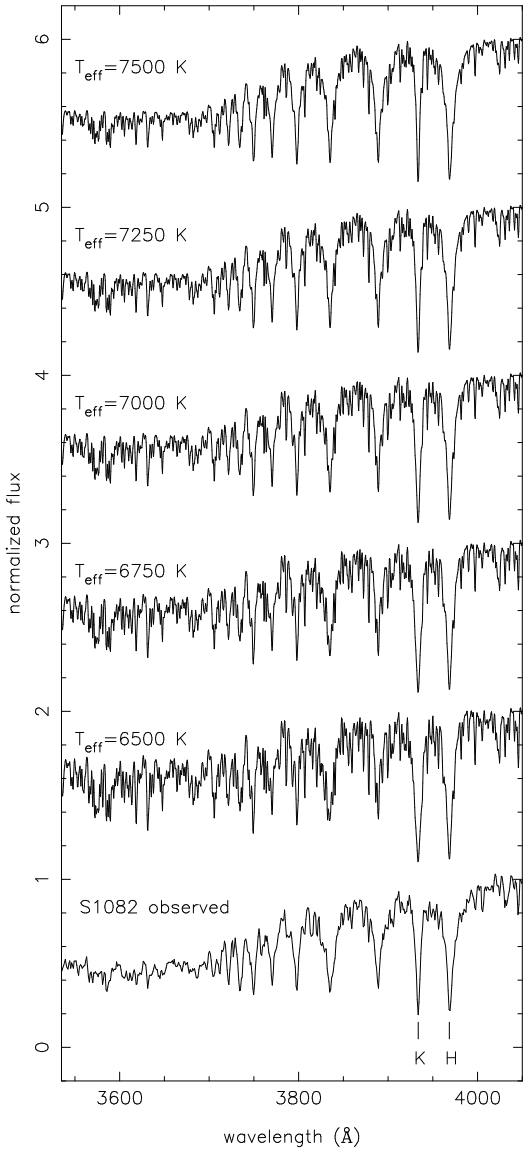

Figure 5.4: Spectrum of S 1082 compared with synthetic spectra of various effective temperatures; surface gravity and projected rotational velocity are fixed at $\log g = 4.5$ and $v_{\rm rot} \sin i = 10$ km s^{-1}. The spectra are normalised to the flux at 4050 Å; each spectrum is offset with 1 unit from the previous spectrum. The relative strength of the Ca II K line and the Ca II H+Hε blend (marked with 'K' and 'H'), and the contrast in the Balmer jump (flux near 4050 Å relative to flux near 3600 Å) are indicators of temperature.

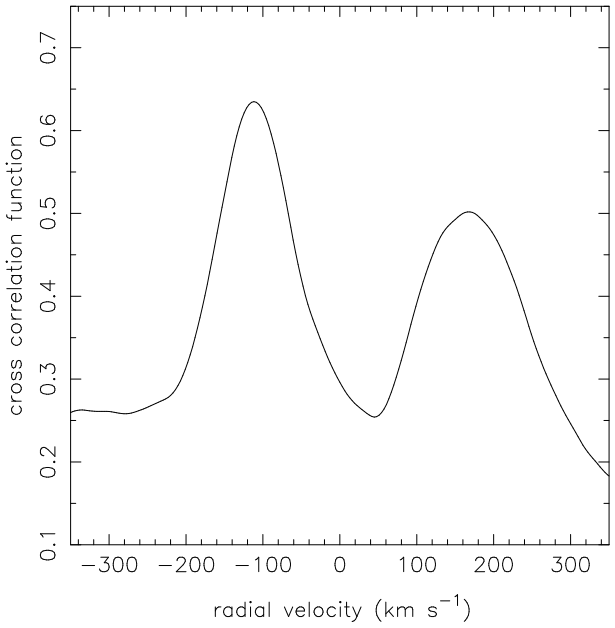

Figure 5.5: Cross correlation function resulting from the residual spectrum taken at photometric phase 0.2535 after the contribution of the hot star is removed. The left peak corresponds to the primary star Aa in the eclipsing binary. The width of the peak corresponding to the secondary Ab is broader which indicates that its spectral lines are more broadened by rotation. For this particular cross correlation the spectrum between 5160 and 5240 Å was used. The radial velocity is given with respect to the hot star B in S 1082.

the region between 5690 and 6090 Å for which the cross correlation functions are very noisy with no clear peaks. A cross correlation peak is sometimes visible at $v_{\rm rad} = 0$ km s^{-1} and represents features of the hot star that were not corrected for (or introduced into the spectrum) by subtraction of the template. The cross correlation functions of most spectra clearly show two peaks with a variable separation (see Fig. 5.5). One peak is smaller and broader than the other, and is redshifted with respect to the template for phases smaller than 0.5; therefore, this peak is identified with the secondary star in the eclipsing binary. This is the first spectroscopic evidence for the third star in S 1082. The measurements of the velocity of the primary near phase 0.1 are probably distorted due to its eclipse by the secondary star. In the following we will refer to the components of the eclipsing binary as Aa and Ab, and to the outer companion as B.

We used the spectrum observed near first quadrature (wavelength region 5160 to 5240 Å containing the Mg I b triplet) to derive an estimate for the projected rotational velocities of both components from the widths of their cross correlation peaks. To that end, we cross correlated a synthetic spectrum of a certain temperature ($\log g = 4.0$, $v_{\rm rot} \sin i = 30$ km s^{-1}) with synthetic templates of the same temperature and surface gravity with $v_{\rm rot} \sin i$ ranging from 10 to 100 km s^{-1}, and with the object spectrum. The peak of the cross correlation functions

HJD− 2 450 000	phot. phase	$v_{\rm rad,B}$ km s^{-1}	$v_{\rm rad,Aa}$ km s^{-1}	$v_{\rm rad,Ab}$ km s^{-1}
142.5101	.09213	33.0±0.1	–	–
142.5790	.1567	33.2±0.1	−97 ± 4	–
142.6837	.2548	32.9±0.2	−108 ± 3	–
1591.3642	.9540	33.5±0.4	–	–
1591.3822	.9709	33.7±0.3	–	–
1591.4170	.003451	34.2±0.3	–	–
1591.4334	.01880	33.7±0.3	–	–
1591.4640	.04750	32.4±0.3	–	–
1591.4805	.06294	32.8±0.3	–	–
1591.4967	.07812	32.7±0.3	−73 ± 4	122±7
1591.5452	.1235	33.2±0.4	−96 ± 3	148±4
1591.5616	.1389	33.3±0.4	−95 ± 2	141±4
1591.5779	.1541	33.3±0.4	−100 ± 2	153±5
1591.5993	.1742	33.1±0.5	−104 ± 2	154±5
1591.6150	.1890	33.5±0.4	−108 ± 2	150±12
1591.6310	.2039	33.9±0.5	−107 ± 3	166±5
1591.6474	.2192	34.2±0.5	−109 ± 2	170±8
1591.6682	.2387	33.8±0.5	−113 ± 2	160±7
1591.6840	.2535	33.9±0.5	−113 ± 3	169±14
1591.7010	.2695	33.9±0.5	−115 ± 2	180±5
1617.4072	.3435	31.8±0.4	−104 ± 2	163±5
1617.4308	.3656	32.7±0.5	−96 ± 2	153±5
1617.6147	.5378	36.0±1.2	28 ± 5	–
1617.6394	.5609	35.2±0.8	–	–
1624.3903	.8832	35.4±0.4	91±3	−130 ± 5
1624.4092	.9009	34.6±0.4	85±4	−132 ± 7
1624.5766	.05765	32.4±0.3	–	–
1624.5949	.07484	32.7±0.3	−80 ± 4	121±6
1624.6131	.09188	32.6±0.4	−90 ± 4	128±5

Table 5.3: Radial velocities of the three stars in S 1082: the components of the eclipsing binary Aa and Ab, and the outer companion B. From left to right: heliocentric Julian date (−2 450 000) at the midpoint of observation; photometric phase computed with the ephemeris of Goranskij et al. (1992); heliocentric radial velocity for star B; radial velocity of the primary Aa and secondary Ab in the eclipsing binary with respect to star B in km s^{-1}. The spectra of phases 0.5378 and 0.5609 were taken under bad observing conditions.

were fitted with gaussian profiles. This was repeated for synthetic spectra of temperatures 5000 to 6750 K in steps of 250 K. With the results we constructed calibration curves for each temperature that give the width of the cross correlation peak as a function of the projected rotational velocity of the synthetic template. The widths of the cross correlation peaks from the object spectrum then give a rough estimate for the $v_{\rm rot}\sin i$ of both stars. For star Aa we obtain a $v_{\rm rot}\sin i$ of 51 km s^{-1} (5750 K) to 58 km s^{-1} (6750 K), for star Ab a $v_{\rm rot}\sin i$ of 83 km s^{-1} (5500, 5750 K) to 87 km s^{-1} (6750 K).

5.4 Parameter estimation for the eclipsing binary

We used the recently written Eclipsing Light Curve (ELC) code of Orosz & Hauschildt (2000) to fit the basic binary observables of S 1082, namely the light curves in the four filters, the two velocity curves and the observed projected rotational velocities of the two stars Aa and Ab. The blue straggler B in this case is modelled as "third light". The addition of a constant (in phase) light will reduce the observed relative amplitudes of the light curves. The ELC code uses model atmosphere specific intensities, so the flux from a third star can be self-consistently added to several different bandpasses (i.e. a blue third light star dilutes the *B*-band light curve of a red binary more than it dilutes the *I*-band light curve). We mainly used the specific intensities derived from the NEXTGEN models (Hauschildt et al. 1999a; 1999b). A few models were also computed using specific intensities derived from Kurucz (1979) models. Only the photometric data of run 1 were used for the light curve fitting as they form the largest set of homogeneous measurements.

We start by estimating the component masses of the eclipsing binary. Unfortunately, we only have radial velocities near one quadrature phase (poor weather prevented us from observing the opposite quadrature), so the velocity amplitudes of the two curves and the binary systemic velocity will not be as constrained as we would like them to be. We fit sinusoids to each of the velocity curves, fixing the period at the photometric period. For star Aa we find $K_{\rm Aa} = 120.8 \pm 6.4$ km s^{-1}, $\gamma_{\rm rel,Aa} = 1.7 \pm 5.8$ km s^{-1}, $\phi_{0,\rm Aa}({\rm spect}) = 0.747 \pm 0.007$, where $\gamma_{\rm rel}$ is the systemic velocity relative to the mean cluster velocity and where $\phi_0({\rm spect})$ refers to the phase of maximum velocity. For star Ab we find $K_{\rm Ab} = 190.1 \pm 12.5$ km s^{-1}, $\gamma_{\rm rel,Ab} = -2.6 \pm 12.5$ km s^{-1}, $\phi_{0,\rm Ab}({\rm spect}) = 0.242 \pm 0.010$. The errors on the individual velocities were scaled to yield $\chi^2_\nu = 1$ for each curve, and the error estimates on the fitted parameters were derived using the scaled uncertainties. The phasing of the curves are consistent with expectations, where star Aa has its maximum velocity one fourth of an orbital cycle before the deeper photometric eclipse. Since systemic velocities are consistent with being zero, we will assume the binary is a cluster member and hence has $\gamma_{\rm rel} = 0$ km s^{-1}. In this case we find for star Aa $K_{\rm Aa} = 119.1 \pm 3.1$ km s^{-1} and $\phi_{0,\rm Aa}({\rm spect}) = 0.748 \pm 0.007$, and for star Ab we find $K_{\rm Ab} = 190.1 \pm 11.6$ km s^{-1} and $\phi_{0,\rm Ab}({\rm spect}) = 0.243 \pm 0.010$. Taking the sinusoid fits at face value, we can immediately compute the mass ratio of the binary. We find $Q \equiv M_{\rm Ab}/M_{\rm Aa} = K_{\rm Aa}/K_{\rm Ab} = 0.63 \pm 0.04$. The minimum masses of the two component stars are then $M_{\rm Aa}\sin^3 i = 2.01 \pm 0.38\,M_\odot$ and $M_{\rm Ab}\sin^3 i = 1.26 \pm 0.27\,M_\odot$ (see Table 5.4 for

parameter	value
$P_{\rm phot}$	1.0677971(7)
T_0	2 444 643.250(2)
V	11.251
$B-V$	0.415
$K_{\rm Aa}$ (km s^{-1})	119.1(3.1)
$K_{\rm Ab}$ (km s^{-1})	190.1(11.6)
Q	0.63(4)
$\gamma_{\rm Aa}$ (km s^{-1})	0.0 [fixed]
$\gamma_{\rm Ab}$ (km s^{-1})	0.0 [fixed]
$M_{\rm Aa}\sin^3 i$ ($M_\odot$)	2.01(38)
$M_{\rm Ab}\sin^3 i$ ($M_\odot$)	1.26(27)
$v_{\rm rot,Aa}\sin i$ (km s^{-1})	56(5)
$v_{\rm rot,Ab}\sin i$ (km s^{-1})	83(5)

Table 5.4: Observed binary parameters. Aa and Ab refer to the stars in the eclipsing binary. V and $B-V$ are taken from Montgomery et al. (1993).

a summary of the observed parameters of the eclipsing binary).

There are a total of twelve free parameters in the model: the filling factors (by radius) of the two stars $f_{\rm Aa}$, $f_{\rm Ab}$, the mean temperatures of the two stars $T_{\rm Aa}$, $T_{\rm Ab}$, the "spin factors" of the two stars $\Omega_{\rm Aa}$, $\Omega_{\rm Ab}$, where Ω is the ratio of the rotational angular velocity to the orbital angular velocity, the inclination i, the mass ratio Q, the orbital separation a, the temperature of the third light star $T_{\rm B}$, the surface gravity of the third light star $\log g_B$, and the third light scaling factor $SA_{\rm B}$. We assume the orbit is circular, and that the third light star B does not vary. The gravity darkening exponent of star Aa was fixed at 0.25, the standard value for a star with a radiative envelope, while the gravity darkening exponent for star Ab was set at the standard convective value of 0.08. The ELC code uses Wilson's (1990) detailed reflection scheme, and for this problem the albedo of star Aa was taken to be 1 and the albedo of star Ab was taken to be 0.5. Three iterations of the reflection scheme were needed to achieve convergence. Both stars in the binary are assumed to be free of spots. A variation of the "grid search" routine outlined in Bevington (1969) was used to optimise the fits. In practice the fitting procedure involved a great deal of interaction where some parameters were temporarily fixed at certain values. Several two-dimensional grids in parameter space were defined (for example a grid of points in the $f_{\rm Aa}$, $f_{\rm Ab}$ plane). For each point, we fixed those parameters at the values defined by the grid location and optimised the other parameters, creating contours of χ^2 values. New parameter sets were optimised using the set of parameters for a nearby point that gave the best previous fit. After the lowest χ^2 value in a grid was found, then a new grid using other parameters was computed using the best solution as a starting point. The fitting took several weeks of CPU time on an Alpha XP 1000, and sampled a wide range of parameter space. We

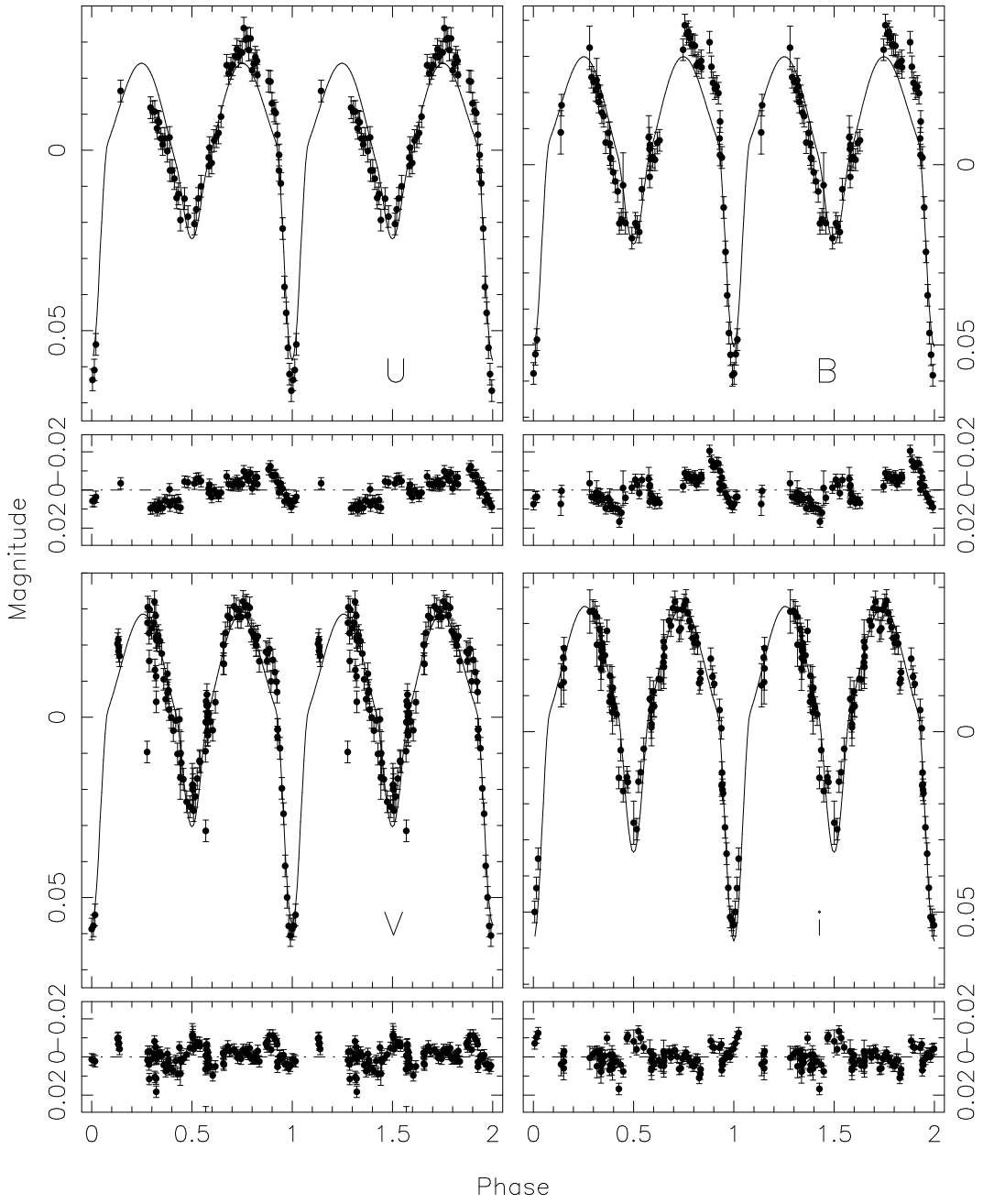

Figure 5.6: Fit to the light curves in the *U*, *B*, *V* and Gunn *i* band. The small panels show the residuals to the fit. Only the data from the first observation run are used.

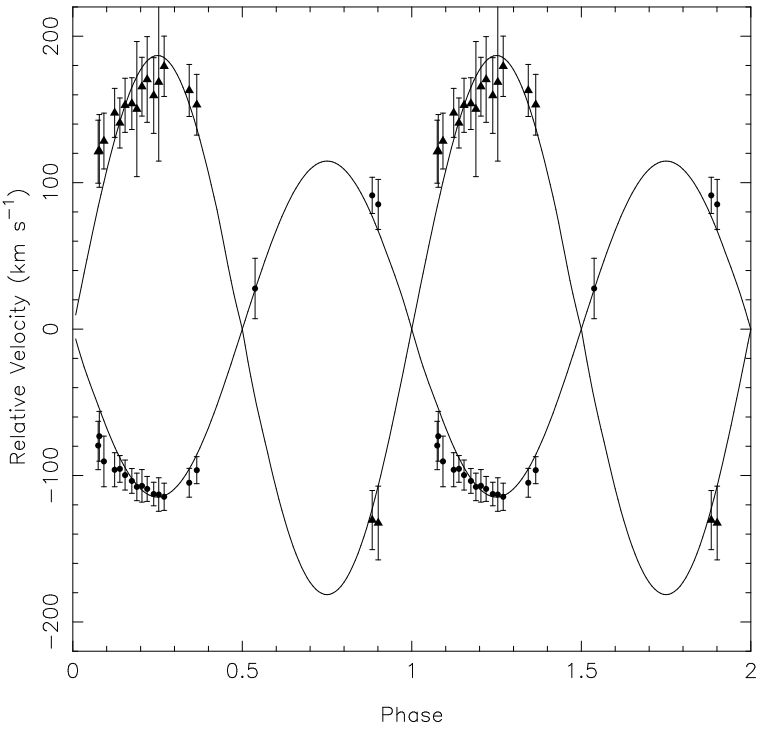

Figure 5.7: Radial-velocity curves of star Aa of the eclipsing binary in S 1082 (filled circles) and star Ab (filled triangles). The lines indicate the best-fitting velocity curves as computed by ELC.

are reasonably confident that our results are at or very near the global χ^2 minimum.

We found a relatively large number of solutions with similar χ^2 values. Fig. 5.6 shows a typical fit. The light curves in the 4 bands are fitted reasonably well, although there are still some systematic deviations, especially near the eclipse phases. The radial velocities are also fitted reasonably well (Fig. 5.7), but again there are some small systematic deviations (the velocity curves seem to be systematically flatter than the sinusoid fits near phase 0.25). In all solutions the binary is detached, i.e. both stars are well within their respective Roche lobes. We applied two additional constraints in order to narrow down the range of parameters. The first constraint is that the total V magnitude and $B-V$ colour of the model should match the observed V magnitude of S 1082. In this case the apparent V magnitude of the model is easy to compute. We used the synthetic photometry computed from the NEXTGEN models[1] to compute the expected absolute V magnitude of each star Aa and Ab in the eclipsing binary from its temperature, radius, and surface gravity. The V magnitude of the blue straggler B then follows from the fitted luminosity scaling. The second constraint is that the implied mass of the blue straggler is roughly consistent with its place in the colour-magnitude diagram. That is, the radius of the blue straggler B can be computed from the distance, the V magnitude, and the temperature. Since the gravity of the blue straggler B is specified in the models, its

[1] `ftp://calvin.physast.uga.edu/pub/NextGen/Colors/`

parameter	Aa	Ab	B
f	0.520(10)	0.700(10)	
R ($R_\odot$)	2.07(7)	2.17(3)	≈ 2.5
$R/R_{\rm Roche}$	0.66(7)	0.86(7)	
Ω	0.49(5)	0.91(5)	
T (K)	6480(25)	5450(40)	7500(50)
$\log g$ (cgs)	4.21(2)	4.0(2)	4.25(5)
M ($M_\odot$)	2.70(38)	1.70(27)	≈ 1.7
V	12.33(11)	13.10(11)	12.24(11)
$B-V$	0.51(2)	0.82(2)	0.33(1)
$i_{\rm A}$ (deg)	64.0(1.0)		
$a_{\rm A}$ ($R_\odot$)	7.2(4)		
V, $B-V$ total	11.30(11), 0.48(2)		

Table 5.5: Fitted binary parameters. Aa and Ab refer to the stars in the eclipsing binary, B to the third, outer star.

mass can then be computed. The blue colour of S 1082 requires a relatively hot third light star ($\approx$ 7500 K), and its surface gravity must be near $\log g = 4.25$ in order for the mass to be near $\approx 1.7\,M_\odot$. The derived astrophysical parameters for the adopted model are summarised in Table 5.5. The errors on the parameters were estimated from the χ^2 values generated in the various grid searches. These error estimates may be too small, given the complicated nature of the model. The errors on the masses were taken to be on the order of 15%, as judged from the quality of the sinusoid fits. The light curves of the three components are shown in Fig. 5.8, and a cartoon of the binary at three phases in Fig. 5.9.

We have assumed that the stars are not spotted and that the eclipsing binary has a circular orbit. A violation of either one of these assumptions could alter the light curves to produce the small systematic deviations seen in the residuals. Bright or dark spots could either add or remove light at certain phases, complicating the analysis. Given the rather large number of free parameters we have now we did not consider adding spots at this time. If this binary is part of a triple, then the orbit could be eccentric (see Sect. 5.5). A slight eccentricity ($e \approx 0.05$ say) could cause the maxima to be asymmetric and the minima to be shifted slightly in phase. Our current velocity curves do not have enough phase coverage to place meaningful constraints on the eccentricity, so any firm conclusions on the eccentricity will have to await the arrival of additional data.

Fig. 5.10 shows the decomposition of S 1082 into its components in a colour-magnitude diagram of M 67. Star Ab is located near the 4 Gyr isochrone that provides the best fit to the observed main-sequence, subgiant and giant stars (Pols et al. 1998). Hence the position of star Ab is consistent with the expected value based on its mass. The positions of star Aa and the blue straggler B are a bit more uncertain since one can "trade off" flux between the two stars (i.e. the blue straggler B can be made brighter at the expense of star Aa in the binary).

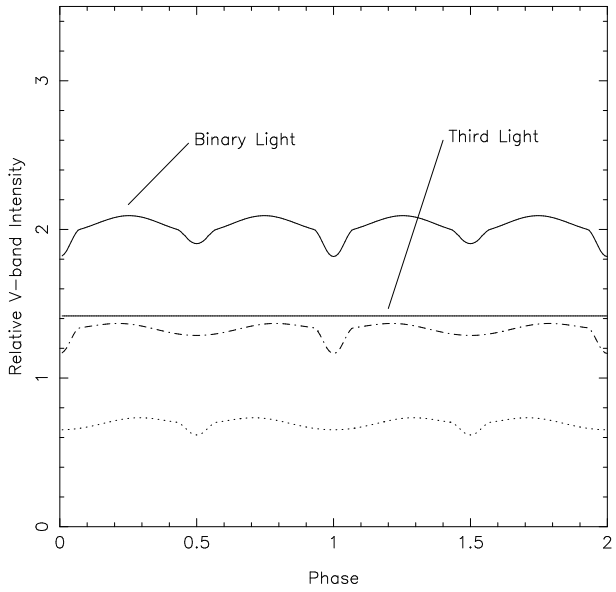

Figure 5.8: Light curves of the three components in S 1082 (dashed-dotted line indicates the primary Aa in the eclipsing binary).

We note that the star Ab is always located (within the errors) on the 4 Gyr isochrone. The error bars shown on the V magnitudes reflect the uncertainties for our adopted model which produces an overall V magnitude of all three stars close to the observed value. In any event, the hotter star Aa is subluminous by at least 2 mag in V (compare with the track for a 2.2 $M_\odot$ star). The position of the blue straggler lies to the red of the extension of the main-sequence as defined by the 1 Myr isochrone.

In order to obtain observed times of primary minimum we use the model light curve as a template to fit the data near the primary minima observed during run 1 and run 2. Seven additional times of minimum are obtained from fitting the data in Table 3 of Goranskij et al. and from the data points of Simoda (1991) (see first column of Table 5.6). A straight line is fitted to the observed times of minimum to find a new period and T_0 (see Table 5.4). The period thus derived is compatible with the period listed by Goranskij et al. (Eq. 5.1). We use the new ephemeris to compute observed minus computed (O–C) times of primary eclipse and the corresponding cycle number with respect to T_0 (second and third column of Table 5.6, and Fig. 5.11). The peak-to-peak amplitude ΔO–C is $\sim$ 39 minutes. If these variations are real and caused by the motion of the eclipsing binary around a third body it would correspond to a minimum semi-major axis in the outer (o) orbit of the binary (b) $a_{\rm o,b} \sin i_{\rm o} = 1/2\ c\ \Delta$ O–C = 2.3 AU. Assuming that the blue straggler (B) has a mass compatible with its position in the colour-magnitude diagram (about 1.7 $M_\odot$) this corresponds to a minimum value of the semi-major axis of the total system $a_{\rm o} \sin i_{\rm o} = a_{\rm o,b} \sin i_{\rm o}\ (1 + M_{\rm A}/M_{\rm B}) \approx 8.4$ AU; combined with the total mass of the system of 6.1 $M_\odot$ and Kepler's third law this gives a minimum period of 10 years. This is not compatible with the period of $\sim$ 3 years found by Milone (1991). We

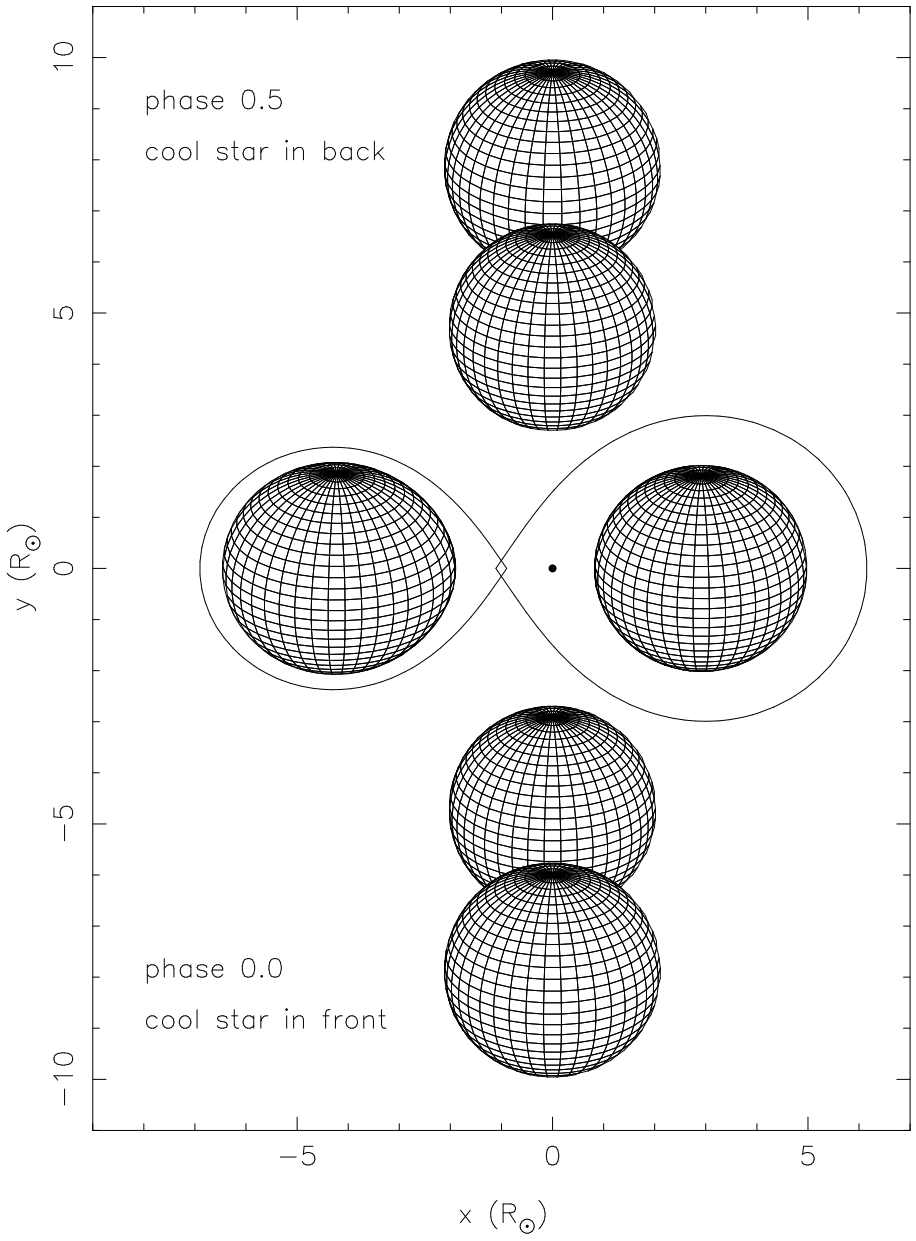

Figure 5.9: Cartoon of the configuration at three orbital phases of the inner binary according to the model listed in Table 5.5. Note that the Roche-lobes of the two stars Aa and Ab slightly overlap due to the fact that neither star corotates with the orbit.

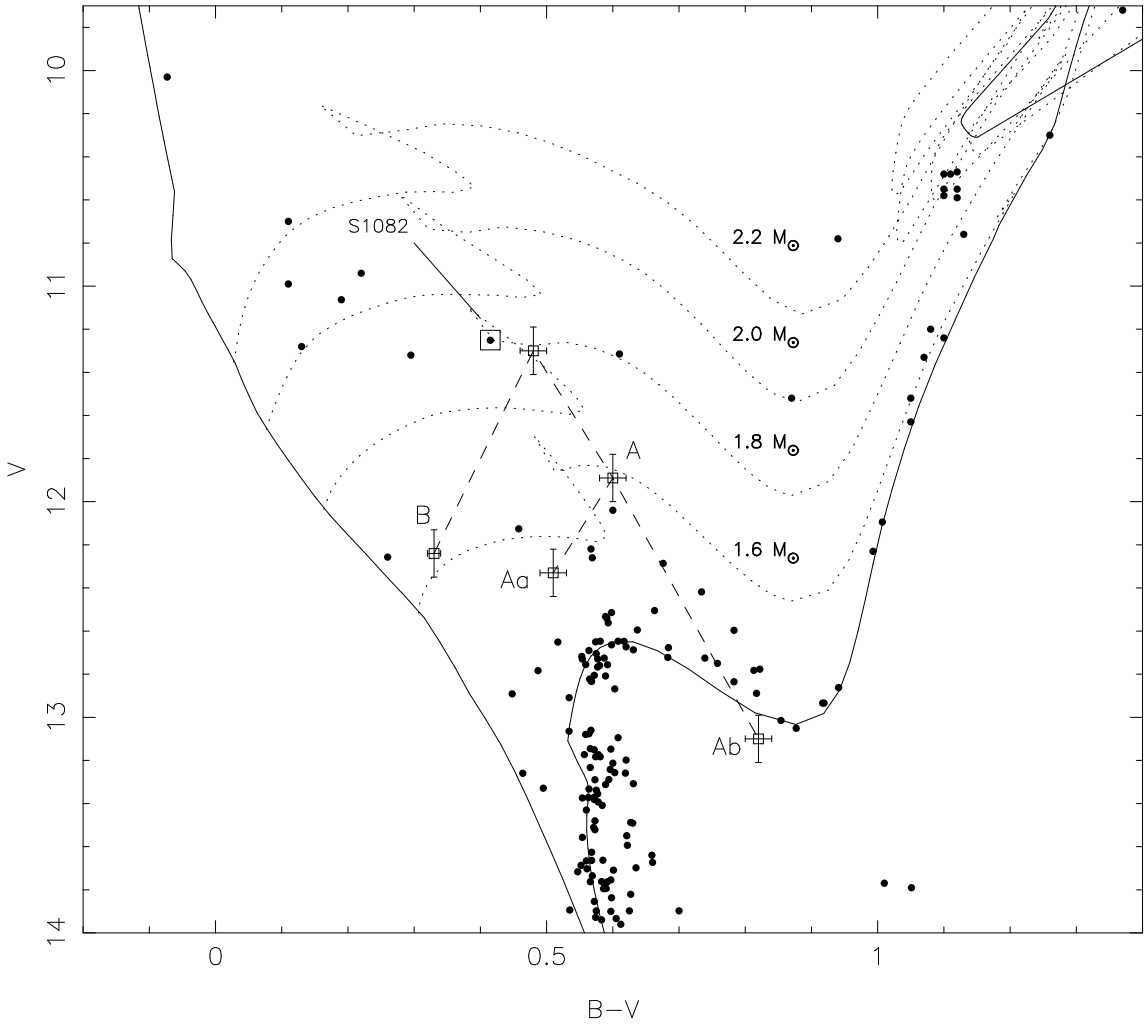

Figure 5.10: Colour-magnitude diagram of M 67 that shows the decomposition of S 1082 into a blue straggler (B) and stars Aa and Ab in the eclipsing binary (A); a dashed line connects their positions. The observed location of S 1082 is indicated with a box; the height of the square equals the depth of the primary eclipse. The dotted lines are evolutionary tracks for 1.6, 1.8, 2.0 and 2.2 $M_{\odot}$ stars corrected for the distance modulus and reddening of M 67 ($Z = 0.02$, Pols et al. 1998). The 4 Gyr-isochrone is included to indicate the expected positions of cluster members; the 1 Myr isochrone is included to give an estimate for the location of the ZAMS (Pols et al. 1998). *B* and *V* magnitudes of M 67 stars are from Montgomery et al. (1993). Only stars with a proper-motion membership probability $> 80\%$ (Girard et al. 1989) are plotted.

HJD −2 440 000	O−C	cycle	source
3191.036	−0.010	−1360	Simoda (1991)[a]
4643.250	0.000	0	Goranskij et al. (1992)
5325.586	0.013	639	idem
6773.492	−0.013	1995	idem
7861.605	0.014	3014	idem
7920.333	0.014	3069	idem
7944.869	−0.010	3092	idem[b]
11218.744	−0.001	6158	run 1
11539.078	−0.006	6458	run 2

[a]Simoda observed two consecutive primary eclipses. These data were combined to measure one time of minimum.
[b]Based on a measurement of a secondary eclipse which we convert to a primary eclipse by adding half a period. We note that if the orbit of the eclipsing binary is eccentric, the two eclipses need not be separated by half a period.

Table 5.6: Times of primary minimum. From left to right: observed time of minimum; O–C difference (in days) between the observed and computed time of eclipse; cycle number of the eclipse with respect to the T_0 of Table 5.4. The errors in the observed times of minimum and the O−C values are 0.005 days.

conclude that not all the variation in O–C is due to light-travel time in the outer orbit. There is no evidence for periodicity in the O–C times, although the time baseline is somewhat short and the coverage is somewhat spotty.

5.5 Discussion

Our new observations of S 1082 confirm the eclipses reported by Goranskij et al. (1992), the small radial-velocity variations of the narrow lines in the spectrum (Mathieu et al. 1986) and the time-variation of a broad-lined component seen in high-resolution spectra (van den Berg et al. 1999 [Chapter 2], Shetrone & Sandquist 2000). In addition, we now have found that the radial-velocity shifts of the broad-lined component *and* of a third component in the spectra vary on the photometric period. This clearly demonstrates that the narrow-lined star, which is a blue straggler on its own, is not part of the eclipsing binary – this solves the seeming contradiction in the properties of this system. The broad variable component of the Hα line discussed by van den Berg et al. (1999) [Chapter 2] is the Stark-broadened Hα line of the hot component Aa of the inner binary. The ultraviolet flux measured by Landsman et al. (1998), higher than expected for a star at the $B-V$ colour of S 1082, is only partly explained as a consequence of the bluer colour, i.e. higher temperature of the third star.

Comparison with Figs. 2 and 3 of Dempsey et al. (1993) shows that the X-ray luminosity

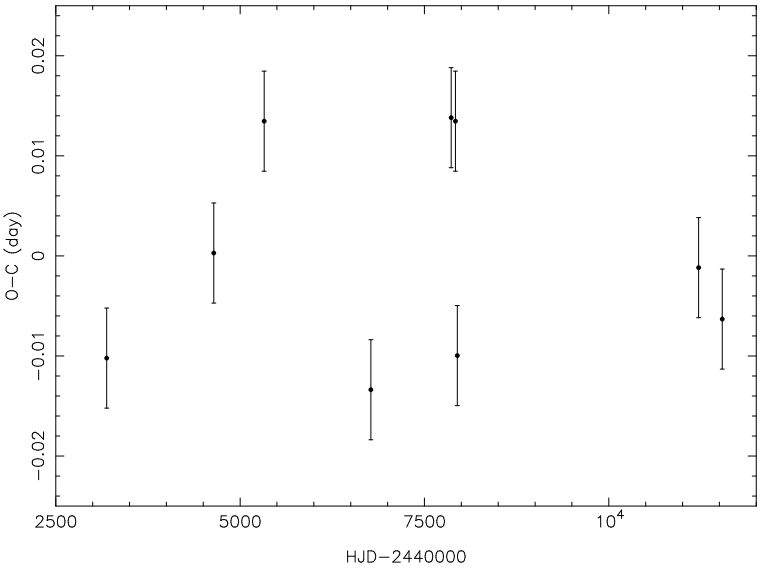

Figure 5.11: O–C times of the primary eclipse in days versus heliocentric Julian date ($-2\,440\,000$) of the measurement.

of S 1082 (Belloni et al. 1998) is typical for a subgiant in an RS CVn system. The X-ray emission could therefore be caused by magnetic activity in the rapidly rotating subgiant Ab. Thus, our model can explain the X-rays of S 1082.

Our solution to the photometry is symmetric (see Fig. 5.8) and does not explain the asymmetry between phases 0.25 and 0.75; nor the variability in the form of the secondary eclipse between our first two observations runs. This indicates that variable spots are present and accordingly that the best-fit parameters of the system are subject to some additional uncertainty. However, we do not think our main conclusions are affected.

We think that the eclipsing binary forms a bound triple with the third star, for two reasons. First, the radial-velocity measurements of the third star B – the narrow-lined system in S 1082 – indicate that it is in a ~ 1000 day orbit around a companion. The systemic velocities of both the 1000 day and the 1.07 day binaries are compatible with the radial velocity of the cluster. A chance alignment of two such bright cluster members is unlikely. Second, if we relax the constraint that the binary is at the cluster distance in solving the photometry, we find that the best solutions tend to be an Algol binary at higher mass ($\gtrsim 4\,M_\odot$) and larger distance (about twice the cluster distance). A high-mass binary at such a large distance from the galactic disc is unlikely.

Assuming then that the binary forms a hierarchical triple with the third star, in M 67, we note that the 1-σ lower bound to the mass of the binary is at about three times the turnoff mass of the cluster. The formation of the binary must thus have involved at least three stars. The third star is a blue straggler on its own account, and thus according to most current models its formation involves two stars. We have to conclude that the formation of S 1082 required the interaction of no less than five stars!

This interaction may have started with a binary-binary encounter, in which two stars collided directly and merged; one of the remaining two stars ended in a close orbit around the merger, the fourth star in a wide orbit around the inner binary. The fourth star must be a blue straggler, which either was already present in the original encounter or was later exchanged into the system. That triples are formed easily by binary-binary encounters, and that they live long enough to undergo subsequent exchange encounters with a binary, is shown for example by the computations of Aarseth & Mardling (2001). It is less obvious that mergers are common in such encounters, as most binary-binary encounters are between relatively wide systems. Merger products tend to be subluminous (Sills et al. 2001), in accordance with the properties of the more massive star Aa in the inner binary. The main problem with this scenario for the formation of the S 1082 system is that a merger product is only subluminous for a very limited period; comparable to its thermal time scale. This reduces the available time within which the outer star of the first encounter is exchanged with a binary or blue straggler in a subsequent encounter, and indicates that the blue straggler was present in the initial binary-binary encounter. Alternatively, an initial encounter between two triple systems can have led immediately to the currently observed configuration. In any case, the probability of catching the merger product while it is strongly subluminous is disconcertingly small.

Aarseth & Mardling (2001) note that the inclination of the outer orbit in a hierarchical triple with respect to the inner orbit can induce a large eccentricity in the inner orbit; subsequently, tidal forces in the inner orbit cause it to shrink. Thus, the inner orbit may be eccentric, and smaller than in the past. Our solution for the inner binary implies that the cool star has a radius which is a sizeable fraction of the binary separation $R_{\rm Ab}/a_{\rm A} \approx 0.3$. According to Eq. 2 of Verbunt & Phinney (1995) the circularisation time scale of the inner binary A is $\sim 10^3$ year; the eccentricity of A and asynchronicity of Ab thus will be determined by the competing effects of the perturbation by the outer star B and the tidal forces in the inner binary. Only if the latter are substantially reduced with respect to the Zahn (1977) formulation – as suggested by e.g. Goodman & Oh (1997) – do we expect measurable eccentricity and asynchronicity.

Whereas our new observations have allowed us to resolve the apparent contradictions in the earlier data and to determine the system parameters, we conclude that these parameters – in particular those of the primary Aa of the inner binary – are hard to understand in terms of standard stellar and binary evolution, even when stellar encounters and mergers are taken into account. This situation is remarkably similar to that in the study of two other members of M 67, located below the subgiant branch in the colour-magnitude diagram, both of which turn out to be binaries (Mathieu et al., in preparation) [Chapter 6]; and indeed to our lack of understanding of the blue-straggler population in the cluster. Many of these stars may be mergers, which raises the question whether the object that results when two stars merge may follow an evolutionary track which is very different from that of an ordinary star of the same mass; and whether they can do so for a period of time which significantly exceeds the thermal time scale.

Further studies of the remarkable triple system S 1082 should provide a better-sampled radial-velocity curve, necessary to determine whether the inner binary is eccentric, and to

measure its systemic velocity more accurately to establish cluster membership. Better-quality light curves may also serve to improve the accuracy of the inner orbit, e.g. if the inner orbit is eccentric the separation of the eclipses is different of 0.5. A long-term sampling of the light curves will be required to improve the interpretation of the O–C in the timings of the primary eclipse.

Acknowledgements – The authors wish to thank Magiel Janson, Rien Dijkstra, Gertie Geertsema, Remon Cornelisse and Gijs Nelemans for doing part of the observations. We also want to thank David Latham for discussions. The William Herschel Telescope, the Isaac Newton Telescope and the Jacobus Kapteyn Telescope are operated on the island of La Palma by the Isaac Newton Group in the Spanish Observatorio del Roque de los Muchachos of the Instituto de Astrofisica de Canarias. The Dutch 0.91-m Telescope is operated at La Silla by the European Southern Observatory. IRAF is distributed by the National Optical Astronomy Observatories, which are operated by the Association of Universities for Research in Astronomy, Inc., under cooperative agreement with the National Science Foundation. MvdB is supported by the Netherlands Organization for Scientific Research (NWO).

References

Aarseth, S. & Mardling, R. 2001, in ASP Conference Series, Vol. 229, Evolution of Binary and Multiple Star Systems, ed. P. Podsiadlowski & et al., in press (astro–ph/0011514)

Bailyn, C. D. 1995, ARAA, 33, 133

Belloni, T., Verbunt, F., & Mathieu, R. D. 1998, A&A, 339, 431

Bevington, P. R. 1969, Data reduction and error analysis for the physical sciences (New York: McGraw-Hill)

Dempsey, R. C., Linsky, J. L., Fleming, T. A., & Schmitt, J. H. M. M. 1993, ApJSS, 86, 599

Girard, T. M., Grundy, W. M., López, C. E., & van Altena, W. F. 1989, AJ, 98, 227

Goodman, J. & Oh, S. P. 1997, ApJ, 486, 403

Goranskij, V. P., Kusakin, A. V., Mironov, A. V., Moshkaljov, V. G., & Pastukhova, E. N. 1992, Astron. Astrophys. Trans., 2, 201

Gray, D. F. 1992, The observation and analysis of stellar photospheres (Cambridge: Cambridge University Press)

Gray, R. O. & Garrison, R. F. 1989, ApJSS, 69, 301

Hauschildt, P. H., Allard, F., & Baron, E. 1999a, ApJ, 512, 377

Hauschildt, P. H., Allard, F., Ferguson, J., Baron, E., & Alexander, D. R. 1999b, ApJ, 525, 871

Honeycutt, R. K. 1992, PASP, 104, 435

Hurley, J. R., Tout, C. A., Aarseth, S. J., & Pols, O. R. 2001, MNRAS, 323, 630

Kurucz, R. L. 1979, ApJS, 40, 1

Landsman, W., Bohlin, R. C., Neff, S. G., O'Connell, R. W., Roberts, M. S., Smith, A. M., & Stecher, T. P. 1998, AJ, 116, 789

Latham, D. W. & Milone, A. A. E. 1996, in The origins, evolution, and destinies of binary stars in clusters (ASP Conf. Ser. 90), ed. E. Milone & J.-C. Mermilliod, 385

Leonard, P. J. T. 1996, AJ, 470, 521

Mathieu, R. D., Latham, D. W., Griffin, R. F., & Gunn, J. E. 1986, AJ, 92, 1100
Mathys, G. 1991, A&A, 245, 467
Milone, A. A. E. 1991, PhD thesis, Univ. of Córdoba
Milone, A. A. E. & Latham, D. W. 1992, in Evolutionary processes in interacting binary stars, ed. Y. Kondo, R. F. Sistero, & R. S. Polidan, 475
Montgomery, K. A., Marschall, L. A., & Janes, K. A. 1993, AJ, 106, 181
Nissen, P. E., Twarog, B. A., & Crawford, D. L. 1987, AJ, 93, 634
Orosz, J. A. & Hauschildt, P. H. 2000, A&A, 364, 265
Pols, O. R., Schröder, K.-P., Hurley, J. R., Tout, C. A., & Eggleton, P. P. 1998, MNRAS, 298, 525
Shetrone, M. D. & Sandquist, E. L. 2000, AJ, 120, 1913
Sills, A., Faber, J. A., Lombardi Jr, J. C., Rasio, F. A., & Warren, A. R. 2001, ApJ, 548, 323
Simoda, M. 1991, IBVS 3675
Stryker, L. L. 1993, PASP, 105, 1081
van den Berg, M., Stassun, K., Verbunt, F., & Mathieu, R. D. 2001, A&A, submitted
van den Berg, M., Verbunt, F., & Mathieu, R. D. 1999, A&A, 347, 866
Verbunt, F. & Phinney, E. S. 1995, A&A, 296, 709
Wilson, R. E. 1990, ApJ, 356, 613
Zahn, J.-P. 1977, A&A, 57, 383

Chapter 6

Sub-subgiants in the old open cluster M 67?

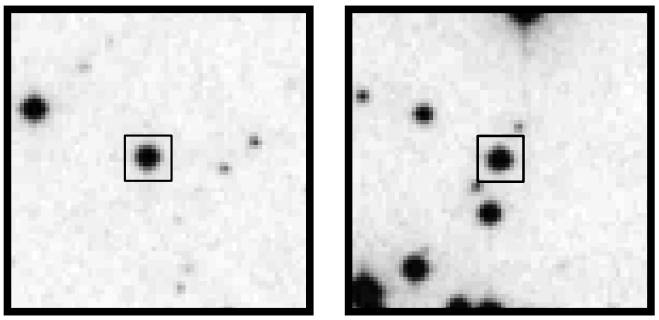

Robert D. Mathieu, Maureen van den Berg, Guillermo Torres,
David Latham, Frank Verbunt & Keivan G. Stassun
to be submitted to The Astronomical Journal

Abstract – We present the orbits of two spectroscopic binaries in M 67 – S 1113 and S 1063 – whose positions in the colour-magnitude diagram place them below the subgiant branch. S 1113 is a double-lined system with a circular orbit having a period of 2.823094±0.000014 days. S 1063 is a single-lined binary with a period of 18.396±0.005 days and an orbital eccentricity of 0.206±0.014. A ROSAT study of M 67 independently discovered these stars to be X-ray sources. The membership in the cluster of these binaries is as secure as can be achieved at present. Both have proper-motion membership probabilities greater than 97%; centre-of-mass velocities are precisely consistent with the cluster mean radial velocity. S 1063 is also projected within one core radius of the cluster centre. We discuss the possible origin and evolutionary state of these binaries which remain as yet unknown.

6.1 Introduction

The open cluster M 67 is one of the most comprehensively studied of all star clusters, and has long been the prototype for old (4-6 Gyr) open clusters in the Galaxy. Indeed, one of the first photo-electric colour-magnitude diagrams was derived for M 67 by Johnson & Sandage (1955). Since that time the precision of stellar photometry has steadily improved, and with it has the definition of the M 67 giant branch (Janes & Smith 1984, Montgomery et al. 1993). Indeed the remarkable narrowness of the M 67 giant branch has served as a precise touchstone against which innumerable single-star evolution models have been tested (e.g., Dinescu et al. 1995).

However, even after application of strict proper-motion membership criteria, the colour-magnitude diagram of M 67 remains littered with stars that do not fall on a single-star isochrone (Fig. 6.1). Some of these seeming anomalies can be accounted for. For example, one luminous star to the blue of the giant branch is a spectroscopic binary whose composite light can be explained by a giant–main-sequence pairing; another is a giant–white dwarf pair with a complicated history (Mathieu et al. 1990, Verbunt & Phinney 1995, Landsman et al. 1997). Many of the stars immediately above the turnoff and subgiant branch are spectroscopic binaries and consequently overluminous. And the parallel sequence of stars to the red of the main sequence are assuredly binaries as well (Montgomery et al. 1993).

However, there remain stars that are not so easily explained. Most famous are the blue stragglers, first noted in M 67 by Johnson & Sandage. The origin of blue stragglers in an open cluster environment is still not securely understood today (Bailyn 1995). Similarly, the yellow giant S 1072, lying 1.2 magnitudes above the main-sequence turnoff, has defied explanation. A kinematic member in all three dimensions and lying in projection in the cluster core, its resolution as a non-member remains possible but not satisfying (Mathieu & Latham 1986, Nissen et al. 1987). In this paper we consider two more stars – S 1063 and S 1113 – who by every indication are cluster members, yet whose location in the M 67 colour-magnitude diagram is dramatically inconsistent with single-star evolutionary theory. Specifically, as shown in Fig. 6.1, these stars lie below the subgiant branch, and as such we call them sub-subgiants.

Our attention has converged on these stars from two directions. We have underway a multi-decade survey of the spectroscopic binary population in M 67 (Mathieu et al. 1990, Latham et al. in preparation). Both S 1063 and S 1113 were found to be spectroscopic binaries, with S 1113 in particular being notable for the rapid rotation of its primary star. Belloni et al. (1998) have undertaken a comprehensive study of stellar X-ray sources in M 67 based on ROSAT observations (Belloni et al. 1998). S 1063 and S 1113 were independently discovered to be X-ray sources, of which there are only 25 known among cluster members. Both binaries are also photometric variables (van den Berg et al. 2001) [Chapter 3], which are infrequent in a cluster of this age (Stassun et al. 2001, in preparation) [Chapter 4]. In this paper we present a comprehensive discussion of the orbital, spectroscopic, and photometric properties of S 1063 and S 1113. Regrettably, like the blue stragglers and S 1072, their interpretation remains a puzzle.

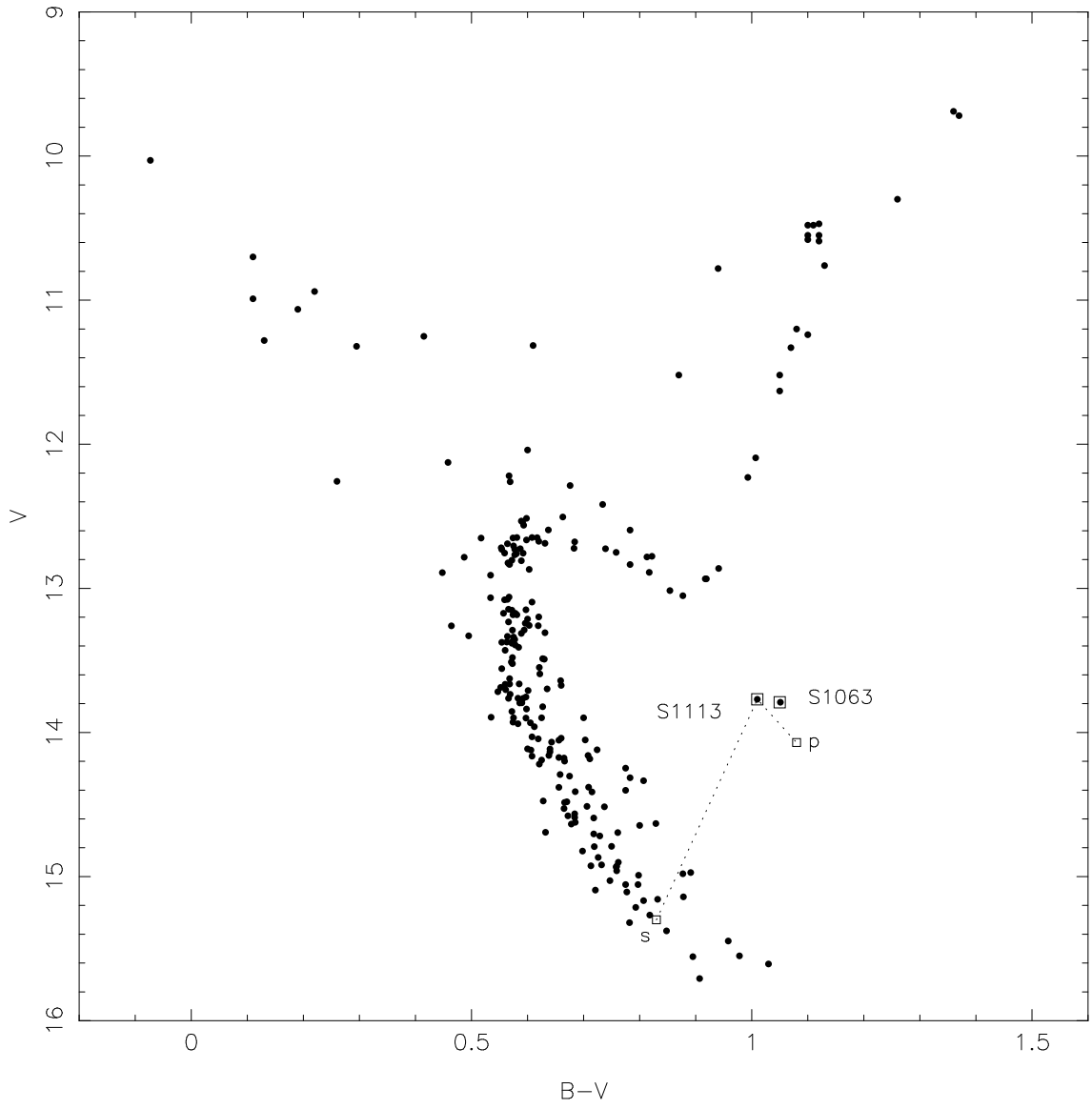

Figure 6.1: Colour-magnitude diagram of M 67 based on the photometry of Montgomery et al. (1993) and including only stars with proper-motion membership greater than 80% (Girard et al. 1989). The suggested sub-subgiants – S 1063 and S 1113 – are highlighted. We also show the decomposition of the light of S 1113 into the primary (p) and secondary (s) which applies if the secondary is a main-sequence star (see also Sect. 6.4).

6.2 The stars

The stars S 1063 and S 1113 had attracted some attention prior to our radial-velocity and X-ray studies. Both stars are included in the highly precise proper-motion study of Girard et al. (1989), in which S 1063 is given a kinematic membership probability of 97% and S 1113 of 98%. Being a bit less than one core radius from the cluster centre, S 1063 has been included in most photometric studies of M 67; S 1113 is located at three core radii, and thus only has been observed in the wider field photometric surveys. Racine (1971) noted that S 1063 was photometrically unusual in that it lies roughly a magnitude in V below the subgiant branch. S 1113 has very similar photometric properties as S 1063, but seems to have escaped notice until mentioned by Kaluzny & Radczynska (1991). In Fig. 6.1 we show the colour-magnitude diagram of M 67 derived from the photometry of Montgomery et al. (1993); S 1063 and S 1113 are marked by filled boxes.

Both stars have been found to be photometric variables. Racine (1971) noted a large range (0.18 mag) in photometric observations of S1063, and its variability was subsequently confirmed by other observers (Rajamohan et al. 1988, Kaluzny & Radczynska 1991). S 1113 has a variable star designation – AG Cnc – and Kaluzny & Radczynska (1991) found S 1113 to be photometrically variable at the 0.05 mag level. Based on their variability (but not light curves) and their location in the colour-magnitude diagram, Kaluzny & Radczynska (1991) suggested that both stars are highly evolved W UMa binaries with extremely small mass ratios and consequently small photometric amplitudes.

Both S 1063 and S 1113 were included in a large survey for spectroscopic binaries among M 67 proper-motion cluster members begun in the mid-1980's (last summarised in Latham et al. 1992). S 1063 was quickly found to be a single-lined spectroscopic binary, with no evident distinction otherwise. S 1113 was immediately recognised as an unusual double-lined spectroscopic binary in that the primary star was a rapid rotator.

Independently, ROSAT PSPC observations of M 67 identified these two stars as among 25 cluster members detected to have X-ray emission (Belloni et al. 1993, 1998). As members of this select group, S 1063 and S 1113 received optical spectroscopic attention by Pasquini & Belloni (1998) and van den Berg et al. (1999) [Chapter 2]. Both stars show strong emission cores in the Ca II H and K lines, indicative of chromospherically active stars. Both stars also show Hα emission. In S1063 the Hα line is asymmetric, showing emission which is blue-shifted with respect to an absorption feature. The absorption line agrees with the velocity of the primary, perhaps suggesting that it can be attributed to the primary star and that the Hα emission originates elsewhere in the system. Alternatively, the Hα line profile is very similar to that seen from HK Lac by Catalano & Frasca (1994), who attribute the emission to a large flare lasting 6 days. In S 1113 the Hα emission is broad and clearly centred on the velocity of the primary star, with an equivalent width of 15 Å.

6.3 Observations and data analyses

6.3.1 Speedometry and orbital solutions

High-precision radial-velocity observations of S 1063 were begun in 1987, and 28 observations were obtained through 1989. 18 radial-velocity observations were obtained for S 1113 between 1989 and 1998. All observations were obtained with the Center for Astrophysics (CfA) Digital Speedometers (Latham 1992). Two nearly identical instruments were used on the Multiple Mirror Telescope and the 1.5-m Tillinghast Reflector atop Mt. Hopkins, Arizona. Echelle spectrographs were used with intensified photon-counting Reticon detectors to record about 45 Å of spectrum in a single order near 5187 Å with a resolution of 8.3 km s^{-1} and signal-to-noise ratios ranging from 8 to 15 per resolution element.

The 28 radial velocities for S 1063 were measured using the one-dimensional correlation package RVSAO (Kurtz & Mink 1998) running inside the IRAF environment. The template spectrum was drawn from a new grid of synthetic spectra (Morse & Kurucz, in preparation) calculated using Kurucz's code ATLAS9. We correlated our observed spectra against an array of solar-metallicity templates spanning effective temperature, surface gravity, and projected rotation velocity. The template giving the highest peak correlation (averaged over all observations) had $\log g = 3.5$, $T_{\rm eff} = 5000$ K, and $v \sin i = 6$ km s^{-1}. The radial velocities derived with this template are presented in Table 6.1. Extensive experience measuring radial velocities of similar stars with the CfA speedometers suggests a typical single-measurement error of 0.7 km s^{-1}.

A single-lined orbital solution with period $P = 18.396$ days is easily derived from these data; the elements are given in Table 6.2 and the orbit curves are superimposed on the data in Fig. 6.2. The centre-of-mass velocity of $\gamma = 34.3 \pm 0.2$ km s^{-1} is consistent with the cluster mean radial velocity of 33.5 km s^{-1} and observed velocity dispersion of 0.5 km s^{-1} (Mathieu 1983), so the star is a kinematic cluster member in all three dimensions. Otherwise, the orbital elements are not notable.

The analyses of the S 1113 spectra were done using the TODCOR machinery of Zucker & Mazeh (1994), as implemented at CfA. A two-dimensional array of templates in effective temperature and projected rotation velocity, again derived from Kurucz spectra, were correlated with all of the S 1113 spectra. The effective temperatures and rotation velocities of the templates were selected based on maximising the correlation peak height, averaged over all available spectra. We find projected rotational velocities $v \sin i$ of 53 km s^{-1} for the primary and 12 km s^{-1} for the secondary, respectively, with a 1-σ uncertainty of 2 km s^{-1} on each. Van den Berg et al. (1999) [Chapter 2] previously measured $v \sin i$ for both stars, finding 45 ± 6 km s^{-1} for the primary and 12 ± 1 km s^{-1} for the secondary. The derived effective temperatures are 4800 K and 5450 K for the primary and secondary, respectively, with a 1-σ uncertainty of 150 K. Finally, we derive a luminosity ratio at 5187Å of 0.352 ± 0.016 (secondary/primary).

The primary and secondary radial velocities derived with these template parameters are given in Table 6.3. A double-lined orbital solution is easily obtained from these data; the elements are given in Table 6.4 and the orbit curves are superimposed on the data in Fig. 6.3.

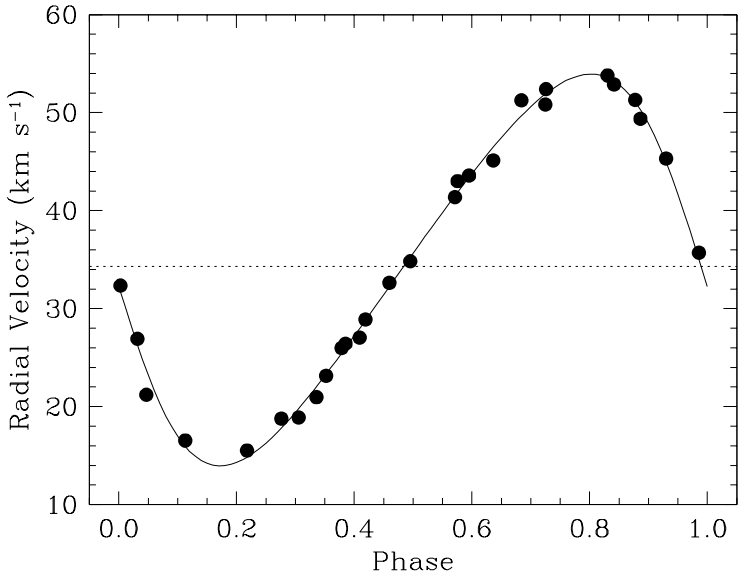

Figure 6.2: The single-lined orbit curve of S 1063 shown with the phased radial-velocity measurements. The dashed line shows the centre-of-mass velocity of the binary.

Again, the centre-of-mass velocity of $\gamma = 33.4 \pm 0.4$ km s^{-1} is consistent with the cluster mean radial velocity. The orbital eccentricity of $e = 0.022 \pm 0.010$ leaves open the possibility that the orbit may not be circular, but at present that conclusion is not statistically secure. Thus we also present in Table 6.4 a circular-orbit solution with eccentricity $e = 0$, the elements of which we will use for the remainder of this paper. The mass ratio of the system is $q = 0.703 \pm 0.012$.

6.3.2 Photometry and variability

Van den Berg et al. (2001) [Chapter 3] have photometrically monitored both stars, with 1-m telescopes at ESO (La Silla), Kitt Peak and La Palma, in order to look for light variations that may provide insight into the nature of the systems. We here summarise their main results.

While S 1063 is definitively variable, as yet no period has been identified in our data. The variability is clearly of a long-term nature. If it is periodic, the 18-days ESO light curve establishes that the period is longer than the pseudo-synchronous period of 14.64 days (Hut 1981). Furthermore, the ESO and Kitt Peak data do not phase up on the orbital period of 18.4 days. Indeed, it is not evident that the Kitt Peak and ESO data can be phased together on any period, as the Kitt Peak data show a steeper slope in their photometric variation. However, this could arguably be the result of a change in the source of the variability during the year between the Kitt Peak and ESO observations (e.g., a different star spot morphology). Alternatively, the variability may simply not be periodic. Longer intervals of continuous observation are required.

S 1063 becomes bluer as it brightens. This effect is small in the $B-V$ colour, and most

HJD	$v_{\rm rad}$ (km s^{-1})
2446899.6818	21.94
7158.0132	26.21
7198.7906	44.67
7216.7438	42.04
7226.7088	17.03
7489.8904	29.52
7493.8852	46.04
7513.9289	52.67
7515.8531	53.39
7516.8802	50.36
7519.8331	21.04
7522.9810	14.87
7524.0551	17.48
7526.0601	26.21
7543.8490	23.10
7544.8949	27.58
7545.8256	33.04
7547.9579	43.67
7549.9533	52.55
7552.8487	52.40
7555.8172	31.66
7574.7462	27.03
7579.7805	19.95
7601.6697	35.60
7608.6951	52.30
7609.6639	46.29
7610.6930	36.26
7845.0409	51.18

Table 6.1: Radial-velocity measurements for S 1063.

P (days)	18.396 ± 0.005
γ (km s^{-1})	34.30 ± 0.20
K (km s^{-1})	20.0 ± 0.3
e	0.206 ± 0.014
ω (deg)	95 ± 5
T (244 + days)	7482.19 ± 0.22
$a_1 \sin i$ (AU)	0.0330 ± 0.0006
$f(m)$ ($M_\odot$)	0.0143 ± 0.0007
Number of observations	28
σ (km s^{-1})	0.99

Table 6.2: Orbital elements for S 1063.

HJD	$v_{\rm rad,p}$ (km s^{-1})	$v_{\rm rad,s}$ (km s^{-1})
2447579.7541	−23.72	114.14
47610.8114	−24.26	117.76
47635.6961	−4.62	87.84
47903.0130	92.82	−48.87
48320.7433	93.49	−48.93
48338.7448	−18.47	103.52
48345.7097	74.53	−22.31
48644.8675	64.94	−5.16
49021.9789	−11.59	105.53
49057.7946	83.51	−38.66
49058.6665	−9.15	103.29
49348.0117	83.93	−36.01
49354.9585	−5.61	86.68
49465.7519	−16.13	103.53
49699.9173	−26.20	112.09
50799.0251	73.97	−28.94
50821.8463	92.94	−53.73
50821.8681	94.91	−53.55

Table 6.3: Radial-velocity measurements for S 1113.

P (days)	2.823094 ± 0.000014	2.823105 ± 0.000015
γ (km s^{-1})	33.4 ± 0.4	33.8 ± 0.4
K_1 (km s^{-1})	60.6 ± 0.9	60.6 ± 0.8
K_2 (km s^{-1})	86.2 ± 0.6	86.2 ± 0.6
e	0	0.022 ± 0.010
ω (deg)	–	333 ± 16
$T_{\rm max}$ (244 + days)	8916.368 ± 0.4	–
T_0 (244 + days)	–	8916.15 ± 0.13
$a_1 \sin i$ (AU)	0.0157 ± 0.0003	0.0157 ± 0.0003
$a_2 \sin i$ (AU)	0.0223 ± 0.0003	0.0223 ± 0.0003
$M_1 \sin^3 i$ ($M_\odot$)	0.544 ± 0.012	0.544 ± 0.012
$M_2 \sin^3 i$ ($M_\odot$)	0.382 ± 0.012	0.382 ± 0.012
q	0.703 ± 0.012	0.703 ± 0.012
Number of observations	18	18
σ_1 (km s^{-1})	3.15	2.94
σ_2 (km s^{-1})	2.10	2.05

Table 6.4: Orbital elements for S 1113. The primary is indicated with '1', the secondary with '2'.

	V	$B-V$	$L/L_\odot$	$T_{\rm eff}$ (K)	$R/R_\odot$
Composite	13.77	1.01			
Primary	14.07	1.08	2.51	4760	2.32
Secondary	15.30	0.83	0.70	5475	0.93
0.94 $M_\odot$			0.66	5475	0.90

Table 6.5: Deconvolved photometry for S 1113. For comparison with the parameters of the secondary star, the parameters for a 0.94 $M_\odot$ star are also listed.

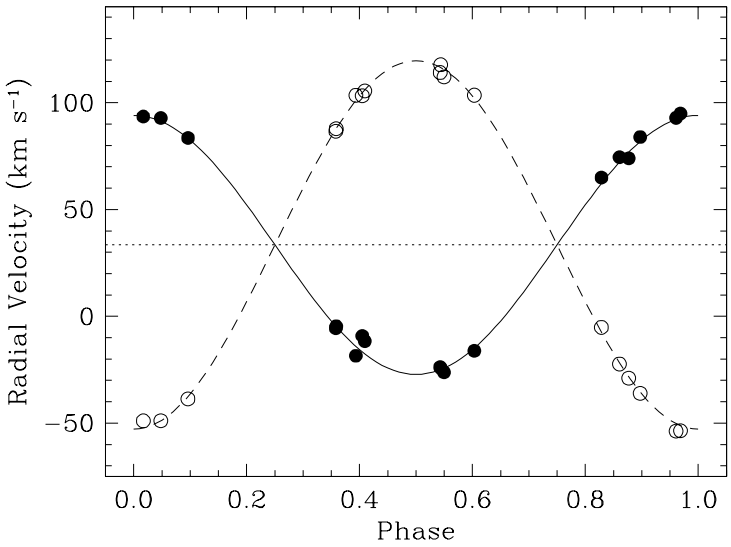

Figure 6.3: The double-lined orbit curve of S 1113 shown with the phased radial-velocity measurements for the primary (filled circle) and secondary (open circle) stars. The dashed line shows the centre-of-mass velocity of the binary.

evident in colours including the *U* and *I* bandpasses. These colour variations are more suggestive of relatively small temperature variations on the primary stellar surface or variable extinction than a contribution from either a hot boundary layer or a cool circumbinary disc.

A periodicity comparable to the orbital period was quickly evident in the S 1113 data. We show in Fig. 6.4 the *V* light curves derived from the 18-day ESO observations and phased to the radial-velocity orbit solution, which is also shown in Fig. 6.4 The morphology of the light curve is sinusoidal with a high degree of symmetry. Maximum brightness occurs at orbital phase 0.5, when the stars are aligned perpendicular to our line of sight and the primary is approaching. As with S 1063, the system becomes bluer as it brightens.

A time-series analysis on all of the photometric data indicates a possible period of 2.822d$\pm$ 0.001 days. This period is very similar to the orbital period of 2.823094d$\pm$0.000014 days, indicating a close association. There is some indication that the light curve shape is not stable. As evident in Fig. 3.5 of van den Berg et al. (2001) [Chapter 3], three sets of photometric observations obtained at intervals of 4-6 weeks and 2 years do not repeat to within the formal photometric errors, suggestive that the source of the photometric modulation has undergone small changes on these time scales.

6.4 Properties of the stars

S 1063 The most notable property of the orbit of S 1063 may be its ordinariness. If S 1063 fell on the main sequence or the subgiant branch, its orbit would merit no further attention.

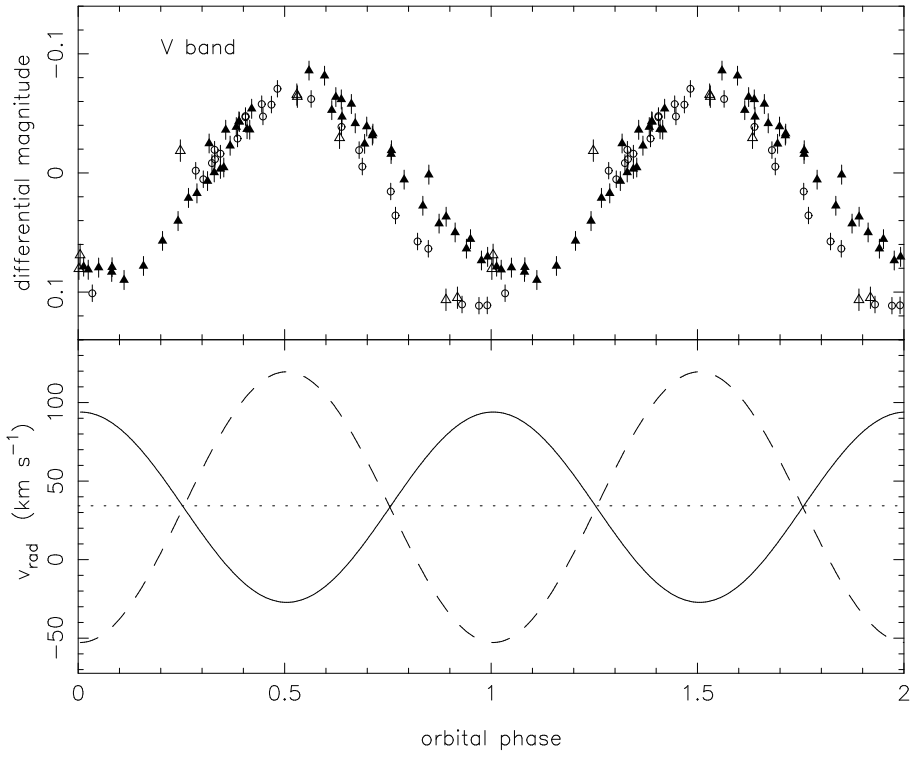

Figure 6.4: Light curve (top) and primary and secondary orbit curves (bottom) for S 1113 phased on the orbital period of 2.823094 days. The light curve shows *V* data taken in January 1998 (open circles), February and March 1998 (filled triangles) and February 2000 (open triangles), taken from van den Berg et al. (2001) [Chapter 3]. Note that maximum light amplitude occurs when the primary star is moving toward us (in projection).

For example, the eccentricity of $e = 0.206$ is quite typical for main-sequence and subgiant binaries in M 67 with periods ~ 20 days (Mathieu, Latham & Griffin 1990).

Evidently the primary star dominates the light at 5187 Å. As noted above, the CfA spectra indicate an effective temperature of $T_{\rm eff} = 5000$ K and a gravity of $\log g = 3.5$. New analyses of the higher S/N spectra of van den Berg et al. (1999) [Chapter 2] yield similar measures. Comparison of the Vanadium I 6251.83 Å/FeI 6252.57 Å line ratio with the spectral analyses of Gray (Gray 1989, Gray & Johanson 1991) yield a $T_{\rm eff}$ of 5150 K for a dwarf and 4900 K for a giant. Alternatively, in Fig. 6.5 we use the spectral diagnostic I_s as defined by Malyuto & Schmidt-Kaler (1997) to derive a spectral type of G8–K0. Such a spectral classification indicates effective temperatures similar to the spectral line results (Schmidt-Kaler 1982, Bessell & Brett 1988, Bessell et al. 1998).

Detailed analyses of the optical spectra obtained by van den Berg et al. (1999) [Chapter 2] indicate that the primary of S 1063 is neither a giant nor a dwarf. We have taken two approaches to determining the surface gravity. First, we have compared the gravity sensitive Mg b lines with Kurucz spectra. In Fig. 6.6 we show the spectrum of S 1063 and Kurucz

spectra at $T_{\rm eff} = 5000$ K over a range of $\log g$. Based on the Mg b triplet line shapes, S 1063 is clearly neither a giant ($\log g = 2.5 - 3.0$) nor a dwarf ($\log g = 4.5 - 5.0$). Spectral fitting (with $T_{\rm eff}$ a free parameter) results in $T_{\rm eff} = 5000$ K, $\log g$ = 3.5, and $v \sin i$ = 8 km s^{-1}, confirming the results obtained from the lower-S/N CfA spectra. In Fig. 6.5 we compare the values of I_s and I_2 for S 1063 with those of stars of all luminosity classes. Again, for stars of similar I_s S 1063 falls between the dwarfs and giants.

Given several lines of evidence that the gravity of S 1063 is intermediate between dwarfs and giants, we interpolate between calibrations for dwarfs and giants and adopt an effective temperature of $T_{\rm eff} = 5000$ K. We use the composite light photometry of Montgomery et al. (1993), their reddening of $E(B-V) = 0.05$, and distance modulus of 9.6. A bolometric correction of 0.4 mag was obtained from the main-sequence calibrations of Bessell & Brett (1988) and Bessell et al. (1998). With these parameters we deduce a luminosity of 3.0 $L_\odot$, and a radius for the primary star of 2.3 $R_\odot$. For any reasonable pair of stellar masses, such a star fits comfortably within its Roche radius at periastron separation.

The orbit places an absolute lower limit on the primary and secondary masses of 0.06 $M_\odot$. If the primary is taken to have the turnoff mass 1.3 $M_\odot$ (Yale 5 Gyr isochrone; Demarque, private communication), then the orbit places a lower limit on the secondary mass of 0.33 $M_\odot$. This lower limit changes by less than 0.1 $M_\odot$ for primary masses between 0.5 $M_\odot$ and 2 $M_\odot$. The non-detection of the secondary in our spectra requires that the secondary star have $V > 16$, roughly two magnitudes fainter than the primary (here taken as equivalent to the composite light). If the secondary is a main-sequence star, then based on this magnitude limit the Yale isochrones give an upper limit on the mass of the secondary of 0.83 $M_\odot$ (Demarque, private communication).

More generally, for primary masses between 0.5 $M_\odot$ and 2 $M_\odot$ and for mass ratios between 0.1 and 1, the mass function implies an orbital inclination angle of 20–45°. For aligned rotational and orbital axes, the true equatorial rotation velocity could be as large as 20 km s^{-1}, and for a primary radius of 2.3 $R_\odot$ the rotational period could be as short as 6 days. Such rapid rotation periods would be consistent with the observed X-ray emission, chromospheric activity, and possible flares. Perhaps most plausibly, the pseudo-synchronous rotation period of 14.64 days (Hut 1981) is permitted, requiring an inclination angle of $i = 47°$ (and, for a primary mass of 1.3 $M_\odot$, a secondary mass of 0.5 $M_\odot$). However, we remind the reader that the photometric data show no evidence of periodicity at this or shorter rotation periods.

Finally, we do not know that the secondary is a main-sequence star; we know only that it is faint at V. If it were instead a white dwarf the expected mass would still be of order 0.6–0.7 $M_\odot$ (Wood 1992, Richer et al. 1998) and the conclusions above regarding the primary star would change little. How the secondary could become a white dwarf without circularising the orbit during its post–main-sequence evolution would need to be explained.

S 1113 The spectroscopic detection of the secondary permits substantially more information to be derived for this binary. Given that the primary star is evidently not on the cluster main sequence, we begin analysis of the system with the presumption that the primary is an evolved cluster member, and initially assume that the primary mass is the same as the cluster

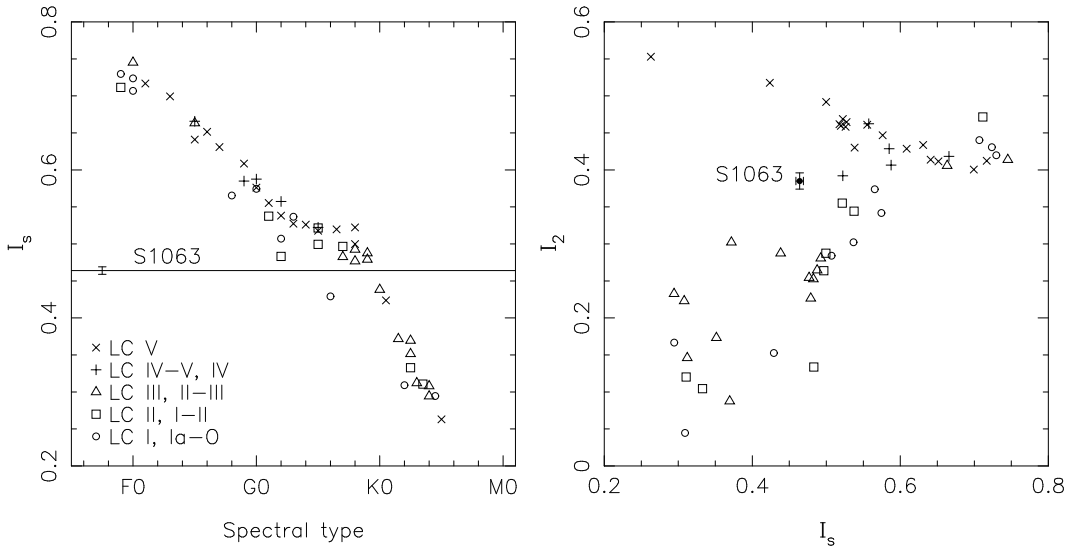

Figure 6.5: Spectral classification of S 1063 according to the classification criteria of Malyuto & Schmidt-Kaler (1997). Left: I_S, based on features between 4215 Å and 4360 Å and 5125 Å and 5290 Å, is an index for spectral type and places S 1063 (solid line) between type G8 and K0. Right: I_2, based on features between 4120 Å and 4280 Å is an index for luminosity class and places S 1063 between dwarfs and giants.

turnoff mass - 1.3 $M_\odot$. Then we immediately derive an orbital inclination angle of 48° and a semi-major axis of 11.0 $R_\odot$. The mass for the secondary then is 0.91 $M_\odot$, for which the Yale isochrones give an effective temperature of 5350 K. This is close to the effective temperature for the secondary of 5450 K derived from the TODCOR analysis (Sect. 6.3.1).

If we assume that the rotational axes of both stars are aligned with the orbital angular momentum vector and that the rotations of both stars are synchronised, then we can derive the radii of the stars from the projected rotation velocities. We find the primary and secondary radii to be 3.9 $R_\odot$ and 0.9 $R_\odot$, respectively. The secondary radius is again consistent with a 0.91 $M_\odot$ main-sequence star, while the primary radius is indicative of an evolved star.

The Roche radii are 4.5 $R_\odot$ and 3.8 $R_\odot$ for the primary and secondary, respectively. Evidently the secondary lies well within its Roche radius. The primary however fills a large fraction of the Roche volume, and the equipotential surface whose volume equals that of a 3.9 $R_\odot$ sphere extends 74% of the way to the L_1 point. Using the Wilson-Devinney formalism we have investigated the expected magnitude of photometric variations due to the ellipsoidal shape of the primary. Adopting the parameters above, a temperature of 4800 K for the primary star, a limb darkening coefficient (linear law) of 0.6 for each star, a gravity brightening coefficient of 0.32, and a reflection coefficient of 0.5, we find the peak-to-peak ellipsoidal variations to be 0.06 mag in V. The synthetic light curve is presented in Fig. 6.7 and shows the expected two peaks per orbital cycle.

Such double-peaked variations are in marked contrast to the single-peaked sinusoidal light

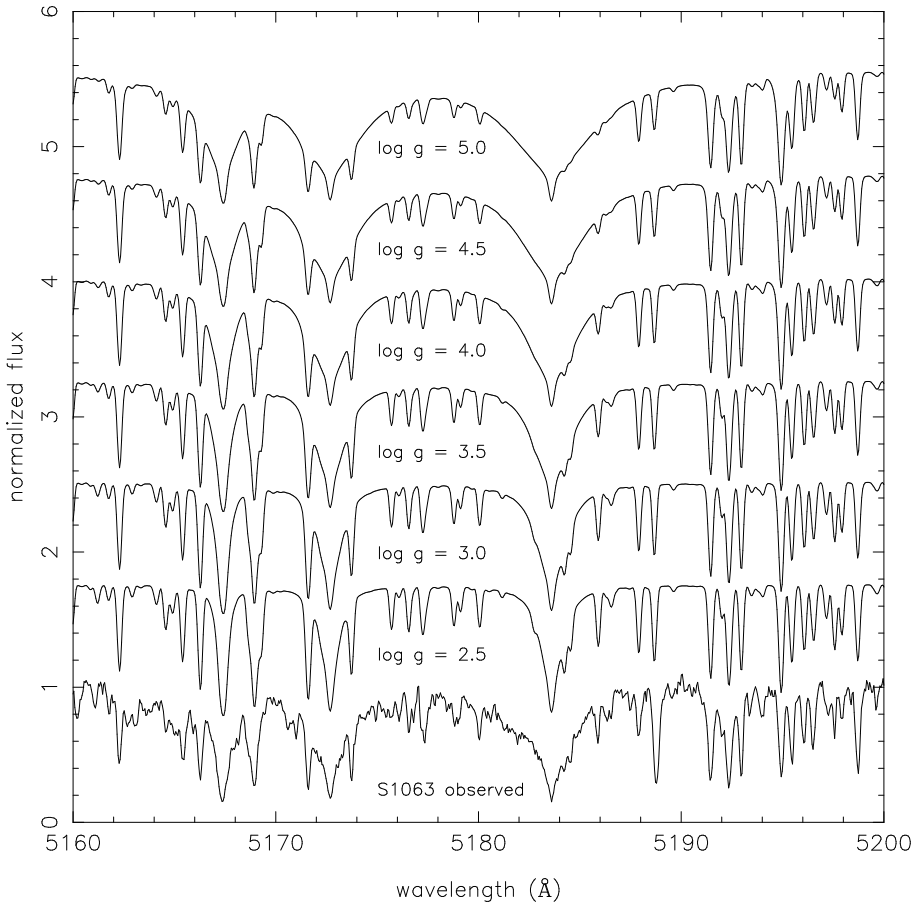

Figure 6.6: Comparison of S 1063 spectrum with synthetic spectra of effective temperature $T_{\rm eff}$ = 5000 K, $v \sin i$ = 8 km s^{-1}, and differing surface gravities (Kurucz 1979). The spectra are normalised to the continuum flux and shifted vertically in steps of 0.75 flux units. S 1063 is best fit by the synthetic spectrum with $\log g$ = 3.5.

curve found by van den Berg et al. (2001) (see Fig. 6.4). It is possible that these small ellipsoidal variations have gone undetected in contrast to the larger photometric variations of the system. We have modelled the binary as described above with the addition of a cool spot in the upper hemisphere of the primary and located 90° from the major axis. (Specifically the spot properties are: latitude 40°, longitude 270°, radius 27°, temperature 0.82 of the stellar surface temperature.) The resultant light curve – including both spot and ellipsoidal photometric variations - is also shown in Fig. 6.7. Evidently the ellipsoidal variations are lost to inspection in this synthetic light curve, which in fact looks very similar to the observed light curve of S 1113. It is not clear whether the ellipsoidal variations should have been detected in our Fourier analyses of the time-series data; certainly there is no indication in the observations of power at half the orbital period. We also note that this resolution of the absence of ellipsoidal variation requires a rather specific (and as yet unmotivated) positioning of the spot.

An independent analysis of the primary and secondary stars can be done from the observed photometry and the measured luminosity difference of $\Delta V = 1.23$ mag. Specifically, we can deconvolve the composite photometry to obtain magnitudes and colours for each star. Adopting again the photometry of Montgomery et al. (1993), the primary and secondary V magnitudes are immediate. To obtain colours we presume that the secondary lies on the cluster main sequence, a position that is uniquely defined by the secondary V magnitude. With this assumption, we find the magnitudes and colours for the primary and secondary stars presented in Table 6.5. These results for the primary and secondary are plotted in Fig. 6.1. The secondary star lies on the M 67 main sequence by construction, while the primary lies somewhat further below the subgiant branch and slightly to the red of S 1063. Adopting again a reddening of $E(B-V) = 0.05$ mag and using again the main-sequence calibrations of Bessell & Brett (1988) and Bessell et al. (1998), we also give in Table 6.5 effective temperatures, luminosities and radii for the stars based on the derived photometry.

The derived properties of the secondary star are indicative of a star of mass 0.94 $M_{\odot}$ based on the Yale isochrones. While slightly higher mass than the 0.91 $M_{\odot}$ estimate derived from assuming the cluster turnoff mass for the primary, the two lines of argument give a very similar picture of the secondary star.

Given its unusual location in the colour-magnitude diagram, the derived properties of the primary star are not subject to comparison with single-star stellar evolutionary models. Nonetheless, the properties of the primary given in Table 6.5 from analysis of the system light are in contradiction to the model of the primary developed above from geometrical arguments. In particular, the photometric radius of 2.3 $R_{\odot}$ is substantially smaller than the geometric radius of 3.9 $R_{\odot}$ derived from the adopted mass of 1.3 $M_{\odot}$ and synchronous rotation. Put simply, the observed flux is too small for such a large, early-K star.

We have explored numerous paths out of this quandary. With respect to the geometric argument, the adoption of a primary mass of 1.3 $M_{\odot}$ was plausible but arbitrary. The primary mass could be as small as 0.54 $M_{\odot}$, given an inclination angle of 90°. However, even at this limit the radius of a synchronised primary star would only be reduced to 2.9 $R_{\odot}$. Equally problematic, the secondary mass would then be only 0.38 $M_{\odot}$, begging the question of how such a low-mass star could be detectable against the luminous primary.

Alternatively, the $v \sin i$ of a synchronously rotating 2.3 $R_{\odot}$ star has an upper limit of 41 km s^{-1} for an inclination of 90°. This result is consistent with 45 ± 6 km s^{-1} of van den Berg et al. (1999) [Chapter 2] far outside the uncertainty in the CfA measurement of 53 ± 2 km s^{-1}.

The assumption of synchronism might also be given up, with the primary taken to rotate super-synchronously. This is unexpected on physical grounds given that the orbit has apparently been circularised (Hut 1981). More problematic is the fact that the system shows periodic photometric variations identical to the orbital period. If these are not due to a brightness variation on the surface of a synchronously rotating primary star, an alternative origin must be found. For such modulations to derive from the secondary, the secondary light must vary by 50%. Variations in secondary light this large are not seen in the CfA spectra. A spot origin resulting from an accretion stream is an intriguing possibility, but the origin of such

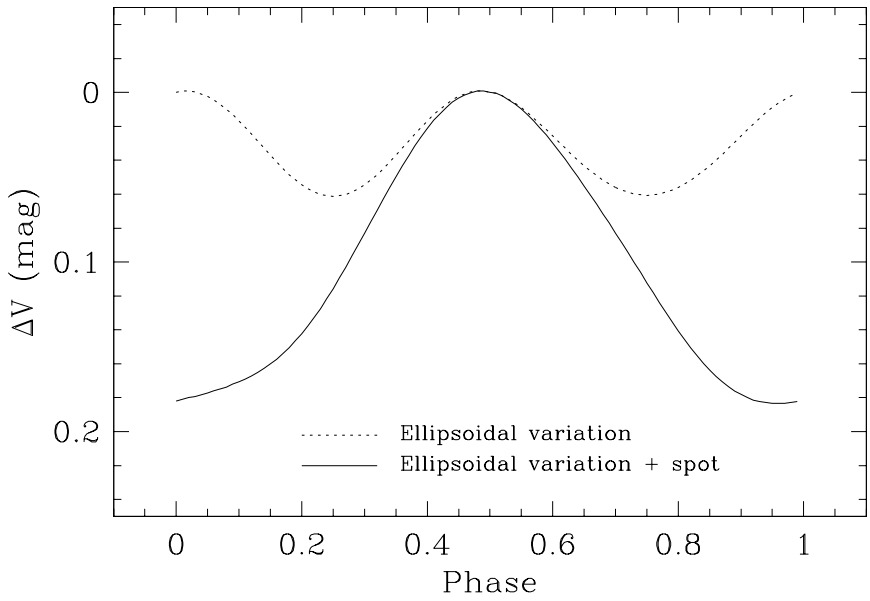

Figure 6.7: Synthetic light curves for S 1113, phased against the binary orbit solution. The upper curve shows expected light variation due to the expected ellipsoidal shape of the primary, given synchronous rotation. The lower curve shows the same light curve combined with the photometric variation due to a spot at longitude 270°. The resulting light curve is very similar to that seen for S 1113 (Fig. 6.4), and the ellipsoidal variations are no longer evident.

a stream is not evident given that the primary does not fill its Roche lobe nor is there any observational evidence for such a stream.

On the photometric side of the argument, the primary needs to be ~ 3 times more luminous at constant temperature to bring the geometric and photometric radii into agreement. Broadband photometric measurements of S 1113 are several and corroborative. The colours and derived effective temperature for the primary are very similar to the effective temperatures derived from our several analyses of high-resolution spectra, indicating both that the effective temperatures are reasonable and that the primary is not heavily reddened. While the photometric analyses have been done in the context of main-sequence calibrations, use of giant calibrations tends to slightly increase the effective temperature and lower both the derived luminosity and stellar radius. Finally, it seems unlikely – but as yet unconstrained – that the bolometric correction is in error by ~ 1 mag. The contradiction between the geometric and photometric derivations of the primary radius can also be resolved by abandoning cluster membership. If S 1113 is located 1.7 times further than the cluster, the photometric radius is immediately brought into agreement with the geometric radius.

In summary, the inconsistency between the geometric and photometric radii derived for the primary remains unresolved. However, both argue that the primary star is larger than any main-sequence member of the cluster.

6.5 Discussion

6.5.1 Membership

Any discussion of seemingly anomalous stars in clusters is premature until the cluster memberships of the stars in question are established. In the absence of a geometrically measured distance, the M 67 memberships of S 1063 and S 1113 are as secure as can be demanded. As noted, Girard et al. (1989) find the proper-motion membership probability of S 1063 to be 98%. Furthermore S 1063 lies within one core radius of the cluster centre in projection. The membership status of S 1113 is essentially the same, except that its position in projection outside the cluster core makes the argument for membership slightly less secure. However, even weighting by cluster position Girard et al. (1989) give it a membership probability of 94%, reflecting the fact that S 1113 lies within the half-mass radius of the cluster (Mathieu 1983).

Even so, in a sample of 300 high-probability ($\geq$90%) proper-motion cluster members a small fraction will in fact be field stars. Given the high-precision of the Girard et al. (1989) proper motions and the consequent excellent separation of cluster members and field stars (246 of the 300 stars have membership probabilities greater than 95%), this fraction is of order 5% or $\sim$ 15 stars. Presuming that radial velocities and proper motions are uncorrelated, and recognising that the radial-velocity dispersion of fields stars is several tens of km s^{-1}, only a few percent of such field star interlopers in the proper-motion sample will also have radial velocities within 1 km s^{-1} of the cluster radial velocity. Finding two such field stars becomes unlikely.

The argument for S 1063 and S 1113 as field stars becomes still more improbable given that they are both RS CVn stars (van den Berg et al. 2001) [Chapter 3]. Duquennoy & Mayor (1991) find the frequency of G-dwarf main-sequence binaries with periods less than 20 days to be of order 5%. These binaries will turn into RS CVns once their more massive component starts to evolve onto the (sub)giant branch; the binary turns into an Algol once the star fills its Roche lobe. Thus an upper limit to the fraction of RS CVns is given by the ratio of the subgiant lifetime to main-sequence lifetime, i.e. less than 10%. Together these arguments roughly predict that less than 1 in 200 field stars is an RS CVn. Presuming that being an RS CVn is independent of stellar kinematics, the probability that two of the few field stars which are kinematically identical to the cluster would by chance also be RS CVn would seem to be very small.

We must be wary of a posteriori reasoning here, since S 1063 and S 1113 were noticed in part because of their X-ray emission. However, even if we grant that S 1063 and S 1113 are a biased sample, it is nonetheless the case that their interpretation as field stars implies that there should be several hundred other field stars among the three-dimensional kinematic members. Presumably these stars should not have the photometric properties of cluster single stars and fall more or less randomly in the M 67 colour-magnitude diagram. Examination of Fig. 6.1 shows this not to be the case.

In summary, that S 1063 and S 1113 are field RS CVns with three-dimensional motions identical to M 67 seems very improbable.

Regrettably, such arguments can never be definitive, and so it is worth considering the nature of S 1063 and S 1113 in the context that they are not cluster members. We have argued above that the primary star of S 1063 has a surface gravity intermediate between giants and dwarfs. We have also argued that the primary star of S 1113, if synchronously rotating, has a radius of order 3–4 $R_\odot$. Both of these arguments are independent of cluster membership, and indicate that the primary stars are neither background K giants nor nearby (350 pc) K dwarfs. Rather, both stars would presently be background near-solar mass stars evolving up the giant branch.

6.5.2 Origins

S 1063

The origin of S 1063 is a challenging problem simply because neither the binary orbit nor the stellar components are remarkable. Even the X-ray emission and chromospheric activity, while notable in a cluster of this age, are understandable in the context of tidally induced rapid rotation of the primary star (van den Berg et al. 2001) [Chapter 3]. Indeed, the most notable feature of the system is the lack of periodic photometric variability associated with such rapid rotation, and the presence of longer term photometric variation. Given a radius of 2.3 $R_\odot$ (Sect. 6.4), the primary star of S 1063 does not approach filling its Roche lobe at periastron, and so the sub-subgiant location cannot be due to the Roche limit set on the primary radius by the presence of a secondary. Furthermore, the eccentric orbit does not suggest a larger primary in the past or prior mass transfer. Consequently we have explored mechanisms by which energy input to a lower-mass main-sequence star might inflate the star to the present position of S 1063.

Given the presently eccentric orbit, tidal circularisation processes must be dissipating energy in the primary star. Using the formalism of Zahn (1977), the rate of energy deposition (defined as the ratio of the energy difference between the current orbit and a circular orbit and the circularisation time) in the primary star is presently very small, of order $10^{-5}\ L_\odot$. This is not adequate to explain the observed excess luminosity.

Alternatively, the present primary may be superluminous because of recent deposition of kinetic energy via a merger of two stars. Here we consider two types of mergers: coalescence and collision. In the coalescence scenario, the S 1063 system was originally a triple system in which the present secondary was the tertiary star. If we assume that the orbital period that we observe now was equal to the period of the original tertiary star, we can use stability arguments to place an upper limit on the period of the original inner binary star. Using the coplanar formulation of Mardling & Aarseth (1998) for the stability of a triple system, and adopting a mass ratio of $q = 0.5$ (outer star to inner binary), we find that an original inner binary would have had an orbital period of less than 2.22 days. Such a period is physically permitted, and so that S 1063 was formerly a triple system is possible. Coalescence via multiple mechanisms is plausible on time scales of a few Gyr (Stępień 1995), and indeed the old (6 Gyr) cluster NGC 188 has many contact binaries (Baliunas & Guinan 1985, Rucinski 1998).

A collision scenario has been suggested as a possible mechanism for the formation of some blue stragglers in M 67 by Leonard & Linnell (1992). In the low density environment of an open cluster, collisions of single stars are improbable. However, binary-binary encounters have substantially higher probabilities, and in the course of such encounters the probability of a stellar collision is not negligible. In this scenario, the present S 1063 would consist of three of the stars involved in the binary-binary encounter, two having merged into the primary and a third being the present secondary.

A prediction of either of these merger scenarios is that the resulting star will rotate rapidly. In the coalescence scenario rapid rotation is expected as a result of synchronous rotation prior to the merger. With respect to the collision scenario, the simulations of Sills et al. (2001) show that a collision product is born with a high rotation rate. We argued in Sect. 6.4 that for aligned rotation and orbital axes, the true equatorial rotation velocity could be as large as 20 km s^{-1}, and for a primary radius of 2.3 $R_\odot$ the rotational period could be as short as 6 days. However such a rotation period is still long compared to those expected from mergers or collisions. In the collision scenario, of course, the primary rotation axis and the orbital axis need not be aligned, particularly since tidal circularisation has not come to completion. As such, the surface rotation velocity of the primary could be significantly higher. A high inclination angle could also possibly explain the lack of periodic photometric modulation. As an aside, merger scenarios have long been suggested for the M 67 blue stragglers, which also do not show evidence for notably high rotation velocities.

Most problematic, these impulsive origins must face the challenge that – even if the merger product would briefly have the properties of the S 1063 primary star – the thermal time scale of the primary is very short compared to the cluster lifetime. If, for the sake of example, we adopt a mass of 0.75 $M_\odot$, the present thermal time scale $E_{\rm pot}/L$ is only 3.4 Myr. A merger product would be expected to readjust to its new mass on such time scales, evolving into either a blue straggler for a merger of main-sequence stars or an FK Comae giant if one of the parent stars was evolved. Given such short time scales, neither of these merger mechanisms can plausibly occur frequently enough to be a plausible mechanism for the formation of S 1063

S 1113

The short orbital period of 2.8 days suggests that the sub-subgiant status of S 1113 might result from Roche limitation of the primary as it evolves off the main sequence, and that the system is presently a semi-detached binary. However, if the primary rotation is both synchronised, as suggested by the photometric periodicity, and aligned with the orbit this cannot be the case. With these assumptions, the measured $v \sin i$ provides directly $R_1 \sin i$ while the orbital solution provides $a \sin i$. Thus $R_1/a = 0.361$ independent of inclination angle. Similarly, for a give mass ratio R/L_1 is also independent of inclination angle. Thus, the ratio $R_1/L_1 = 0.74$ derived in Section 4 for the specific case of $M_1 = 1.3\,M_\odot$ is in fact general.

A slight (8°) misalignment of the primary rotation axis and orbital axis would allow a Roche-filling primary. However, the distorted shape of such a primary would lead to larger amplitude ellipsoidal photometric variability, which is not seen in our light curves. Follow-

ing the formalism in Section 6.4, we have explored the ellipsoidal variations resulting from a Roche-filling primary. The peak-to-peak amplitude increases to 0.12 mag; these larger variations are difficult to mask with concurrent photometric variations from a spot.

Thus every indication is that the primary star of S 1113 does not fill its Roche lobe, nor is there any observational indication of mass flow in the system.

6.6 Summary

The stars S 1063 and S 1113 in the M 67 field have attracted attention for their location in the cluster colour-magnitude diagram roughly 1 magnitude below the cluster subgiant branch (Fig. 6.1), for which we have called them sub-subgiants. Comprehensive photometric (optical and X-ray), spectroscopic, and astrometric study have shown them to be early-K RS CVn-like systems with observed three-dimensional motions the same as that of the cluster to high measurement precision.

Specifically, S 1063 is a single-lined spectroscopic binary with a period of 18.4 days and an eccentric orbit ($e = 0.2$). Spectroscopic surface gravity measurements indicate that the primary is neither a dwarf nor a giant, consistent with its location in the cluster colour-magnitude diagram which implies a radius of 2.3 $R_\odot$. The strong X-ray emission suggests rapid rotation of the primary, although the measured $v \sin i$ is only 6 km s^{-1}. Pseudosynchronous rotation at a period of 14.6 days is permitted by all observations to date. Oddly there is no indication of short-period photometric variability associated with such rapid rotation. Also unexplained is long-term photometric variation that is clearly not periodic on time scales of shorter than 18 days.

S 1113 is a double-lined spectroscopic binary with a circular orbit having a period of 2.8 days. The mass ratio of the system is 0.7. The composite light is variable with a period identical to or very near the orbital period. Synchronous rotation of the primary and the large measured $v \sin i$ of 53 km s^{-1} shows the primary to fill 74% of its Roche lobe, with a lower limit on the primary radius of 2.9 $R_\odot$. If the primary star is taken to be an evolved cluster member with a mass of 1.3 $M_\odot$, then the secondary star is consistent with a 0.9 $M_\odot$ main-sequence cluster member. However, the observed fluxes and colours indicate a primary radius of 2.3 $R_\odot$ under the assumption of cluster membership. This discrepancy between geometric and photometric determinations of the primary radius have not been resolved. Both argue that the primary is an evolved star.

We have been unable to develop a successful model for the origin and evolution of either S 1063 or S 1113 within the context of cluster membership. While disappointing, this failure is not unique – decades of work have not securely resolved the status of blue stragglers in open clusters. More uncomfortable is the lack of certainty regarding the membership of these binaries in M 67. Their anomalous properties can be quickly resolved simply by assigning them to the background field population, despite the unusually strong statistical arguments indicating cluster membership. In so doing, however, we run the risk of missing a new alternative evolutionary path in stellar astrophysics.

The issue of membership can only be securely resolved with parallax measurements. At the distance of M 67 these are a challenge, but we note that even 10% relative measurement precision would be sufficient to distinguish whether the difficulties in the primary radius of S 1113 can be resolved by a background location. Higher precision parallax measurements will be within the scope of planned space missions.

Until then, S 1063 and S 1113 merit more detailed study in search of more clues to their nature. In particular we encourage infrared studies to search for extended material that would be indicative of previous interactions in these systems.

Acknowledgements – We thank R. Davis, E. Horine, A. Milone and J. Peters for acquiring many of the CfA spectra. We are grateful to J. Orosz for assistance in computing the ellipsoidal variation light curves. RDM and KS are supported by National Science Foundation research grant AST 9731302. MvdB is supported by the Netherlands Organization for Scientific Research.

References

Bailyn, C. D. 1995, ARAA, 33, 133
Baliunas, S. L. & Guinan, E. F. 1985, ApJ, 294, 207
Belloni, T., Verbunt, F., & Mathieu, R. D. 1998, A&A, 339, 431
Belloni, T., Verbunt, F., & Schmitt, J. H. M. M. 1993, A&A, 269, 175
Bessel, M. S. & Brett, J. M. 1988, PASP, 100, 1134
Bessel, M. S., Castelli, F., & Plez, B. 1998, A&A, 333, 231
Catalano, S. & Frasca, A. 1994, A&A, 287, 575
Dinescu, D. I., Demarque, P., Guenther, D. B., & Pinsonneault, M. H. 1995, AJ, 109, 2090
Duquennoy, A. & Mayor, M. 1991, A&A, 248, 485
Girard, T. M., Grundy, W. M., López, C. E., & van Altena, W. F. 1989, AJ, 98, 227
Gray, D. F. 1989, ApJ, 347, 1021
Gray, D. F. & Johanson, H. L. 1991, PASP, 103, 439
Hut, P. 1981, A&A, 99, 126
Janes, K. A. & Smith, G. H. 1984, AJ, 89, 487
Johnson, H. L. & Sandage, A. R. 1955, ApJ, 121, 616
Kaluzny, J. & Radczynska, J. 1991, IBVS 3586
Kurtz, M. J. & Mink, D. J. 1998, PASP, 110, 934
Kurucz, R. L. 1979, ApJS, 40, 1
Landsman, W., Aparicio, J., Bergeron, P., di Stefano, R., & Stecher, T. P. 1997, ApJ, 481, L93
Latham, D. W. 1992, in Complementary Approaches to Double and Multiple Star Research, IAU Colloquium 135, ed. H. A. McAlister & W. I. Hartkopf, ASP Conf. Series 32, 110
Latham, D. W., Mathieu, R. D., Milone, A. A. E., & Davis, R. J. 1992, in Binaries as tracers of stellar formation, ed. A. Duquennoy & M. Mayor (Cambridge: Cambridge University Press), 132
Leonard, P. J. T. & Linnell, A. P. 1992, AJ, 103, 1928
Malyuto, V. & Schmidt-Kaler, T. 1997, A&A, 325, 693

Mardling, R. & Aarseth, S. 1999, in The Dynamics of Small Bodies in the Solar System, A Major Key to Solar System Studies, ed. B. A. Steves & A. E. Roy (Kluwer Academic Publishers), 385
Mathieu, R. D. 1983, PhD thesis, University of California, Berkeley
Mathieu, R. D., Latham, D. W., & Griffin, R. F. 1990, AJ, 100, 1859
Mathieu, R. D., Latham, D. W., Griffin, R. F., & Gunn, J. E. 1986, AJ, 92, 1100
Montgomery, K. A., Marschall, L. A., & Janes, K. A. 1993, AJ, 106, 181
Nissen, P. E., Twarog, B. A., & Crawford, D. L. 1987, AJ, 93, 634
Pasquini, L. & Belloni, T. 1998, A&A, 336, 902
Racine, R. 1971, ApJ, 168, 393
Rajamohan, R., Bhattacharyya, J. C., Subramanian, V., & Kuppuswamy, K. 1988, Bull. Astr. Soc. India, 16, 139
Richer, H. B., Fahlman, G. G., Rosvick, J., & Ibata, R. 1998, ApJ, 116, L91
Rucinski, S. M. 1998, AJ, 116, 2998
Sills, A., Faber, J. A., Lombardi Jr, J. C., Rasio, F. A., & Warren, A. R. 2001, ApJ, 548, 323
Stępién, K. 1995, MNRAS, 274, 1019
van den Berg, M., Stassun, K., Verbunt, F., & Mathieu, R. D. 2001, A&A, submitted
van den Berg, M., Verbunt, F., & Mathieu, R. D. 1999, A&A, 347, 866
Verbunt, F. & Phinney, E. S. 1995, A&A, 296, 709
Wood, M. A. 1992, ApJ, 386, 539
Zahn, J.-P. 1977, A&A, 57, 383
Zucker, S. & Mazeh, T. 1994, ApJ, 420, 806

Chapter 7

An optical study of X-ray sources in the old open clusters NGC 752 and NGC 6940

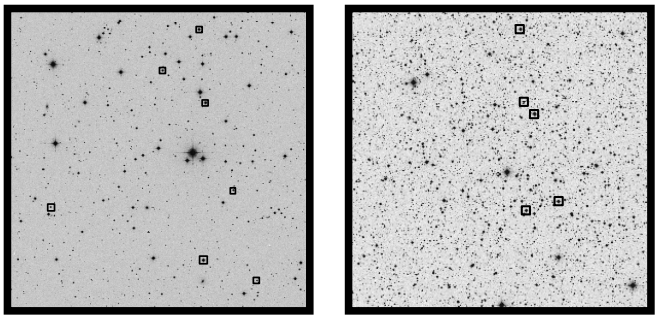

Maureen van den Berg & Frank Verbunt
Astronomy & Astrophysics 2001, 375, 387

Abstract – We observed the optical counterparts of X-ray sources in the old open clusters NGC 752 and NGC 6940 to search for the origin of the X-rays. The photometric variability reported earlier for the blue straggler H 209 is not confirmed by our light curves, nor is an indication for variability seen in the spectra; thus its X-rays remain unexplained. The X-rays of VR 111 and VR 114 are likely not a result of magnetic activity as these stars lack strong Ca II H&K emission, while in VR 108 the level of activity could be enhanced. The short-period binary H 313 is a photometric variable; this supports the interpretation that it is a magnetically active binary. From the detection of the Li I 6707.8 Å line, we classify the giant in VR 84 as a first-ascent giant; this leaves its circular orbit unexplained. As a side-result we report the detection of Li I 6707.8 Å in the spectrum of the giant H 3 and the absence of this line in the spectrum of the giant H 11; this classifies H 3 as a first-ascent giant and H 11 as a core-helium-burning clump star, and confirms the faint extension of the red-giant clump in NGC 752.

7.1 Introduction

X-ray observations of open clusters older than 1 Gyr led to the detection of many magnetically active binaries (e.g. Belloni 1997). This is not unexpected: at these high ages single late-type stars are believed to rotate too slowly to emit detectable X-rays, and tidal interaction in a close binary is therefore necessary to maintain rotation at a higher rate than is typical for stars of that age. However, our interest is mainly in the stars whose X-rays are not as easily explained: binaries with orbital periods too long for tidal interaction, and stars whose evolutionary statuses are poorly understood. Such peculiar X-ray sources were pointed out in M 67 (Belloni et al. 1998) and were selected by us for an optical follow-up study (van den Berg et al. 1999) [Chapter 2]. This revealed interesting results (e.g. the blue straggler S 1082 turned out to be a complex triple system, van den Berg et al. 2001a [Chapter 5]) but in several cases the X-rays remain unexplained. The failure to explain the origin and properties of these stars demonstrates that our understanding of the X-rays and stellar interactions in old open clusters is still limited. We have observed similar peculiar X-ray sources in two other old clusters, NGC 752 and NGC 6940, to look for for optical signatures for the X-ray emission and to compare their properties with those of the ones found in M 67. The properties of the X-ray sources in the two clusters are summarised in Table 7.1.

NGC 752 is a nearby ($\sim$ 450 pc, Daniel et al. 1994) open cluster with an estimated age of 2 Gyr (Dinescu et al. 1995). Seven X-ray sources were identified with optical cluster members (Belloni & Verbunt 1996; not counting the probable detection of the short-period binary DS And). Our study is focused on the blue straggler H 209, the only X-ray source in NGC 752 that is not located along the cluster's main sequence (see Fig. 7.1). H 209 is a spectroscopic binary with a long orbital period (Latham et al. private communication). Magnetic activity in the early-type star is not expected, but also the orbital period is too long to generate magnetic activity in a possible late-type secondary. Low-amplitude (0.05 mag) photometric variability was noted by Hrivnak (1977). Three of the remaining X-ray sources (H 205, H 313 and the contact binary H 235) are binaries with orbital periods less than 2 days; hence their X-rays are likely a result of magnetic activity. The same could be the case for the rapid rotator H 214 (Daniel et al. 1994). The radial-velocity measurements of H 182 by Daniel et al. (1994) show no indication of binarity while no measurements are made of H 156.

NGC 6940 is somewhat younger than NGC 752. It is considered to be an old cluster (Janes & Phelps 1994) with age-estimates ranging from 0.6 Gyr (Carraro & Chiosi 1994) to 1.1 Gyr (van den Bergh & McClure 1980). Four X-ray sources were identified with cluster members (Belloni & Tagliaferri 1997, Fig. 7.2). VR 111 is a spectroscopic binary with a 3595 day eccentric orbit, too wide for tidal interaction (Verbunt & Phinney 1995). For VR 108 the limit on the radial-velocity variations excludes orbital periods shorter than 4000 days (Mermilliod & Mayor 1989). VR 114 is not a proper-motion member (Sanders 1972) and therefore not included in photometric and radial-velocity studies. However, Belloni & Tagliaferri derived that it is located at a similar distance as the cluster ($\sim$ 900 pc, Larsson-Leander 1964) and suggested that the star could somehow be related to the cluster. We are mainly interested in these three stars. The other sources, VR 100 and VR 84, are spectroscopic binaries with

ID	V	B–V	$P_{\rm orb}$ (days)	ctrate (s^{-1})	sp.type (lit)	sp.type	$F_{\rm Ca}$ (erg s^{-1} cm^{-2})	$v_{\rm rad}$ (km s^{-1})	$v_{\rm rot} \sin i$ (km s^{-1})
NGC 752									
H 156	13.77	0.87		0.0036(6)		G9-K0V			
H 182	12.24	0.61		0.0038(6)		F5-7V			
H 205	9.92	0.42	1.45	0.0045(6)	F3IV-Vp				
H 209	9.74	0.061	1574[a]	0.0018(5)	B9.5V			10(3)	
H 214	10.47	0.38	rot	0.0039(6)	F2IV			6.1(4)	64(5)
H 235	11.47	0.48	0.4118	0.0020(4)	F5				
H 313	13.39	0.83	1.95	0.0062(7)					
H 3[b]	9.57	1.00		<0.0084	K0III	gG4-G8	8.7(2.2) 10^{-14}	4.7(2)	–
H 11[b]	9.29	0.97		<0.0014		gG		5.2(2)	–
NGC 6940									
VR 84	10.91	0.83	54.2	0.0020(5)	F8	F4-F6		1.4(4)	4–5
VR 100	10.43	0.74	82.5	0.0011(4)	F5[c]	F4-F6		–15.8(1)	1–2
VR 108	11.19	1.04		0.0018(5)	gG5	gG4-G8	1.3(0.3) 10^{-14}	7.7(1)	5–6
VR 111	11.56	1.05	3595	0.0011(4)	gG5	gG5-G9	5.8(1.5) 10^{-15}	10.0(6)	3–4
VR 114	11.17	1.27		0.0012(5)	gG8	gG9-K0	2.4(0.6) 10^{-15}	–9.1(7)	1–2
VR 92[b]	11.77	1.20	549.2	<0.0010	gG8	gG5-G9	6.4(1.6) 10^{-15}	8.1(4)	2–3
VR 152[b]	10.84	1.07		<0.0005	gG8	gG5-G9		8.2(5)	1–2

[a] preliminary solution by Latham et al. (private communication)
[b] comparison stars, 2σ-upper limit to the PSPC count rate determined from re-analysis of ROSAT data)
[c] spectrum is composite (Bidelman suggests G8II+A7, see Walker 1958)

Table 7.1: Properties of the stars in NGC 752 and NGC 6940 discussed in this paper. We list the star identification number (Heinemann 1926, Vasilevskis & Rach 1957), V magnitude and $B-V$ colour (Daniel et al. 1994, Larsson-Leander 1964), the orbital period $P_{\rm orb}$ (see Belloni & Verbunt (1996) for references on NGC 752; rot=rapid rotator $v_{\rm rot} \sin i > 30$ km s^{-1}, Daniel et al. (1994); see Mermilliod & Mayor (1989) for NGC 6940), the X-ray count rate in PSPC channels 41-240 corresponding to 0.4-2.4 keV (Belloni & Verbunt 1996, Belloni & Tagliaferri 1997), the spectral type from literature (Garrison 1972; Rebeirot 1970; Larsson-Leander 1964), the spectral type as derived from our low-resolution spectra, the flux in the Ca II H&K lines $F_{\rm Ca}$, the heliocentric radial velocity $v_{\rm rad}$ and projected rotational velocity $v_{\rm rot} \sin i$.

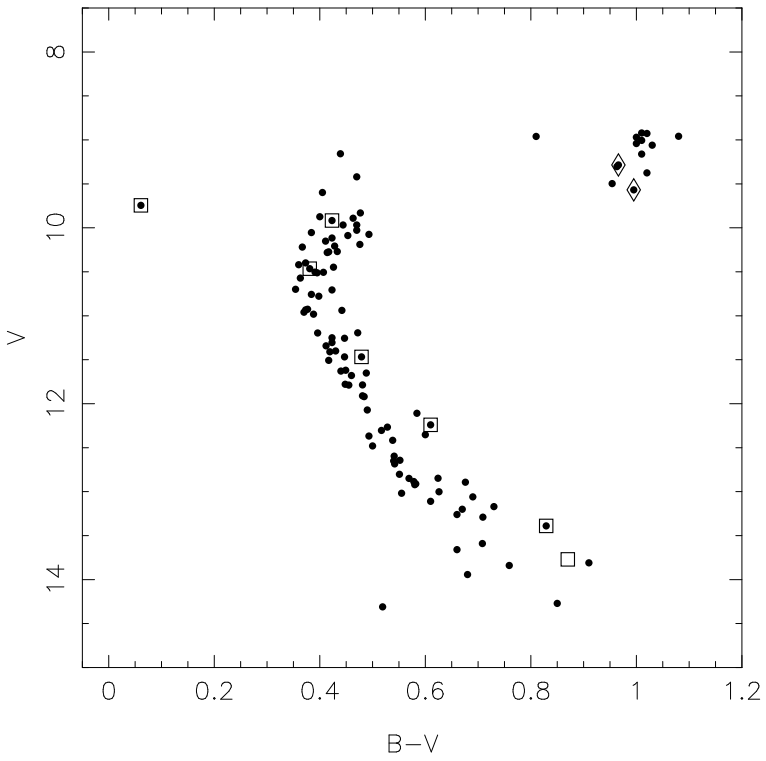

Figure 7.1: Colour-magnitude diagram of NGC 752 showing the member stars according to Daniel et al. (1994). X-ray sources are indicated with squares, our comparison stars with diamonds. The empty square is at the position of H 156 that is classified as a possible member by Daniel et al.

circular orbits shorter than 100 days, indicative for tidal interaction. VR 100 is a double-lined spectroscopic binary which explains its position in the colour-magnitude diagram between the turnoff stars and the giants.

We have obtained low- and high-resolution spectra to look for optical signatures of X-ray activity. In particular we studied the Ca II H&K lines that are optical indicators of magnetic activity, and we determined projected rotational velocities. For the X-ray sources in NGC 752 we also obtained multi-colour light curves. Sect. 7.2 describes our observations and data-analysis. The results are presented in Sect. 7.3 and are discussed in the last section.

7.2 Observations and data reduction

7.2.1 Spectroscopy

Low- and high-resolution spectra were obtained with the 4.2-m William Herschel Telescope on La Palma on the nights of July 29 and 30 1999. Weather conditions were good with a typical seeing of $1''$. An overview of the spectroscopic observations is given in Table 7.2.

		ISIS		UES-b		UES-r	
ID	n	UT	t_{exp}	UT	t_{exp}	UT	t_{exp}
X-RAY SOURCES							
H 156	2	2:43	360				
H 182	2	2:51	120				
H 209	1	3:34	20	4:59	720	4:07	360
						4:19	360
						5:15	720
						5:30	600
						5:43	300
	2	2:58	20	4:09	720	3:54	720
						4:47	900
						5:05	900
						5:44	600
H 214	2	2:54	30			5:23	600
VR 84	2	0:36	90/40	23:30	600	21:41	750
				23:43	600		
VR 100	1	2:39	30/15	23:20	750	21:11	900
		2:43	60/30				
VR 108	2	0:33	90	22:54	600	21:14	600
				23:12	600	21:27	600
VR 111	1	2:52	180/	0:19	900	22:02	1200
			120	0:37	900		
VR 114	1	2:56	180/90	0:55	900	22:26	1200
	2	0:28	180/90	23:57	900		
COMPARISON STARS							
H 3	1	3:37	30/20	4:57	500	4:28	600
H 11	2	2:56	20/10	4:26	360	3:44	360
VR 92	1	2:48	120	23:44	1000	21:46	1500
				0:06	1200		
VR 152	2	0:39	90/30	21:58	600	22:41	750
		0:40	–/30	22:28	600		
FLUX STANDARD							
BD+284211	1	3:21	30				
	2	1:01	30				
		1:03	30/–				
RADIAL-VELOCITY STANDARDS							
HD 187691[a]	1			1:27	20	2:12	40
	2			20:51	80	20:57	80
HD 212943[b]	1			1:41	20	1:57	40
	2			0:00	20	3:29	20

[a]F8V, [b]K0III-IV (Astronomical Almanac)

Table 7.2: Log of the spectroscopic observations. From left to right: star number; date of observation: n(ight) 1=July 29, 2=July 30 1999; UT at start of the exposure and exposure time t_{exp} in seconds for ISIS (where appropriate, t_{exp} is listed separately for the blue/red arm), and the blue and red setup of UES.

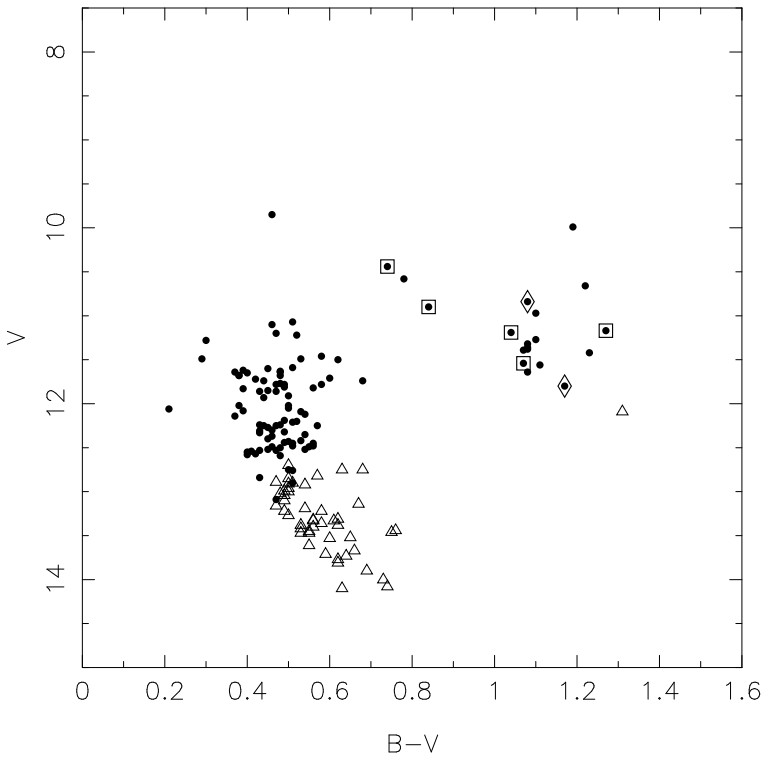

Figure 7.2: Colour-magnitude diagram of NGC 6940 showing the stars with proper-motion membership probability larger than 70% (filled circles; Sanders 1972). No proper-motion information is available for the fainter stars, indicated with open triangles. X-ray sources are indicated with squares, our comparison stars with diamonds. The empty square is at the position of VR 114 that is not a proper-motion member according to Sanders (1972).

Low-resolution spectra

Low-resolution (R $\approx$ 1000) spectra were obtained with the double-beam spectrograph ISIS used in combination with the 5700-dichroic. The blue arm was centred on 4504 Å. The 300 lines mm^{-1} grating gives a dispersion of $\sim$ 0.86 Å pixel^{-1} which results in a wavelength coverage of 2743–6260 Å. The atmosphere blocks flux below 3200 Å. The red arm was centred on 7191 Å and was used with the 158 lines mm^{-1} grating. The dispersion of $\sim$ 2.90 Å pixel^{-1} results in a red spectrum of 5778–8726 Å. Program stars were observed with a 4″ slit width; the slit was widened to 8″ for the observations of the flux standard BD+28 4211.

IRAF routines were used to reduce the data. First a bias correction was applied to the frames. The dichroic leaves a signature in the blue spectra between 4000 and 4600 Å that consists of wiggles with an amplitude of up to 6% of the count level. This is not entirely removed by dividing the bias-corrected frames through a normalised flatfield image. Instead, the effect was reduced by extracting a spectrum from an unflatfielded image and next dividing it by a flatfield spectrum extracted from the same region on the CCD as the object spectrum.

Wavelength calibration was done with CuNe-lamp spectra. A dispersion solution was derived by fitting second (blue) and first (red) order cubic splines to the position of the arc lines on the CCD. Counts were converted to absolute flux using spectra of BD+28 4211 and the flux table by Massey et al. (1988) and the atmospheric extinction curve for La Palma (King 1985).

High-resolution spectra

The Utrecht Echelle Spectrograph (UES) was used in a blue (central wavelength 4253 Å) and red (central wavelength 6565 Å) setup to obtain high-resolution (R $\approx$ 49 000) spectra. The spectrograph was combined with the 31 lines mm^{-1} grating and SITe1 CCD, resulting in a total wavelength coverage of 3620 to 9930 Å. Exposures of a Tungsten lamp served as flatfield images; Thorium-Argon lamp spectra were taken for the purpose of wavelength calibration.

The images were processed with the IRAF packages CCDRED and ECHELLE. They were corrected for a bias signal and flatfielded before spectra were extracted for each echelle-order. Sixth-order polynomials were fitted in both directions of the CCD to the positions of the ThAr-lines. The maximum residuals to the fit are $\sim$ 0.01 Å (or 0.6 km s^{-1} at 5000 Å). Polynomials were fitted to the spectra for continuum normalisation. The orders containing the Ca II H&K lines of a given star were calibrated in units of absolute flux with the calibrated low-resolution spectra of the same star.

7.2.2 Photometry

The X-ray sources in NGC 752 were monitored in the *U*, *B*, *V* and *I* bands during the seven nights of December 20 to 26 1999 with the 1-m Jacobus Kapteyn Telescope on La Palma. The typical seeing varied between 1.6″ and 3″. The telescope is equipped with a 2148x2148 pixel^2 SITe2 CCD which has an unvignetted field of view of $\sim$ 10x10 arcmin^2. The field around the blue straggler H 209 was observed intensively with 4 to 5 exposures per filter per hour. Roughly every two *UBVI*-sequences the pointing was changed between a field that in addition includes either the X-ray source H 156 or H 182. The frames were exposed for typically 80 s in *U*, 25 s in *B* and 15 s in *V* and *I*. Two fields including H 205, H 214, H 235 and H 313 were observed only once or twice per night with typical exposure times of 180 s (*U*), 120 s (*B*), 60 s (*V*, *I*) for H 313 and 80 s (*U*), 15 s (*B*), 10 s (*V*, *I*) for the other sources. The locations of the fields that were observed are shown in Fig. 7.3.

Bias removal and flatfielding were done in IRAF. Aperture photometry for all the stars in the fields was done with the DAOPHOT.PHOT task. The method of ensemble photometry (Honeycutt 1992) was used to compute differential light curves.

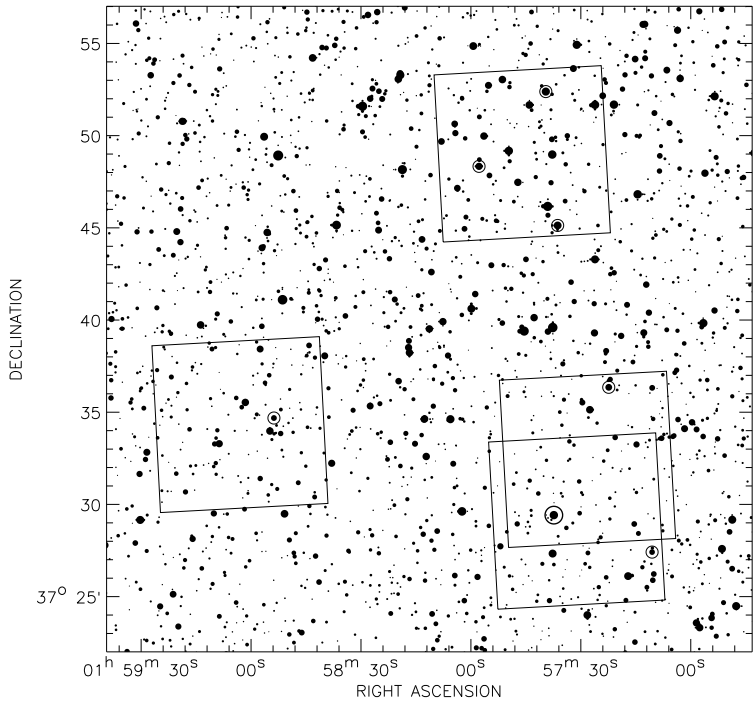

Figure 7.3: Map of a 35 x 35 arcmin^2 region of NGC 752 centred on α_{J2000}=1^{h}58^{m}11^s.3, δ_{J2000} = 37°39′34.0″. The fields that were monitored are indicated, X-ray sources are encircled. The coordinates of the stars in the field are taken from the USNO-A1.0 catalogue.

7.3 Results

7.3.1 Photometric variability

The light curves in each filter were tested for variability with a χ^2-test. A star was labelled as a probable variable if the probability that its light curve is compatible with being constant is smaller than 0.3%. Two stars were thus found to be variable: H 313 and, as expected, the contact binary H 235. We computed Lomb-Scargle periodograms (Scargle 1982) to search for periodicity in the light curves of H 313, that contain only $\sim$ 10 points. A periodogram was computed at 1000 frequencies between a minimum period and maximum period that correspond to twice the sampling period (3 hours) and the length of the observation run (7 days). We chose the highest peak in the periodogram as a first estimate for the period of the variability. A false-alarm probability (fap) for the period detection was computed (van den Berg et al. 2001b [Chapter 3]) to estimate the chance detection of the periodicity. We accept periods with a fap less than 1% as significant, but the candidate periods all had higher faps. However, when the data points are folded on the binary period of 1.95 days, photometric variability on that period looks suggestive (Fig. 7.4). As an accurate photometric period of 0.4118 days is known for H 235 (Milone et al. 1995), we did not search for a period in its light

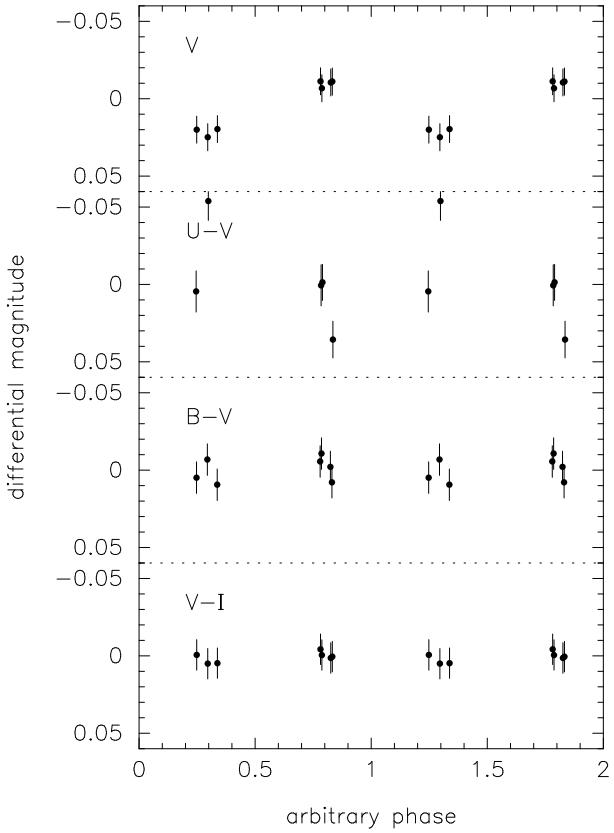

Figure 7.4: Light and colour curves of H 313 folded on the orbital period of 1.95 days. The magnitudes are plotted with respect to the average V-magnitude and colours.

curves of only $\sim$ 10 points.

The light curves of our main target H 209 are constant within $<$0.01 mag.

7.3.2 Spectral classification

With the classification criteria of Malyuto & Schmidt-Kaler (1997) for F- to K- type stars, spectral types were assigned to H 156 and H 182, for which no classifications were found in literature. The method is based on features in the wavelength region 3640 to 5305 Å that define the classification indices I_1, I_2, I_3 and I_S. We computed the values for these indices with the low-resolution spectra. A spectral class of G9-K0 V is derived for H 156 and of F5-F7 for H 182; the values of the classification indices of H 182 are insensitive to luminosity class in that specific region, but its position in the colour-magnitude diagram shows it to be a dwarf. The comparison giant H 11 is classified as a G-type giant (luminosity class III or brighter). For the other stars we find spectral types that are in agreement with earlier classifications to within two subclasses (see Table 7.1). The spectral types of H 209 and H 214 are too early to be classified with the criteria of Malyuto & Schmidt-Kaler.

With the low-resolution spectrum of VR 114 we derive its spectroscopic distance. The luminosity classification is refined using the calibration of the equivalent width of the Ca II infrared lines at 8498.02 and 8542.09 Å against luminosity class by Mallik (1994). The equivalent width of 4.8 Å (determined from the high-resolution spectrum between the ranges used by Mallik) indicates that VR 114 is probably of luminosity class II or III. $B-V$ (1.24 ± 0.14) and $U-B$ (1.08 ± 0.14, no measurement found in literature) colours are computed by folding the spectrum calibrated in absolute-flux units with U, B and V filter transmission curves. Errors are estimated from comparison of the magnitudes thus derived for the flux standard with tabulated values. The reddening and distance can now be derived from comparison with the colours and absolute magnitudes of standard giant (class III) and bright giant (class II) stars. If VR 114 is a giant, then $E(B-V) \approx 0.3$ (for type K0) and the distance ~ 810 pc, similar to the value found by Belloni & Tagliaferri; if VR 114 is a bright giant, then $E(B-V) \approx 0.16$ (for type K0) and the distance ~ 4 kpc. As the reddening in the direction of NGC 6940 was found to vary between 0.2 and 0.3 (Larsson-Leander 1964), the classification of VR 114 as a class III giant seems to be more plausible. We thus confirm that VR 114 lies at about the same distance as NGC 6940.

7.3.3 Ca II H&K emission

Emission cores in the centre of the broad Ca II H&K absorption lines are often used as optical indicators for magnetic activity in late-type stars (e.g. Fernández-Figueroa et al. 1994). Therefore, strong emission in these lines would be an indication that the X-rays are of coronal origin. The high-resolution spectra of our late-type target and comparison stars in the region around the 3933.67 Å Ca II K line are shown in Fig. 7.5. Emission above the level of the absorption profile is seen in all X-ray sources, but the emission is of similar strength as in the non–X-ray sources H 3 and VR 92. The flux in the emission lines was estimated with the IRAF task SPLOT: the pseudo-continuum of the absorption line is estimated by eye; the flux above this level is obtained by summing the pixel values above a straight line connecting the continuum on both sides of the emission (see Table 7.1). We adopt an error of $\sim 25\%$ accounting for the fact that the choice of the continuum is a bit arbitrary. We choose this method to measure emission fluxes as it is similar to the way fluxes were determined for the stars in our comparison sample (Fernández-Figueroa et al. 1994); higher-order fits to the continuum, as used by Fernández-Figueroa et al., instead of a straight line to estimate the continuum gave similar results for the stars discussed in van den Berg et al. (1999) [Chapter 2]. No emission flux is determined for VR 100, that has a composite spectrum, and for VR 84, whose spectrum could also be composite judging from its position in the colour-magnitude diagram. For VR 100 the predicted position of the K line lies to the left of the centre in the composite absorption profile. Apparently, the relative contribution of the companion star is strong in the blue.

A comparison with magnetically active binaries is made by combining the information from the X-ray and H&K emission. In Fig. 7.6 the emission in both activity indicators is

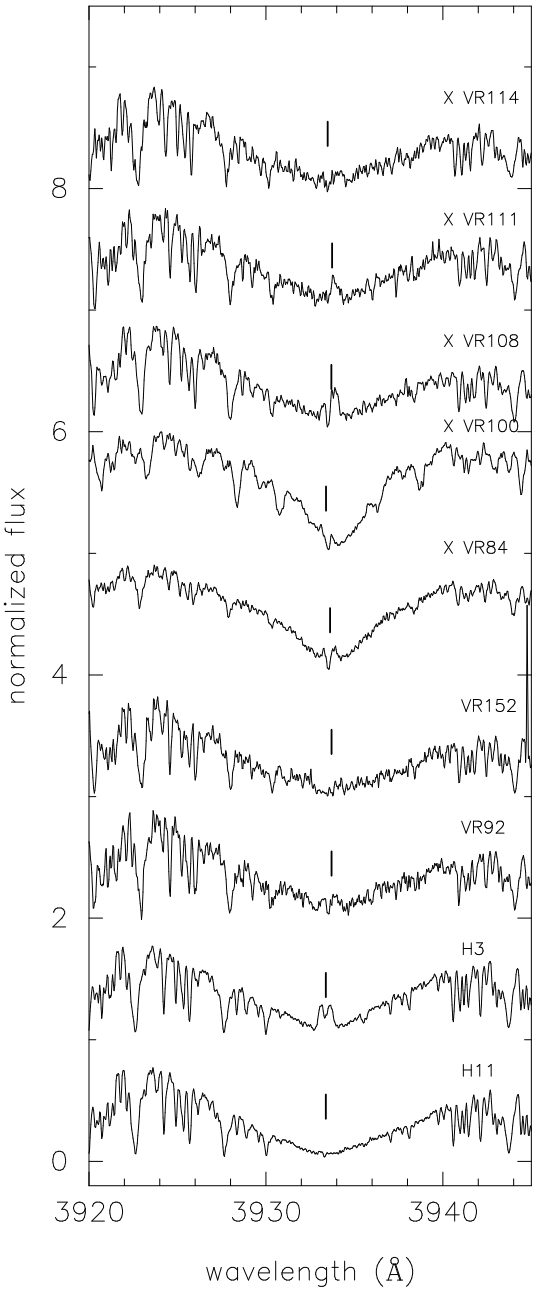

Figure 7.5: Ca II K line in our late-type X-ray sources ('X') and the non–X-ray sources comparison giants H 3, H 11, VR 92 and VR 152. The expected position of the K-line centre as derived from the radial-velocity measurements of Sect. 7.3.4 is marked with the vertical line; from the position of this line to the left of the centre of the absorption profile it is clear that the spectrum of VR 100 is composite. The spectra are normalised to the continuum near 3915 and 4000 Å. A vertical offset is applied for clarity to all spectra but that of H 11.

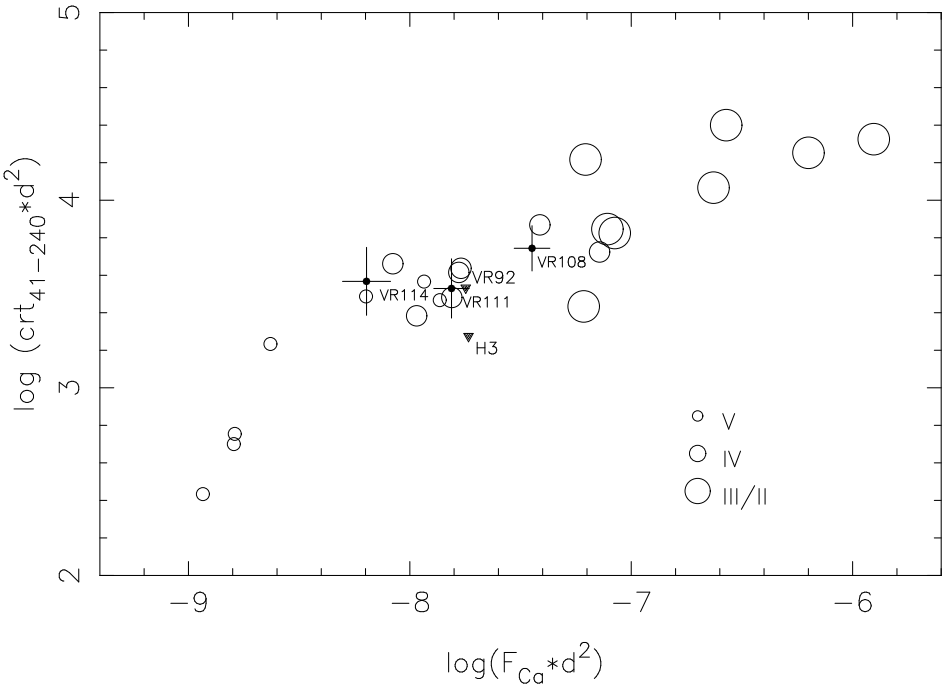

Figure 7.6: Comparison of the Ca II H&K and X-ray emission of our targets with that of magnetically active binaries. Fluxes in the Ca II H&K emission lines $F_{\rm Ca}$ (in erg s^{-1} cm^{-2}) and X-ray count rates between 0.4 and 2.4 keV (channel 41-240 of the ROSAT PSPC) are multiplied with the square of the distance d in parsec to eliminate the effect of distance. The luminosity class of the active star in the comparison sample is indicated with the size of the symbol. The comparison giants H 3 and VR 92 are indicated with filled triangles using the upper limits to the PSPC count rates listed in Table 7.1.

plotted for the same sample of magnetically active binaries as used in van den Berg et al. (1999) [Chapter 2] to study magnetic activity of stars in M 67. The H&K fluxes were taken from Fernández-Figueroa et al. (1994), the X-ray emission is given as the count rate in the 0.4 to 2.4 keV band of the ROSAT PSPC. A description of the sample and the determination of the X-ray count rates can be found in van den Berg et al. (1999) [Chapter 2]. The fluxes and count rates are multiplied by the square of the distance in parsecs so that stars at different distances can be compared. To correct for the absorption towards NGC 6940, we multiply the X-ray count rate and Ca II H&K optical fluxes as listed in Table 7.1 by 3.8 and 3.3, respectively. Our target stars lie in the region where active binaries are found, but the level of activity in VR 111 and VR 114 appears to be low for their luminosity class. This makes it unlikely that the X-ray emission arises through coronal activity in these giants. As the position of VR 108 lies closer to the active giants, activity could be enhanced in VR 108.

No H&K emission lines are visible in the low-resolution spectra of H 156, H 182 and H 214.

We also checked the X-ray sources for emission in the Hα line, another optical signature for activity, but found no indication for emission. The nine spectra of H 209 show no

variability in the Hα-profile.

7.3.4 Radial and rotational velocities

Radial velocities were determined through cross correlation of the high-resolution spectra against the spectra of the radial-velocity standards. We adopt the velocity resulting from correlation with the template that gives the highest correlation peak (better spectral match). The orders between 4960 and 5510 Å for the blue exposures and 4970 and 5530 Å for the red exposures were used; Table 7.1 lists their average. The systematic errors in the measurements for the rapid rotator H 214 will be larger than in the other measurements as our radial-velocity standards are slow rotators and therefore give a bad match between object and template spectrum. The radial velocity of H 209 was measured by cross correlating the spectrum between 5145 and 5225 Å with a synthetic spectrum (Kurucz 1979) of $T_{\rm eff} = 9750$ K, gravity $\log g = 4.0$ and $v_{\rm rot} \sin i = 50$ km s^{-1} (we adopt the parameters for H 209 as derived by Schönberner & Napiwotzki 1994).

The results for H 3, H 11, VR 152 and VR 108 agree with the values found by Mermilliod et al. (1998) and Mermilliod & Mayor (1989) within 1 km s^{-1}; the velocity we find for H 214 is 2 km s^{-1} off from the value of Daniel et al. (1994). For the proper-motion non-member VR 114 we find a radial velocity that does not agree with the cluster mean (7.75±0.13 km s^{-1}, Mermilliod & Mayor, 1989). Comparison with Fig. 5 of Mermilliod & Mayor (1989) shows that the radial velocities of the binaries in NGC 6940 are roughly as expected, except for VR 84 for which we observe a radial velocity that is ~ 7 km s^{-1} lower than expected. We do not know the reason for this; the period of Mermilliod & Mayor is too accurate to allow such a large deviation at the orbital phase at which we observed VR 84 (137.75±0.04).

The red spectra of H 209 were also cross correlated against each other to look for radial-velocity variations on time scales of hours. We found no variation within the errors (1–2 km s^{-1}).

As stellar rotation and magnetic activity are closely linked, we also determine projected rotational velocities. Rotational velocities were measured from cross correlations with synthetic spectra (Kurucz 1979). Synthetic spectra of $T_{\rm eff} = 5500$ K, gravity $\log g = 3.0$, turbulent velocity $v_{\rm turb} = 2$ km s^{-1} and $v_{\rm rot} \sin i$ varying between 0 and 19 km s^{-1} in steps of 1 km s^{-1} were calculated between 4970 and 5040 Å. The object and synthetic spectra were correlated against the $v_{\rm rot} \sin i$=0 km s^{-1} spectrum; the peak of the cross correlation functions are fitted with gaussian profiles. With the results we make a calibration curve that gives the width of the cross correlation peak as function of rotational velocity. The rotation for the objects then follows from comparison of the measured widths of their peaks with this calibration curve (see Table 7.1). The widths of the correlation peaks from H 3 and H 11 are smaller than the smallest widths in the calibration curve. We note that the velocity thus derived is sensitive to the spectral type of the template. For example, correlation with a template of $T_{\rm eff} = 5000$ K (same $\log g$) gives rotation velocities that are ~ 1 km s^{-1} lower.

For the rapid rotator H 214 $v_{\rm rot} \sin i$ was determined with the method of Fourier-Bessel

transformation (see Piters et al. 1996, Groot et al. 1996) that we also applied to the spectrum of the rapid rotator S 1113 in M 67 (van den Berg et al. 1999) [Chapter 2]. We used three Fe I lines at 6400.15, 6408.03 and 6411.54 Å to find an average $v_{\rm rot}\sin i$ of 64 km s^{-1}, a typical value for a star of this spectral type (Groot et al. 1996). The error in the cleanest line is 1.6 km s^{-1}, in the most noisy line 10 km s^{-1}. We determined no rotational velocity for the blue straggler H 209 for which Schönberner & Napiwotzki (1994) determined a value of $v_{\rm rot}\sin i$ of 50 km s^{-1} from high-resolution spectra.

7.3.5 Lithium 6708 Å

As the element Lithium is easily destroyed at temperatures higher than $\sim 2\ 10^6$ K, it can be used to discriminate between first-ascent giants, with outer layers that are not yet completely mixed to deeper, hotter layers by the development of a convective envelope, and clump stars. Discrimination between the two evolutionary phases can be difficult based on the position of a star in the colour-magnitude diagram alone as the position of the clump is close to the track of the first-ascent giants. Verbunt & Phinney (1995) suggested that the orbital eccentricity of binaries containing a giant can be of help: the present radius of a clump giant is smaller than its radius at the tip of the giant branch; as the time scale for tidal circularization $\tau_{\rm circ}$ is very sensitive to the ratio of the radius of the star with the dissipative tides R to the semi-major axis a ($\tau_{\rm circ}^{-1} \sim (R/a)^8$), clump stars can have circularized orbits that are too wide to be circularized by first-ascent giants with the same radius. Based on the circular orbits of VR 84 and VR 100 Verbunt & Phinney therefore concluded that the giants in these binaries must be clump stars. We can test this prediction now by looking at the presence of the Lithium 6707.8 Å line: whereas it is absent in VR 100 - as expected from the prediction of Verbunt & Phinney - the line is visible in the spectrum of VR 84 which implies that the giant in VR 84 is a first-ascent instead of a clump giant (see Fig. 7.7).

How can it be that the orbit of VR 84 is circular? One possibility is that the decomposition of VR 84 into the two binary components (Mermilliod & Mayor 1989) underestimates the radius of the giant. However, according to the calculations by Verbunt & Phinney the radius has to increase to $\sim$16 $R_\odot$ which cannot be accounted for by varying the reddening or distance modulus within the ranges that are found for NGC 6940 ($0.2 < E(B-V) < 0.3$, $(m-M)_0 = 9.7$; Larsson-Leander 1964) or by making the giant cooler (if $T_{\rm eff} = 4420$ K then $R \approx 15 R_\odot$ according to the tables of Schmidt-Kaler; however this gives an observed $B-V = 1.42$ which is redder than all the giants in NGC 6940). Alternatively, the orbit was not circularized by the present giant but during the giant-phase of its companion that in that case would be a white dwarf now. To account for the observed blue colours of VR 84 the companion white dwarf must be young and bright. The probability that we see both stars in VR 84 in relatively short-lived evolutionary phases is small. A white-dwarf companion is not excluded by the spectroscopic orbit that places a lower limit on the mass of the companion of 0.65 $M_\odot$.

As an aside, we report on the observation of the Li I 6708 Å line in the two comparison giants H 3 and H 11. The red clump of core-helium-burning stars in NGC 752 has attracted

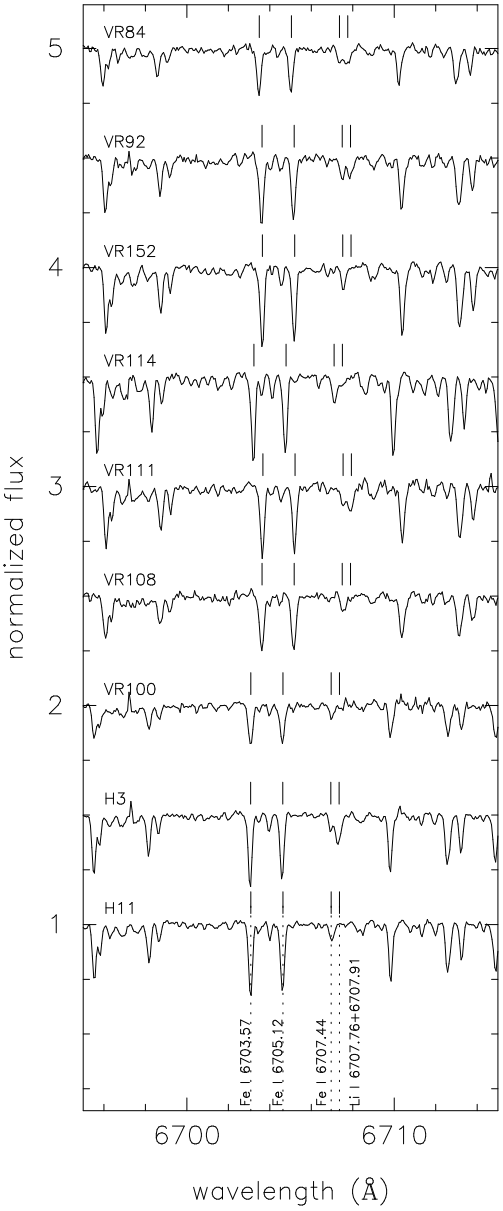

Figure 7.7: The region around the Li I 6707.76 Å, 6707.91 Å doublet. The expected positions of the lines are derived from the radial-velocity measurements.

some attention: Mermilliod et al. (1998) pointed out four stars, including H 3 and H 11, below and to the blue of the main clump whose position is not reproduced by theoretical isochrones. Knowledge about the evolutionary phase of H 3 and H 11 could provide more insight into the situation. Daniel et al. (1994) predicted that H 11 would be depleted of Lithium, whereas Lithium would be present in H 3, that lies more towards the first ascent track; no Lithium was found in the other two stars below the main clump (Pilachowski et al. 1988).

These expectations are confirmed by our observations (see Fig. 7.7) that show the Li I doublet in H 3, while it is absent in H 11. Thus the three bluest stars under the clump likely form a real extension to the clump. Girardi et al. (2000) suggested that the spread seen in the clump of NGC 752 results from the simultaneous presence of clump stars that have undergone the helium flash (the main clump) and of more massive stars that start helium burning more quiescently (at fainter magnitudes); a similar spread near the clump has been observed in the open cluster NGC 7789 that has about the same age as NGC 752.

7.4 Discussion and conclusions

In this paper we report on photometric and spectroscopic observations of four X-ray sources in the old open clusters NGC 752 and NGC 6940, for which the X-rays are unexplained. We conclude that our observations have not provided an answer to the question why these stars emit X-rays. Could it be that the optical identifications of the X-ray sources are wrong? Belloni & Verbunt (1996) show that the probability for a chance identification in the field of NGC 752 is only 1%. In NGC 6940, the suggested optical counterparts are so bright (between 11.5 and 10.4) that the probability for a misidentification is small. We conclude that the stars that we have studied are indeed the optical counterparts to the X-ray sources.

The light curves of the blue straggler H 209 in NGC 752 do not confirm earlier reports of variability (Hrivnak 1977); nor is an indication for variability seen in the spectra. Two other blue stragglers in open clusters (in M 67 and in IC 4651) were detected in X-rays. The former turned out to contain a 1.07-day period binary that could have a late-type magnetically active component (van den Berg et al. 2001a) [Chapter 5]. No evidence for a similar system is seen in H 209. The source of the X-ray emission in H 209 and its blue-straggler nature remain a mystery.

The giants VR 108, VR 111 and VR 114 in NGC 6940 are of later spectral type and therefore magnetic activity in their convective outer layers could in principle be a cause for X-ray emission; though strong activity would be surprising as VR 111 is a wide binary and VR 108 shows no indication for binarity. The Ca II H&K emission fluxes that we measure in VR 111 and VR 114 are indeed lower than is typical for magnetically active stars of their luminosity class; the asymmetric emission cores in the Ca II H&K lines could be a signature of mass outflow as suggested by Dupree et al. (1999), who found similar emission cores in giants of various masses and temperatures. Also, the stars are not found to be rapid rotators. Therefore the X-rays are probably not a result of enhanced magnetic activity in the giants themselves. Similar optical counterparts to X-ray sources – with long orbital periods or no indication for

binarity – were identified in the older cluster M 67 (S 1237, S 760, S 775, S 1270). Apparently another mechanism than activity gives rise to the X-rays of the giants. Alternatively, these stars are triples that contain a hitherto undetected close binary, e.g. because the close binary is relatively faint or because its spectral signature is masked by rapid rotation of the component stars. Activity could be enhanced in VR 108; interestingly, the rotation velocity that we measure is somewhat higher than in the other giants. The reason for an enhanced activity level is not clear.

We confirm that VR 114 is located at about the same distance as the cluster. The information that we add here is that, like its proper motion, its radial velocity is not compatible with the cluster average. More radial-velocity measurements are needed to establish its binary nature.

We find that the short-period binary H 313 in NGC 752 is a photometric variable, and that its light curve suggests variability on the orbital period. If the latter can be confirmed, the rotation of one or both of the stars is likely tidally locked to the orbit. The X-rays – and the photometric variability – can thus be explained as coming from an active, spotted, rapidly rotating star, as suggested by Belloni & Verbunt (1996).

Acknowledgements – The authors wish to thank Gertie Geertsema and Marco Kouwenhoven for their help with the observations, and Keivan Stassun for providing the routines to perform the light curve and photometric variability analysis. We also want to thank David Latham for the information on the binarity of H 209; the measurements were taken as part of a larger study to monitor the radial velocities of blue stragglers in open clusters carried out by D. Latham and A. Milone. This research made extensive use of the WEBDA Open Cluster Database developed and maintained by J.-C. Mermilliod. The Jacobus Kapteyn Telescope and the William Herschel Telescope are operated on the island of La Palma by the Isaac Newton Group in the Spanish Observatorio del Roque de los Muchachos of the Instituto de Astrofisica de Canarias. IRAF is distributed by the National Optical Astronomy Observatories, which are operated by the Association of Universities for Research in Astronomy, Inc., under cooperative agreement with the National Science Foundation. MvdB is supported by the Netherlands Organization for Scientific Research (NWO).

References

Belloni, T. 1997, in Cool stars in clusters and associations: magnetic activity and age indicators, ed. G. Micela, R. Pallavicini, & S. Sciortino, Vol. 68, 993
Belloni, T. & Tagliaferri, G. 1997, A&A, 326, 608
Belloni, T. & Verbunt, F. 1996, A&A, 305, 806
Belloni, T., Verbunt, F., & Mathieu, R. D. 1998, A&A, 339, 431
Carraro, G. & Chiosi, C. 1994, A&A, 287, 761
Daniel, S. A., Latham, D. W., Mathieu, R. D., & Twarog, B. A. 1994, PASP, 106, 281
Dinescu, D. I., Demarque, P., Guenther, D. B., & Pinsonneault, M. H. 1995, AJ, 109, 2090
Dupree, A. K., Whitney, B. A., & Pasquini, L. 1999, ApJ, 520, 751

Fernández-Figueroa, M. J., Montes, D., de Castro, E., & Cornide, M. 1994, ApJS, 90, 433
Garrison, R. F. 1972, ApJ, 177, 653
Girardi, L., Mermilliod, J.-C., & Carraro, G. 2000, A&A, 354, 892
Groot, P. J., Piters, A. J. M., & van Paradijs, J. 1996, A&AS, 118, 545
Heinemann, K. 1926, Astr. Nach., 227, 193
Honeycutt, R. K. 1992, PASP, 104, 435
Hrivnak, B. J. 1977, IBVS 1293
Janes, K. A. & Phelps, R. L. 1994, AJ, 108, 1773
King, D. L. 1985, ING Technical Note, 31
Kurucz, R. L. 1979, ApJS, 40, 1
Larsson-Leander, G. 1964, ApJ, 140, 144
Mallik, S. V. 1994, A&AS, 103, 279
Malyuto, V. & Schmidt-Kaler, T. 1997, A&A, 325, 693
Massey, P., Strobel, K., Barnes, J. V., & Anderson, E. 1988, ApJ, 328, 315
Mermilliod, J.-C., Mathieu, R. D., Latham, D. W., & Mayor, M. 1998, A&A, 339, 423
Mermilliod, J.-C. & Mayor, M. 1989, A&A, 219, 125
Milone, E. F., Stagg, C. R., Sugars, B. A., McVean, J. R., Schiller, S. J., Kallrath, J., & Bradstreet, D. H. 1995, AJ, 109, 359
Pilachowski, C. A., Saha, A., & Hobbs, L. M. 1988, PASP, 100, 474
Piters, A. J. M., Groot, P. J., & van Paradijs, J. 1996, A&AS, 118, 529
Rebeirot, E. 1970, A&A, 4, 404
Sanders, W. L. 1972, A&A, 16, 58
Scargle, J. D. 1982, ApJ, 263, 835
Schönberner, D. & Napiwotzki, R. 1994, A&A, 282, 106
van den Berg, M., Orosz, J., Verbunt, F., & Stassun, K. 2001a, A&A, 375, 375
van den Berg, M., Stassun, K., Verbunt, F., & Mathieu, R. D. 2001b, A&A, submitted
van den Berg, M., Verbunt, F., & Mathieu, R. D. 1999, A&A, 347, 866
van den Bergh, S. & McClure, R. D. 1980, A&A, 88, 360
Vasilevskis, S. & Rach, R. A. 1957, AJ, 62, 157
Verbunt, F. & Phinney, E. S. 1995, A&A, 296, 709
Walker, M. F. 1958, ApJ, 128, 562

Hoofdstuk 8

Samenvatting

Een verlaten strand en een onbewolkte lucht, zoals op de voorkant van dit proefschrift, zijn ideaal om te genieten van de sterren: overdag van de Zon – de dichtstbijzijnde ster – en 's nachts van een hele hemel bezaaid met sterren. Bekeken met het blote oog zien alle sterren er ongeveer hetzelfde uit – er zijn subtiele kleurverschillen en de één is misschien wat helderder dan de andere, maar dat is het wel zo'n beetje. Wanneer we sterren nu in meer detail bekijken, met speciaal daarvoor ontworpen instrumenten zoals telescopen en satellieten, kunnen we veel meer informatie uit deze lichtpuntjes halen.

Het onderzoek in dit proefschrift gaat over sterren die röntgenstraling uitzenden. Omdat we sommige eigenschappen van deze sterren niet begrijpen hebben we veel nieuwe waarnemingen gedaan. Ik zal eerst iets vertellen over sterren in het algemeen, zodat duidelijker wordt *wat* we niet begrijpen aan deze sterren.

8.1 Sterren en sterrenhopen

Het heelal is niet alleen gevuld met sterren en planeten, maar ook met grote wolken stof en gas. Een ster wordt gevormd wanneer zo'n wolk onder haar eigen gewicht begint in te storten. Op een gegeven moment zijn de druk en de temperatuur binnen in de wolk zo hoog opgelopen dat losse deeltjes samensmelten tot één deeltje. Bij dit proces, dat kernfusie wordt genoemd, komt energie vrij die er voor zorgt dat het instorten van de wolk stopt: de wolk is dan een echte ster geworden. Een deel van de energie die in het binnenste van een ster wordt opgewekt wordt aan het oppervlak van de ster in de vorm van licht uitgezonden. Sterren zijn dus hete gasbollen die licht uitstralen. Als er binnen in de ster geen deeltjes meer zijn die kunnen samensmelten stopt de kernfusie en houdt de ster op met stralen.

Er zijn lichte en zware sterren. Zware sterren verbruiken meer energie dan lichte sterren, om het instorten tegen te gaan, en zullen daarom meer licht uitstralen en sneller uitdoven. Aan de helderheid van een ster (aan de hemel) is niet direct te zien hoe zwaar ze is: een lichte ster die dichtbij staat kan nog steeds helderder zijn dan een zware ster op grote afstand. Ook kunnen de eigenschappen van een ster in de loop van de tijd veranderen: aan het eind van haar

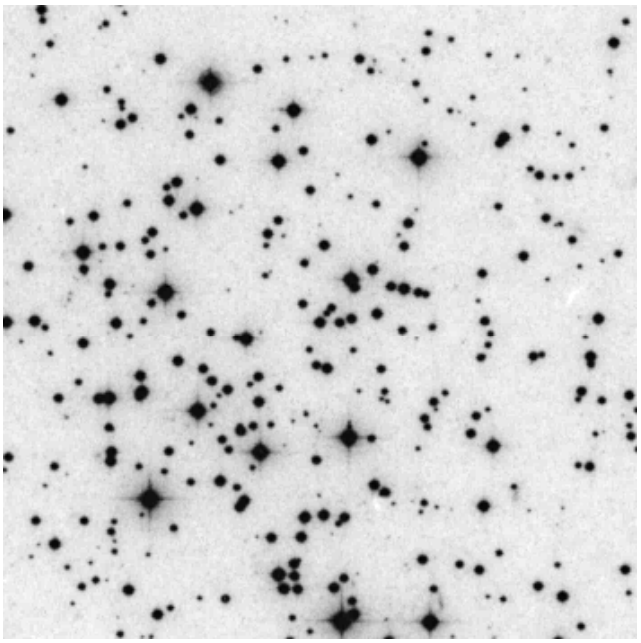

Figuur 8.1: Het binnengebied van de open sterrenhoop M 67.

leven zal een ster enorm opzwellen en daarbij veel helderder worden, voordat ze ophoudt met stralen. Om de eigenschappen van een ster goed te begrijpen is het dus belangrijk dat we haar afstand tot ons weten en de levensfase waarin zij is.

Sterren worden vaak niet alleen geboren, maar met honderden tot honderdduizenden tegelijk. Een groep van een paar honderd of een paar duizend sterren noemen we een open sterrenhoop. Een open sterrenhoop die je gemakkelijk met het blote oog kunt zien is de Pleiaden, een groep sterren die ongeveer 100 miljoen jaar geleden is gevormd. Het onderzoek in dit proefschrift heb ik gedaan aan sterren in sterrenhopen van een paar miljard jaar oud. Ik heb me vooral gericht op de sterren in de sterrenhoop M 67 – of Messier 67 – vernoemd naar Charles Messier die een catalogus heeft gemaakt van nevelachtige hemelobjecten en sterrenhopen. Op 6 april (mijn verjaardag!) 1780 voegde hij nummer 67 aan zijn lijst toe. De sterren in M 67 zijn zo'n vier tot vijf miljard jaar geleden gevormd en zijn daarmee ongeveer net zo oud als onze Zon. Figuur 8.1 is een foto van M 67. Naast M 67 heb ik ook sterren onderzocht in de oude sterrenhopen NGC 752 en NGC 6940.

Het bestuderen van sterrenhopen heeft zo zijn voordelen: de sterren zijn allemaal even oud en ze staan ongeveer even ver van ons weg. Dat maakt het gemakkelijker om de eigenschappen van de sterren met elkaar te vergelijken, zonder de precieze afstand en leeftijd te weten. Van dit voordeel wordt veel gebruik gemaakt, omdat het achterhalen van de afstand en leeftijd van een "alleenstaande" ster niet gemakkelijk is. M 67 heeft daarbij nog als voordeel dat ze relatief dichtbij staat zodat de sterren vrij helder zijn, en dat er weinig materiaal tussen ons en M 67 instaat dat het zicht op deze sterrenhoop belemmert.

8.2 Röntgenstraling van sterren

De sterren die Messier zag en die wij 's nachts zien, nemen we waar in het licht waar onze ogen gevoelig voor zijn: het optisch of visueel licht. Sterren stralen ook ander licht uit dat onzichtbaar is voor onze ogen, van radiostraling tot röntgenstraling.

Met de röntgentelescoop van de satelliet ROSAT is gezocht naar straling van de sterren in M67. Van sterren die net zo oud zijn als de Zon (en dat zijn de sterren in M67) verwachten we eigenlijk dat ze te weinig röntgenstraling uitzenden om door ROSAT gezien te worden: de Zon straalt ook röntgenlicht uit, maar als je de Zon net zo ver weg zou zetten als de sterren in M 67 zou ROSAT haar niet meer zien. Als we *wel* een ster van M 67 in röntgenlicht zien moet er dus iets speciaals met die ster aan de hand zijn. Het zou bijvoorbeeld een *dubbelster* kunnen zijn ...

8.3 Dubbelsterren

De meeste sterren staan niet alleen, maar vormen met een andere ster een paar, of een dubbelster, dat heel regelmatig om elkaar heen beweegt. Als een dubbelster ver weg staat is het voor ons moeilijk om de twee sterren afzonderlijk te zien, zelfs met een telescoop. Gelukkig zijn er wel indirecte manieren om af te leiden dat een ster dubbel is. Bijvoorbeeld, als twee sterren zo om elkaar heen draaien dat gedurende een deel van de tijd de ene ster tussen ons en de andere ster in staat, dan zal de dubbelster even wat minder helder worden. Dit is een beetje te vergelijken met wat er gebeurt als de Zon tijdens een zonsverduistering wordt afgedekt door de Maan.

Sterren die dicht bij elkaar staan zullen elkaar beïnvloeden door middel van getijdenkrachten, net zoals de Aarde en de Maan dat doen (eb en vloed). Het effect van die krachten is dat de vorm van de baan waarin de twee sterren om elkaar heen draaien steeds meer op een cirkel begint te lijken. Ook de snelheid waarmee de sterren om hun eigen as draaien zal veranderen: de getijdenkrachten proberen ervoor te zorgen dat de tijd waarin een ster één keer om haar as draait net zolang wordt als de tijd waarin de sterren één rondje om elkaar hebben gedraaid. Als een ster alleen is, zal ze in de loop van de tijd steeds langzamer om haar as draaien (de beweging wordt afgeremd), maar als een ster onderdeel is van een dubbelster kan een ster door getijdenkrachten toch snel om haar as blijven draaien, ondanks de hoge leeftijd.

Waarom dit verhaal over dubbelsterren en ronddraaiende sterren? Sterren die snel ronddraaien kunnen magneetvelden opwekken in hun buitenlagen – we noemen ze *magnetisch actieve* sterren. Die magneetvelden zorgen ervoor dat er een laag gas om de ster heen wordt gevormd die zo heet is (een paar miljoen graden) dat hij röntgenlicht uitstraalt. Op grond hiervan zou je dus verwachten dat veel van de röntgenbronnen die ROSAT in M 67 heeft gezien dubbelsterren zijn, waarin getijdenwisselwerking plaatsvindt. Voor veel van de röntgenbronnen in M67 blijkt dit inderdaad te kloppen.

8.4 Rare röntgenbronnen

In dit onderzoek wilden we vooral meer te weten komen over sterren waarvan we röntgenstraling hebben gezien, maar waarvoor we geen aanwijzingen hebben dat de ster een dubbelster is. In andere gevallen is een ster wel een dubbelster, maar de twee sterren staan dan zo ver van elkaar af dat ze elkaars aanwezigheid nauwelijks merken. In zo'n geval verwachten we ook niet dat er röntgenstraling wordt opgewekt. Waarom die sterren zo helder zijn in röntgenlicht is dus nog een raadsel.

We hebben nog meer rare röntgenbronnen onderzocht. In het begin van dit hoofdstuk beschreef ik dat er verbanden bestaan tussen de helderheid en de massa van een ster, en tussen de massa en de levensduur. Niet alle sterren in M 67 lijken zich hier aan te houden; zeker toen bleek dat sommige van deze sterren in röntgenlicht te zien waren trokken ze onze aandacht. Dit was een extra aanwijzing is dat er iets raars aan de hand moet zijn. Een paar van deze sterren hebben we ook bestudeerd.

Waarom willen we meer te weten komen over deze sterren? Onze sterren gedragen zich anders dan we verwachten en kunnen ons daarom nieuwe dingen leren. Eén van de mogelijkheden is dat ze in contact zijn geweest met een andere ster. In een dubbelster komt het wel eens voor dat de ene ster gas overdraagt aan de andere; misschien is dit in het verleden ook gebeurd in de sterren die wij hebben onderzocht. Verder staan de sterren in een open sterrenhoop relatief dicht bij elkaar, zodat botsingen tussen sterren ook niet uit te sluiten zijn. Over de sterren die ontstaan uit botsingen weten we helaas nog niet zo veel.

8.5 Dit proefschrift

Om onze rare röntgenbronnen te onderzoeken hebben we veel nieuwe waarnemingen gedaan in optisch licht. Daarvoor hebben we telescopen gebruikt in Chili, de Verenigde Staten en op de Canarische Eilanden. We hebben op twee manieren naar de sterren gekeken. Ten eerste door het licht uit elkaar te rafelen in verschillende kleuren (een spectrum), en ten tweede door te zoeken naar veranderingen in de helderheid van de sterren in de loop van de tijd. Het is niet gelukt om alle vragen die we hadden te beantwoorden, soms zijn er zelfs nieuwe vragen bijgekomen, maar we hebben nu wel beter inzicht in de eigenschappen van de sterren. In het kort geef ik een paar resultaten.

In hoofdstukken 2 en 7 hebben we in spectra gezocht naar aanwijzingen voor een hete gaslaag rondom de ster. Voor sommige sterren heeft dit weinig opgeleverd, voor andere gevallen hebben we wel aanwijzingen voor zo'n heet gas gezien ook al is het niet altijd even duidelijk wat de oorzaak is voor de aanwezigheid van dat gas.

Een kenmerk van actieve sterren is dat het steroppervlak door de magneetvelden niet overal even veel licht uitstraalt. Tijdens het ronddraaien van een ster zal de helderheid dan ook regelmatig veranderen; deze veranderingen zien er anders uit dan de sterverduisteringen waar ik het eerder over had. Wanneer zo'n veranderlijke ster deel uitmaakt van een dubbelster, kunnen we de periode van de helderheidsveranderingen vergelijken met de periode waarmee

de sterren om elkaar heen draaien. Als die twee gelijk zijn is dit een duidelijke aanwijzing voor de werking van getijdenkrachten. Voor een aantal “normale” röntgenbronnen hebben we op deze manier het idee dat we hadden over de oorzaak van hun röntgenstraling bevestigd. Slechts voor een enkele van de rare röntgenbronnen hebben we ook helderheidsveranderingen gezien. Deze metingen worden beschreven in hoofdstukken 3 en 7.

Bij het doen van dit soort waarnemingen, meet je automatisch ook de helderheid van sterren die in de buurt staan van de sterren waarin je bent geïnteresseerd; de resultaten hiervan zijn beschreven in hoofdstuk 4. We hebben een aantal sterren gevonden die regelmatig van helderheid veranderen, maar waarvan verder weinig bekend is. Misschien zijn het tot nu toe onbekende dubbelsterren. We zijn van plan ze in de toekomst beter te onderzoeken.

Ik zal nu het stuk onderzoek samenvatten dat ik zelf het leukst vind en dat beschreven is in hoofdstuk 5. De ster S 1082 in M 67 is een ster die opvalt omdat zij langer lijkt te leven dan we verwachten op grond van haar massa: ze had al lang dood moeten zijn. Zulke sterren worden wel vaker gezien in sterrenhopen en worden blauwe dwaalsterren (*blue stragglers*) genoemd. Een oplossing voor dit probleem zou zijn als de ster niet zo lang geleden “verjongd” is, doordat zij er extra massa (=brandstof) heeft bijgekregen, bijvoorbeeld via een begeleider in een dubbelster of via een botsing met een andere ster. Het probleem met S 1082 was dat ze niet om een andere dichtbijzijnde ster leek te bewegen, hetgeen ook de röntgenstralen onverklaard liet. *Wel* waren er helderheidsveranderingen gemeten met een korte periode van iets meer dan een dag die lijken op verduisteringen van een ster door een andere ster. Omdat deze twee waarnemingen elkaar leken tegen te spreken, en waarschijnlijk ook omdat dit resultaat gepubliceerd was in een weinig toonaangevend tijdschrift, werd er met het resultaat van de helderheidsveranderingen weinig gedaan. Onze bijdrage is geweest dat we de helderheidsveranderingen hebben bevestigd, *en* in het spectrum van S 1082 twee extra sterren hebben gevonden die wel in die ene dag om elkaar heen bewegen. Dit kan de röntgenstralen verklaren: we denken dat ze worden opgewekt door magnetische activiteit in de dubbelster. Het lijkt er zelfs op dat alle drie de sterren om elkaar heen bewegen. Toch lossen onze resultaten niet alle problemen op: we vinden dat twee van de drie sterren nog steeds te oud zijn voor hun massa. Als ze verjongd zijn via een botsing of door het overdragen van gas, dan betekent dit dat er nog meer sterren bij de vorming van S 1082 betrokken waren. Met andere woorden, dit is een aanwijzing dat botsingen en wisselwerkingen tussen sterren in clusters echt gebeuren.

Curriculum vitae

Geboorte datum	6 april 1972
Geboorte plaats	Maastricht
Middelbare school	Stedelijke Scholengemeenschap Maastricht (1984–1990)
Studie Sterrenkunde	Universiteit Utrecht (1990–1996)
Promotie onderzoek Sterrenkunde	Sterrenkundig Instituut Universiteit Utrecht (1996–2001)